

Deep Learning Methods for Partial Differential Equations and Related Parameter Identification Problems

Derick Nganyu Tanyu^{†*}, Jianfeng Ning[†], Tom Freudenberg[‡], Nick Heilenkötter[‡],
Andreas Rademacher[‡], Uwe Iben[§], and Peter Maass[‡]

[‡]Centre for Industrial Mathematics (ZeTeM), University of Bremen, Germany

[†]School of Mathematics and Statistics, Wuhan University, China

[§]Robert Bosch GmbH, Germany

*Corresponding author: derick@uni-bremen.de

December 7, 2022

Abstract

Recent years have witnessed a growth in mathematics for deep learning—which seeks a deeper understanding of the concepts of deep learning with mathematics, and explores how to make it more robust—and deep learning for mathematics, where deep learning algorithms are used to solve problems in mathematics. The latter has popularised the field of scientific machine learning where deep learning is applied to problems in scientific computing. Specifically, more and more neural network architectures have been developed to solve specific classes of partial differential equations (PDEs). Such methods exploit properties that are inherent to PDEs and thus solve the PDEs better than classical feed-forward neural networks, recurrent neural networks, and convolutional neural networks. This has had a great impact in the area of mathematical modeling where parametric PDEs are widely used to model most natural and physical processes arising in science and engineering. In this work, we review such methods and extend them for parametric studies as well as for solving the related inverse problems. We equally proceed to show their relevance in some industrial applications.

1 Motivation

Arguably, partial differential equations (PDEs) provide the most widely used models for a large variety of problems in natural sciences, engineering and industry. The ever increasing complexity of these models such as digital twins for high-tech industrial applications require most efficient solvers.

These models follow the full life cycle of products from classical simulation and optimization during the development phase to process monitoring and control during production. Such models typically rely on accurate calibration of critical parameters, which might be scalar parameters or even distributed spatial-time varying parameter functions. The calibration process itself requires multiple runs of the model and increases the need for efficient solvers even more.

Not surprisingly, data-driven concepts and in particular neural network approaches have been studied extensively over the last few years as they have the potential to overcome three major obstacles in PDE simulations: First of all, no mathematical-physical model is ever complete, however, even the finest detail or tricky non-linearity is contained in a sufficient data set; secondly, the parameters to be determined most often are not arbitrary but follow an unknown, application specific distribution, which can be recovered and exploited from training data; thirdly, as already mentioned, the complexity of PDE-based modeling has reached a level such that conventional and most widely used methods such as finite elements or finite difference

do require computational times beyond reasonable limits, while neural network concepts after training are most efficient.

This is matched by our own experience over the last few years, where an increasing number of our industrial and engineering collaboration partners started to experiment with deep learning (DL) concepts based on neural networks for PDE problems. However, they as much as we were overwhelmed by the somewhat confusing variety of different DL concepts for these tasks. These span from general approaches for large classes of problems to very specifically tailored approaches for individual equations. The present paper is based on our endeavor to provide an unbiased overview of the most common general approaches and to provide a limited, but scientifically based guidance on how to select appropriate methods. We are well aware of the many extension of the mentioned methods and the exploding body of literature dealing with such problems, and we readily apologize to those scientists, whose research we neglected to include. To be more precise, we are considering second-order partial differential equations, which depend on a parameter function λ :

$$\mathcal{N}(u, \nabla u, \Delta u, u_t; \lambda) = 0 \tag{1}$$

$$\lambda : \Omega \rightarrow \mathbb{R} \tag{2}$$

In this general notation, \mathcal{N} encodes the differential equation as well as boundary conditions. We always assume, that the parameter-to-state operator F , which maps a given parameter λ to the solution of the PDE, is well-posed. I.e. we assume a function space setting such that the solution u of the PDE is unique and depends continuously on the parameter λ . We will consider three related classes of problems:

Level 1: Forward problem: solving a single PDE: given λ , compute $u = F(\lambda)$

Level 2: Parametric studies: given many parameters, $\lambda \in \{\lambda_1, \dots, \lambda_N\}$, compute corresponding u 's

Level 3: Parameter identification (inverse problem): given a measured u^δ or its values Pu^δ under a measurement operator P , determine a corresponding λ , e.g. solve $F(\lambda) \sim u^\delta$.

Our main target is the third class of problems, i.e. inverse problems stated as parameter identification problems for PDEs. These problems are typically non-linear and ill-posed, even if the differential equation is linear and the forward operator is well-posed. Nevertheless, we start with the first problem and review the most common DL approaches for solving the forward problem. We then discuss their potential for parametric studies and parameter identification problems. As an underlying motivation for using DL concepts in this setting, we assume that an evaluation of the forward operator F by classical methods, e.g. finite difference schemes or finite elements, is computationally expensive and not suitable for large-scale parametric studies.

We have two remarks for clarifying the scope of the present survey. First of all, parameter identification problems are inverse problems and can be attacked by well-established general regularization schemes for operator equations. For a recent overview of such data-driven concepts for inverse problems and their regularization properties, see e.g. [4]. However, these concepts, e.g. unrolled iteration schemes, typically involve an evaluation of the forward operator or its adjoint. This will not lead to efficient schemes in our framework, where the evaluation of F is assumed to be too costly for large-scale parametric studies. We will remark shortly on that in our section on the state of the art. Hence, in the present paper, we only consider DL concepts, where the forward operator itself, i.e. the parameter-to-state operator, or its inverse are replaced by a neural network. Secondly, there exists a growing number of highly optimized DL concepts for very specific PDE problems e.g. for coupled physics systems, molecular dynamics, or complex fluid dynamic problems. These approaches do have a limited potential for transfer to other problems, and we will not address these concepts. We will rather focus on general classes of DL concepts that apply to a larger variety of PDE-based problems. However, we will highlight some of those successful but specialized approaches in the section on the state of the art.

1.1 Classical methods for solving PDEs numerically

Let us first comment on the main competitors for data-driven concepts, namely the classical and well established concepts of finite difference (FDM), finite element (FEM), boundary element Method (BEM), finite volume (FVM) or particle methods.

The so-called finite difference method (FDM) is based on the replacement of the occurring derivatives by difference quotients. In this process, the function values of the solution are approximated at individual discrete grid points. The result is a so-called grid function. We refer, e.g., to [92] for a more detailed description. The great advantage of the FDM is its straight forward realisation. However, its extension to more complex problems is limited and rather unrealistic smoothness assumptions are necessary for its analysis.

The finite element method (FEM) overcome the mentioned disadvantages of FDM methods to a large extent. In contrast to the FDM, it is based on the weak formulation of the PDE under consideration and searches for the discrete solution over a finite-dimensional subspace of the underlying function space, see [10] for more details. Especially in connection with adaptive and domain decomposition methods it shows its full potential. An interesting variant are discontinuous Galerkin (dG) methods, in which the smoothness assumptions for the discrete solution, which stems from the weak formulation of the PDE, is only enforced by penalty terms.

The boundary element methods (BEM) follows a different idea. In this concept, the PDE is transformed into a boundary integral equation, which, however, is only possible in special cases. This reduces the dimension of the problem. The boundary integral equation is then discretised by means of FEM, for example. However, the resulting system of equations is dense and its numerical solution is often tricky and numerically very elaborate. Nevertheless, the BEM offers great advantages for exterior space problems in which an unbounded area is considered. We refer for instance to [37] for more information.

The Finite Volume Method (FVM) brings together ideas from the FEM and the FDM and combines them with arbitrary control volumes, see e.g. [58]. The FVM is particularly well suited for the discretisation of hyperbolic equations and convection-dominated problems. However, its theoretical analysis is not yet that advanced.

Another approach are particle methods or discrete element methods (DEM), see e.g. [13], which are based on a completely different approach. Here, individual particles and their interaction with each other are considered. By using different approaches to describe the interaction, different materials and processes can be simulated. They thus achieve very good accuracy in many applications, e.g. in the simulation of sand, which are difficult to simulate with the other methods.

The mentioned concepts are well established for solving PDE based forward problems and all of them have been adapted to inverse problems, in particular in the context tasks of optimal control or numerical parameter identification. They lead to accurate results in this context. However, two main difficulties have to be mentioned: Firstly and as said already in the previous section, solving these inverse problems require to solve the forward problem multiple times, which leads to unacceptable overall computing times at least for large problems. Furthermore, the optimisation algorithms for solving the above-mentioned parameter identification tasks require the first and, if possible, also the second derivative with respect to the unknown parameters. At first, it is often unclear whether the mentioned derivatives exist at all. In addition, their calculation is algorithmically very complex and time-consuming, especially for time-dependent problems. We refer, for example, to [98] for a detailed discussion.

In summary, the classical methods are well researched and reliable and should be used whenever possible within the given restrictions of data and computer power. Hence, we once again stress, that the present paper refers to potential applications where solving the forward problem multiple times is simply too costly.

1.2 Deep learning for PDE solvers and scope of this survey

The main purpose of this section is to list the DL methods considered in this present survey. In the subsequent sections, we will then analyze their potential for parametric studies and inverse problems.

As already mentioned, mesh-based methods for solving PDEs such as finite element methods, finite difference methods, and finite volume methods, are the dominant techniques for obtaining numerical solutions of PDEs. When implementing these methods, the computational domain of interest should be first discretized using a set of mesh points and the solution is then approximated at the chosen grid points. The solutions are usually obtained from a finite linear space by solving a linear or non-linear system of equations. The classical methods are very stable and efficient for low dimensional problems and regular geometries. They have been well understood in terms of existence, stability and error estimate, and we can usually achieve desired accuracy by increasing the resolution of the discretization. In addition to the more general remarks above, the

classical methods have several additional drawbacks and limitations. Firstly, the curse of dimensionality has limited the use of mesh-based methods, since the number of discretization points will increase exponentially with the dimension, and there is no straightforward way to discretize irregular domains in high dimensional spaces. Secondly, traditional methods are designed to model one specific instance of the PDE system, not the parameter-to-state operator. Thus, for any given new instance of the PDE system, the problem has to be solved again. Thirdly, the numerical solution is only computed at the mesh points and evaluation of the solution at any other point requires interpolation or some other reconstruction method. Fourthly, classical methods require the knowledge of the underlying analytic system of differential equations, but sometimes the exact physics are unknown. Lastly, solving inverse problems by classical problems is often prohibitively expensive and requires complex formulations, repeated computation of forward problems, new algorithms and elaborate computer coding.

Deep learning methods have shown great power on addressing the above difficulties. Since there are many different deep learning methods for PDEs, and each method has its particular properties, we will discuss them one by one. We should add, that the theoretical investigation of deep learning concepts for PDEs, beyond more or less direct applications of the universal approximation theorem, is still scarce. This is in contrast to the classical PDE theory, where there exists an exhaustive literature on the analytic properties of different types of PDEs. The theoretical characterization of PDEs, as well as the type of theoretical background needed for proving solvability and uniqueness, differentiates between linear and non-linear elliptic, parabolic or hyperbolic equations and in terms of the given boundary conditions. Analytic tools are different for these different classes, hence it is somewhat surprising that DL concepts for PDEs do hardly ever use this classical classification but rather use a classification based on whether or not the PDE (no matter which type of PDE) is known, which type of data is given for training and which type of network architecture as well as which loss function for training is used.

We follow this data driven classification scheme. Our first level of characterization is based on the input and output structure of the network. Either a function approximation, i.e. a regression problem for the function u , is solved. Hence, the network takes x or (t, x) as input and outputs a one-dimensional scalar value, which is sought to approximate $u(x)$ or $u(t, x)$. Otherwise, one aims at an operator approximation for the parameter-to-state map and uses networks which take a parameter function, either in discretized form or as a vector of precomputed feature values, as input and outputs the full solution function u . The solution u again is delivered either in discrete form or as a related feature vector, that can be turned into a proper function representation in a post-processing step. The general idea of these two characterization is summarized in the following Figures 1-2:

- Function evaluation, neural network $\Phi_{\Theta}(t, x)$ based on the PINN concept, [88]

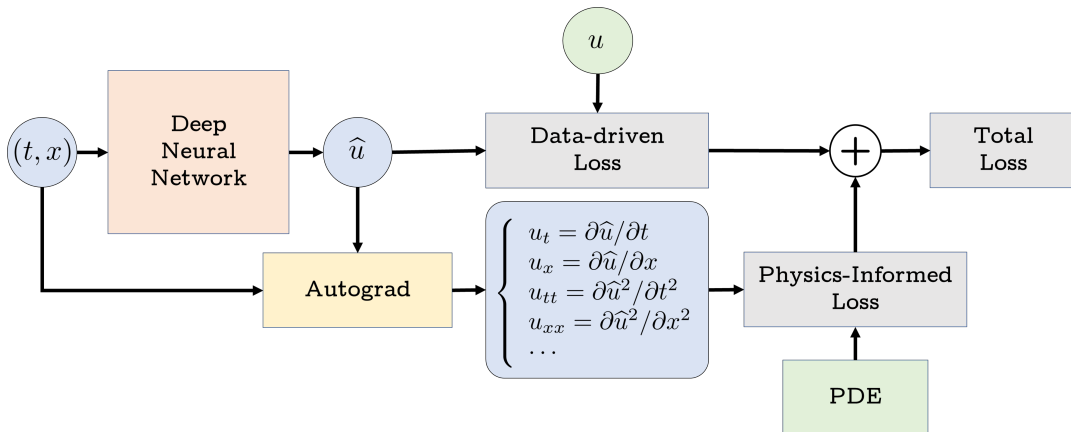


Figure 1: A network with a low input dimension for (t, x) , which outputs a scalar or low-dimensional $u(t, x)$. During training automatic differentiation by backpropagation is used to compute all necessary derivatives for checking, whether the PDE is satisfied. The loss function typically sums up over several values of (t, x) and their corresponding function points. After training only the first part of the network is used and u can be evaluated at arbitrary points (t, x) .

- Operator evaluation, neural network $\Phi_{\Theta}(\lambda)$ following the PCANN concept [8]

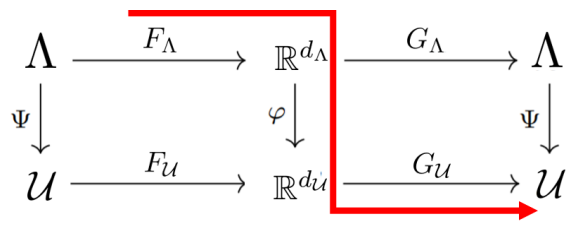


Figure 2: A typical setup for an operator approximation scheme. Here an order reduction model in combination with a neural network is employed. First, the parameter λ is reduced to a feature vector by determining its scalar products with a pre-computed reduced basis, i.e. $c_k = \langle \lambda, b_k \rangle$ which in case of an orthonormal system is equivalent to $\lambda \sim \sum c_k b_k \in X$. Only the feature vectors are mapped by the neural network. The output features \tilde{c} are then used to determine an expansion of the sought for solution u , $\phi_\Theta : c \mapsto \tilde{c}$, $u = \sum_\ell \tilde{c}_\ell \tilde{b}_\ell$ in terms of a basis $\{\tilde{b}_\ell\}$ in the state space. (see [8])

Networks	PDE usage	Data usage	Neural Network approximation	Discretization		Reference
				Parameter	Solution	
Deep Ritz	yes	no	function	no	no	[65, 110]
PINN	yes	no	function	no	no	[88]
WAN	yes	no	function	no	no	[5, 112]
PCANN	no	many	operator	free grids	free grids	[8]
FNO	no	many	operator	free grids	free grids	[61]
UFNO	no	many	operator	free grids	free grids	[106]
MWT	no	many	operator	free grids	free grids	[36]
DeepONet	no	many	operator	fixed	no	[69]
PINO	yes	if needed	operator	free grids	free grids	[64]
PI-DeepONet	yes	if needed	operator	fixed	no	[101]

Table 1: The list of DL-concepts considered in this survey is based on a pre-selection mirroring our own interest in inverse problems. Hence, concepts for operator approximation are preferred. In their original papers, most of these concepts were designed for Level 1 problems only. Hence, we need to specify in later sections how to extend them for Level 2 or Level 3 problems. Also, we will later refine the features characterizing the different methods in terms of limitations, e.g. which PDE equations are most suitable and which are not.

Typical examples of DL concepts aiming for a function approximation are Deep Ritz method [65, 110], Physics-Informed Neural Network (PINN) [88], Deep Galerkin Method (DGM) [91], Weak Adversarial Networks [112], and Deep Splitting Approximation methods [7]. In all these concepts, information of the underlying physics must be used when training the neural network, i.e. the PDE must be known analytically. These concepts are usually mesh-independent and accurate, while they require the knowledge of the governing laws of the PDEs, and the optimization problem needs to be solved for every new instance. This is similar to classical methods.

Examples for the second type, i.e. methods aiming at an operator approximation, include Model reduction neural network (PCANN) [8], Deep Operator Network (DeepONet) [69] and its extensions [35, 101], Fourier neural operator (FNO) [61] and its physics-informed extension–Physics Informed Neural Operator (PINO) [64], Graph Kernel Network [62, 63], Bayesian deep convolutional encoder-decoder networks [114], Wavelet Neural Operators [97], Multiwavelet based operator (MWT) [36] and many more. These operator methods usually learn the neural network with some paired input-output (parameter-solution) observations with or without the knowledge of the physical system (using the physics information could sometimes alleviate the need for much data as in the case of PINO and PI-DeepONet) as highlighted in Table 1. Thus, the neural network only needs to be trained once, and a new parameter identification task can be directly solved by a forward pass of the network. Some of these deep learning methods still need to discretize the domain of interest, and the solutions are sought in a finite linear space [114]. A recently published paper [20] aims at comparing some of these operator approximation concepts for solving various PDEs. The primary criterion

for comparison in this well written paper is the cost-to-accuracy curve. Accordingly, the authors compare results obtained with different network sizes. However, their comparison includes the basic methods PCANN, DeepONet and FNO which in our tests did not yield the best results. Also, the numerical test stay in a range of - when compared with FEM methods - rather large approximation errors. This matches our experience, it is hard to get to high precision for forward solvers with DL concepts. Anyway, our focus is on inverse problems, which are not covered in the mentioned paper.

In terms of the involved computational load, the computational cost of classical methods for solving linear PDEs is mainly determined by the need to solve a large linear system. For deep learning methods it is the training process (optimization) of the neural network. As a general rule of thumb, for low dimensional problems with regular geometries, classical methods are in general more powerful and efficient than deep learning methods. Ignoring rounding errors, the main error of the classical methods arises from the step size of the discretization. There exists a trade-off on the resolution: coarse grids are fast but less accurate; fine grids are more accurate but slower. On the other hand, for DL-approaches one usually has to carefully choose the neural network, optimization method and the hyperparameters in consideration of the underlying differential equation. Additionally, the error of deep learning methods is usually difficult to estimate and consists of several factors. The accuracy can be characterized by dividing the total error into three main types: approximation, optimization, and generalization. In other words, the error relies on the network architecture, the loss function, the optimization algorithm, and the amount of training data, as well as modelling information of the PDE.

The selection of DL-based PDE solvers which are further investigated in this survey is based on our endeavour to cover a most complete range of different concepts. Hence we included the basic concepts of learned DL solvers as well as some recent improvements of these.

A more detailed description of these approaches, their algorithmic implementation and their analytical properties will be given in the subsequent sections. There we will also highlight, how these methods, which were typically designed as PDE-forward solvers can be extended to parameter identification problems.

1.3 Some remarks on concepts not covered in this survey

In this section we want to highlight those directions of research, which are not covered in this survey.

First of all there exist several specialized and powerful DL concepts for complex but specific PDEs. Research on neural networks for such specialized cases of PDEs as well as related parametric studies and inverse problems is exploding and it is impossible to give an exhaustive list of reference. Hence, we only want to highlight areas of research, which have reached a certain level of maturity in terms of experimental success as well as mathematical rigor. Again, this selection is based on personal preferences and we apologize to those, who quite rightly might want to see their own work included.

A particular successful area for DL applications are coupled-physics systems, which lead to some of the most complex inverse problems. Typically, those inverse problems cannot be solved by standard concepts, neither in the classical analytical regularization setting nor in data-driven frameworks. Hence, such problems, e.g. opto-acoustic tomography, require specialized concepts, which typically integrate domain specific expert knowledge or at least partially draw their motivation from analytic reconstruction formulae, see e.g. [3, 17, 40, 95]. Another class of papers do take numerical schemes for PDEs as a starting point for developing network architectures, see e.g. [38, 89]. In these papers, the different layers of a neural network are regarded as a time stepping in a discretized scheme. In particular, this allows to specifically mimic and to improve numerical schemes for parabolic equations, which e.g. are the basis for many imaging problems based on diffusion processes. Simulation of turbulent flows also is an area, where DL concepts have shown good success. We only list some papers, which in our opinion together with the cited literature therein allow an overview on this topic [24, 76, 99]. One should also mention the spectacular results on simulating molecular dynamics [9, 48] and many other fields of applications, where DL simulations lead to groundbreaking novel insights.

We also do not cover the topic of DL for stochastic PDEs and recent results, which we regard to be more on the side of PDE theory and simulation. Hence, we do not cover recent developments as e.g. described in [12, 22, 104].

Secondly, we want to remark on general regularization schemes for inverse problems using a data-driven approach, which can be applied to but are not particularly tailored for PDE-based parameter identification problems. Typically these general data-driven regularization schemes for parameter identification problems

do need an evaluation of F or any form of its adjoints. For reference to this type of schemes we refer to [4] or to [1] for a recent paper, which embeds the learning of the network together with the parameter identification into a regularization scheme. We would like to remark that unrolled iteration schemes such as LISTA or unrolled primal-dual, are somewhat hybrid methods and could be included in our survey. However, LISTA is predominately successful for linear forward operators A and it still needs the adjoint A^* for initializing the input of the network. One could extend such DL schemes, which are derived from classical regularization theory, in such a way that the evaluation F or its adjoint would be done by training an embedded network for every operator evaluation. However, this leads to a rather complex training task and this extension is not part of the scope of the original papers for e.g. primal-dual, NETT or DeepPrior or similar [2, 22, 59].

2 Characterization of DL concepts for PDEs

Having specified the restricted scope of the present survey, we will now list the concepts under consideration in the following sections. Before starting the introduction of the individual methods we include some general remarks on the characterization of deep learning methods for PDEs. As already mentioned, the characterization of DL concepts for solving PDEs differs considerably from the analytic characterization of PDEs. They are mainly characterized in terms of the information needed for applying them. The two main classes of information are data and physical models, where 'physical models' refers to the mathematical formulation of the differential equations and their boundary conditions.

2.1 Data

Data driven methods rely on the availability of sufficiently large data sets of good quality. The data provided can be sampled values of a single or multiple solutions, where sampling can be done either on a predefined grid or with arbitrary sampling points. Some of the most advanced theoretical investigations do start from assuming a sampling in function space, which opens the path for incorporating functional analytical machinery in their analysis, see e.g. [1, 8, 87].

However, the volume of available data is usually rather scarce, e.g. useful experimental data is generally limited or even intractable for many practical scenarios and high-fidelity numerical simulations are often computationally expensive. Sometimes it is also a challenge to extract interpretable information and knowledge from the data deluge. Moreover, purely data-driven methods may fit observations very well, but predictions may be physically inconsistent or implausible. Theoretically, finite data can not fully and correctly determine a mapping which maps a infinite set to a infinite set. However, we can still see the success of data-driven methods, which is mainly due to two reasons: first of all the searched for solution or parameter typically follows a certain prior distribution, which we might be able to approximate well with few samples; and secondly most problems are continuous, which in connection with suitable regularization schemes leads to good generalization properties even for limited sets of training data, [88]

In addition to sampled data, there exists a wealth of domain specific expert knowledge for most applications. This information may come in form of observational, physical or mathematical understanding of the system under consideration. Integrating data and these prior knowledge can yield more interpretable machine learning methods and can improve the accuracy and generalization performances without large amount of data.

In our context information from physics may come in different forms: most commonly, the system of partial differential equations as well as boundary conditions are specified. Otherwise some energy functionals or a weak formulation may be given. Also, certain approaches [90] incorporate conservation laws in the network architecture. Whenever such information is used, the concept is typically called 'physics informed'.

Different from data-driven methods, the physics information may uniquely determine the systems, however, only within the limitations of the chosen model. For example, given the PDE formula and some initial and boundary equations, the solution is uniquely determined if the system is well-posed. In other word, mathematical formulae may inherently contain all information of the physical systems, while data are just some observations and reflection of the physical systems and thus can not fully reveal the whole information of the systems.

The most common approach is to use this physics information in the loss function during training of the network. Hence, the type of physics information determines the loss function.

2.2 Network training and application

Training the resulting networks typically leads to additional problems. This may require extensive hyper-parameter search, data preprocessing or subtle parameters settings for controlling the convergence of the training scheme. We have listed the respective training concepts for each method in the Appendix A.

As pointed out in [49], specific to physics-informed learning, there are currently three pathways that can be followed separately or in tandem to accelerate training and enhance generalization of ML models by embedding physics in them. The first one is **observational biases** from observational data, which is the foundation of data-driven methods in machine learning. The second is **inductive biases** by designing special NN architectures that can automatically and exactly satisfy some properties and conditions. The most common example are convolutional NNs which can be designed to respect properties, such as symmetry, rotations and reflections. Other examples are Graph neural networks [62] which are adapted to graph-structured data. Another concept is based on Quadratic residual networks(QREs) [11], which add a quadratic residual term to the weighted sum of inputs before applying activation functions in the neural networks. They were shown to have good performance on learning high frequency patterns. Specific architectures can also be designed to satisfy the initial/boundary conditions. The last pathway is **learning biases**, where the physics constraints are imposed in a soft manner by appropriately penalizing the loss function of conventional NN approximations. Representative examples include Deep Ritz method and PINN.

We also want to comment on the arguably most important tools for physics-informed machine learning, namely automatic differentiation [6]. In principle, this general concept us to compute exactly the derivatives of the network output with respect to the input variables. Hence, we can incorporate weak or strong formulations of the underlying PDE conveniently. However, compared to conventional numerical gradients such as finite difference, the automatic differentiation method is usually slower and require more memory.

Moreover, after training, the methods will again differ substantially in their scope of applicability. Methods might allow to sample a solution of a PDE at arbitrary points. In this case the method is called meshfree, which is one of the most desirable properties of most DL concepts for PDEs. Another important property, in particular for Level 2 and Level 3 problems, is the computational load needed for applying the network to a different parameter of the PDEs. This is most efficient for most operator learning schemes but might require re-training or the computation of specific feature vectors.

In conclusion, different deep learning methods for PDEs are mainly different in terms of their neural network architecture and the particular choice of the loss function for training.

2.3 General DL concepts for PDE based inverse problems

So far we have sketched two main approaches for solving PDEs (forward problem), namely function or operator approximation schemes. In the following sections we will introduce these methods and their baseline implementation in more detail. We will also include, whenever appropriate, the related concepts for the PDE-based inverse problems.

The extension of function approximations $\Phi_{\Theta}(t, x)$ for solving inverse problems is not straight forward and differs from method to method. In contrast to that, the application of learned operator approximation schemes $\Phi_{\Theta}(\lambda)$ to inverse problems is always based on one of the two following concepts:

- The direct (or backward) method, where the network is trained with reversed input-output. In other words, the solution of the PDE is the input of a neural network which outputs the parameter function. This method is similar to the forward problem, but we learn the backward operator.
- Tikhonov Regularisation, for this case, the forward operator $\Phi_{\Theta}(\lambda)$ is trained as usual. For an inverse problem with given noisy data u^{δ} we then approximate a suitable parameter λ by minimizing a Tikhonov functional with respect to λ

$$\|\Phi_{\Theta}(\lambda) - u^{\delta}\|^2 + \alpha R(\lambda) .$$

The choice of the penalty term R adds to the flexibility of the method and can encode further properties of the solution such as smoothness, sparsity or piece-wise constant structures. Minimization is done iteratively via gradient descent, where the differentiation with respect to λ can be implemented using backpropagation with respect to the input but with fixed weights Θ . We exemplify the procedure for

the model reduction concept PCANN in Algorithm 6. A similar idea can be applied for the other solution operators mentioned in Sections 4.2 and 4.3.

3 DL concepts based on function approximation

In this section we list the DL concepts based on function approximation for PDE forward solvers and their related inverse problems.

3.1 Deep Ritz Method

3.1.1 Motivation

The Deep Ritz method [110] is a function evaluation concept based on a combination of the classical Ritz method (variational method) and deep learning. The Deep Ritz method assumes that a variational formulation of a PDE as stated in Equation (1) exists, i.e. there exists a $\Psi : \mathbb{R} \rightarrow \mathbb{R}$ such that the unique solution \hat{u} of the PDE is given by

$$\hat{u} = \operatorname{argmin}_{u \in H} I(u) \quad (3)$$

where

$$I(u) = \int_{\Omega} \Psi(u(x)) dx \quad (4)$$

and H is the set of admissible functions. Hence, the Deep Ritz method is a physics informed method.

The idea of the Deep Ritz method is to replace u by a neural network u_{Θ} which has a scalar or vectorial x as input. The network is trained by choosing suitable collocation points x_i and by replacing the integral in the variational formulation by a finite sum

$$\min_{\Theta} \sum_{i=1}^N \Psi(u_{\Theta}(x_i)) . \quad (5)$$

After training, u_{Θ} can be evaluated efficiently at arbitrary points in the domain of definition.

3.1.2 Network architecture

For the numerical examples for our standard test problems, see Section 5, we used the network shown in Figure 3. The main building block of the Deep Ritz neural network consists of two stacked fully-connected (FC) layers which are each followed by a non-linear somewhat "smooth" activation function. A residual connection links the input of the first FC layer to the output of the second FC layer. Several blocks are then stacked to complete the architecture of the network.

Consider the i -th block of the neural net. Let $W_{i,1}, W_{i,2} \in \mathbb{R}^{m \times m}$ and $b_{i,1}, b_{i,2} \in \mathbb{R}^m$ be the respective weight and bias of the first and second FC layers. A block which receives an input s , performs the operation

$$B_i(s) = \phi(W_{i,2} \cdot \phi(W_{i,1}s + b_{i,1}) + b_{i,2}) + s, \quad (6)$$

where ϕ is the activation function. From experience,

$$\phi(x) = \max \{x^3, 0\}, \quad (7)$$

provides a good balance between accuracy and simplicity. It's smoothness contributes to the accuracy of the Deep Ritz method. To match the input, resp. output, dimensions of the considered problem, an appropriate FC layer is used at the entrance (resp. exit) of the first (resp. last) layer of the first (resp. last) block of the neural network. Figure 3 shows the architecture of the Deep Ritz network.

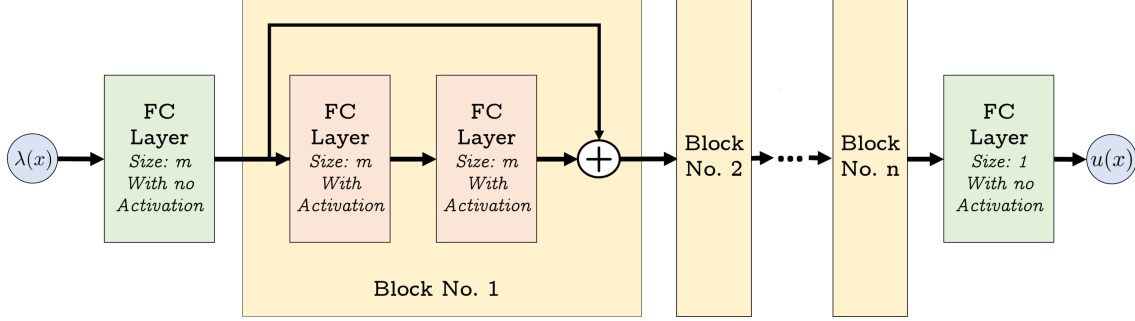


Figure 3: Deep Ritz network with n blocks and with appropriate input and output FC linear layers. The first FC linear layer can be replaced by zero padding

3.1.3 The algorithm

The training of the network does not need any information or data of the solution u , hence, with this respect it is equivalent to classical numerical PDE solvers. It, however, needs the PDE in its variational formulation, hence, it is a physics informed concept. The network architecture will be of the type ‘function approximation’, i.e. a rather small network with two or three nodes in the input level and a single value for output. This can be adjusted for higher-dimensional PDEs accordingly. The training of the network uses a loss function, which is simply a discretization of the variational formulation. A second term is added for ensuring the boundary conditions. Hence, first of all it requires to sample a suitable set of evaluation points $x_i, i = 1, \dots, N$ in the domain of definition and on the boundary. This can be done via stochastic sampling of a uniform distribution over the domain of definition (Monte Carlo integration) on a fixed grid. The training itself is then done by classical stochastic gradient descent. The sampling points may be changed during training after a fixed number of epochs.

We specify the approach for the classical Poisson problem

$$\begin{aligned} \Delta u &= \lambda \text{ on } \Omega \subset \mathbb{R}^2 \\ u &= g \text{ on } \partial\Omega \end{aligned} \quad (8)$$

This has the variational form: $I(u) = \int_{\Omega} (\frac{1}{2}|\nabla u(x)|^2 - \lambda(x)u(x)) dx$, see Algorithm 1.

Algorithm 1: Deep Ritz Method

Input:

- $N_{\mathcal{L}}/N_{\mathcal{B}}$: number of inner/boundary collocation points
- τ : learning rate

- 1 Initialize the network architecture u_{Θ}
 - 2 **while** not converged **do**
 - 3 Sample collocation points $\{x_{\mathcal{L}}^i \in \Omega : i = 1, \dots, N_{\mathcal{L}}\}$ and $\{x_{\mathcal{B}}^j \in \partial\Omega : j = 1, \dots, N_{\mathcal{B}}\}$
 - 4 Compute $E_{\mathcal{L}}(u_{\Theta}) = \frac{1}{N_{\mathcal{L}}} \sum_{i=1}^{N_{\mathcal{L}}} (\frac{1}{2}|\nabla u_{\Theta}(x_{\mathcal{L}}^i)|^2 - \lambda(x_{\mathcal{L}}^i)u_{\Theta}(x_{\mathcal{L}}^i))$, via backpropagation
 - 5 Compute $E_{\mathcal{B}}(u_{\Theta}) = \frac{1}{N_{\mathcal{B}}} \sum_{j=1}^{N_{\mathcal{B}}} (u_{\Theta}(x_{\mathcal{B}}^j) - g(x_{\mathcal{B}}^j))^2$
 - 6 Add loss values $L = E_{\mathcal{L}}(u_{\Theta}) + E_{\mathcal{B}}(u_{\Theta})$
 - 7 Optimise Loss, L using the appropriate optimisation algorithm.
 - 8 Update $\theta \leftarrow \theta - \tau \nabla_{\theta} L$
 - 9 **end**
-

It has been numerically shown that the Deep Ritz has the power to solve high dimensional problems, this is mainly due to the use of Monte Carlo algorithm for approximating the integral. In addition, Deep Ritz is potentially a naturally adaptive algorithm that can solve problems with corner singularities. One drawback of Deep Ritz method is that the neural network parameterizes the solution function instead of

the parameter-solution operator. Hence, the Deep Ritz method is less suited for parametric studies, since it requires a new training of the full network for every new parameter. Note that the loss function of Deep Ritz method can be negative and the minimal value is usually unknown, this also causes some challenges in the training process. In addition, The minimization problem that results from Deep Ritz is usually not convex even when the original problem is. The treatment of the essential boundary condition is not as simple as for traditional methods.

3.1.4 Theoretical Background

The convergence properties of the Deep Ritz methods have been analyzed intensively over the last years [23, 25, 46, 81]. The most far reaching results - to the best of our knowledge - are described in [23]. This paper also contains a nicely written survey on the state of the art of other results concerning convergence properties. This paper use techniques from Γ -convergence for proving, that under rather mild assumptions on the network architectures the loss function of the network training Γ -converges to the true variational formulation and also the minimizers converge weakly to the true solution of the PDE, see Theorem 7 [23].

3.2 Physics-informed Neural Network (PINN)

3.2.1 Motivation

The notion of 'physics informed neural networks' is now used in more general terms. In this section, however, we discuss the baseline version of a PINN as introduced in the original paper [88]. Similar to the previously described Deep Ritz method, this original PINN concept parameterizes the solution function as a neural network and requires the knowledge of the underlying PDE. In contrast to the Deep Ritz method, PINNs use the strong form of the PDE, thus their application to general PDEs is straightforward. To describe the method, we split up the operator \mathcal{N} in equation (1) into a differential operator \mathcal{L} encoding the PDE and the initial/boundary operator \mathcal{B} . The problem then reads

$$\begin{aligned} \mathcal{L}(u; \lambda) &= 0 & \text{in } \Omega \\ \mathcal{B}(u; \lambda) &= 0 & \text{on } \partial\Omega. \end{aligned} \tag{9}$$

The neural network u_Θ is again substituted into the PDE, where the differential operator \mathcal{L} can be applied to u_Θ via automatic differentiation (backpropagation). We note that $\mathcal{L}(u_\Theta; \cdot)$ and $\mathcal{B}(u_\Theta; \cdot)$ rely on the same set of parameters Θ as u_Θ , which is crucial for the optimization of PINNs. To fit u_Θ to the PDE, we penalize the residuals of both operators by their mean squared error on previously sampled points. This leads to the training objective

$$\min_{\Theta} (MSE_{\mathcal{L}}(u_\Theta) + MSE_{\mathcal{B}}(u_\Theta)), \tag{10}$$

where

$$MSE_{\mathcal{L}}(u_\Theta) = \frac{1}{N_{\mathcal{L}}} \sum_{i=1}^{N_{\mathcal{L}}} |\mathcal{L}(u_\Theta; \lambda)(x_{\mathcal{L}}^i)|^2 \quad \text{and} \quad MSE_{\mathcal{B}}(u_\Theta) = \frac{1}{N_{\mathcal{B}}} \sum_{j=1}^{N_{\mathcal{B}}} |\mathcal{B}(u_\Theta; \lambda)(x_{\mathcal{B}}^j)|^2. \tag{11}$$

During optimization, $MSE_{\mathcal{B}}$ enforces the initial or boundary conditions of a given problem and $MSE_{\mathcal{L}}$ checks the differential equation at the collocation points. A visual representation of the general idea, is shown in Figure 4.

3.2.2 Network architecture

The architecture of the neural network u_Θ allows a lot of freedom, the original paper [88] uses a simple fully-connected architecture. Depending on the underlying differential equation, different network structures can lead to better approximation results. This promotes the existence of a great variety of extensions of the PINN approach, either focused on individual problems or designed for broader classes of equations. In Section 3.2.6 we will mention a few of these methods.

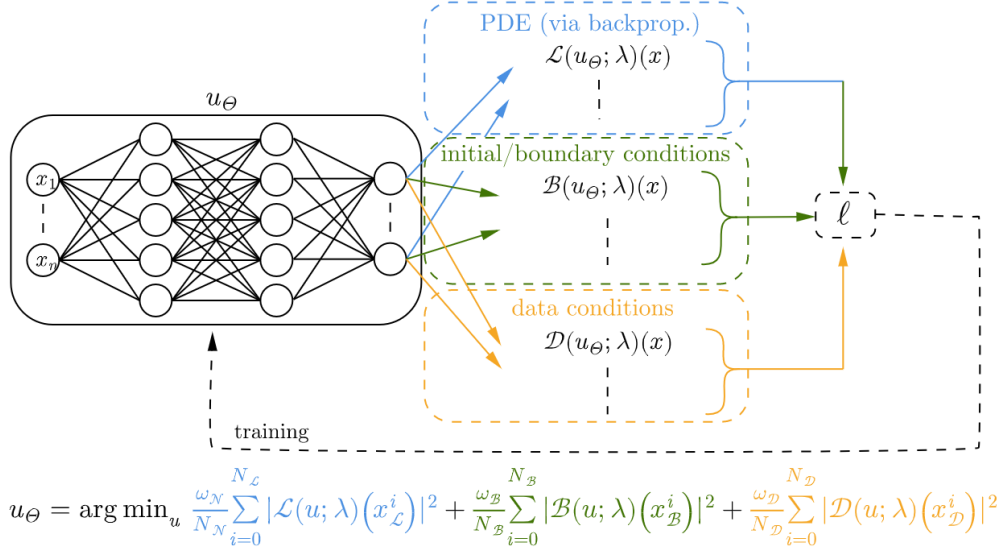


Figure 4: General training procedure of the PINN approach. As compared with the conditions in (11), we included a data condition in this figure.

3.2.3 The algorithm

The general training procedure is comparable to the Deep Ritz algorithm 3.1.3. Again, the network itself is optimized to approximate the solution as a function, therefore the number of input nodes corresponds to the dimensionality of Ω and the amount of output nodes denotes the dimensionality of the possibly vector-valued solution. The training requires the underlying PDE and some evaluation points $x_{\mathcal{L}}^i, x_{\mathcal{B}}^j, i = 1, \dots, N_{\mathcal{L}}, j = 1, \dots, N_{\mathcal{B}}$ to compute the residuals. The sampling strategy and therefore the distribution of these points can be chosen freely and may be changed throughout the training. Summarizing the approach for the Poisson problem of Equation 8, the general algorithm is shown in 2.

Algorithm 2: Physics-Informed Neural Networks

Input: $N_{\mathcal{L}}/N_{\mathcal{B}}$: number of inner/boundary collocation points,
 τ : learning rate

- 1 Initialize the network architecture u_θ
 - 2 **while** not converged **do**
 - 3 Sample collocation points $\{x_{\mathcal{L}}^i \in \Omega : i = 1, \dots, N_{\mathcal{L}}\}$ and $\{x_{\mathcal{B}}^j \in \partial\Omega : j = 1, \dots, N_{\mathcal{B}}\}$
 - 4 Compute $MSE_{\mathcal{L}}(u_\theta) = \frac{1}{N_{\mathcal{L}}} \sum_{i=1}^{N_{\mathcal{L}}} |\Delta u_\theta(x_{\mathcal{L}}^i) - \lambda(x_{\mathcal{L}}^i)|^2$, via backpropagation
 - 5 Compute $MSE_{\mathcal{B}}(u_\theta) = \frac{1}{N_{\mathcal{B}}} \sum_{j=1}^{N_{\mathcal{B}}} |u_\theta(x_{\mathcal{B}}^j) - g(x_{\mathcal{B}}^j)|^2$
 - 6 Add loss values $L = MSE_{\mathcal{L}}(u_\theta) + MSE_{\mathcal{B}}(u_\theta)$
 - 7 Update $\theta \leftarrow \theta - \tau \nabla_{\theta} L$
 - 8 **end**
-

The generality of PINN allows to extend the loss function to include several additional conditions. For example, if some observed data is available, it can be seamlessly incorporated into the loss function. In addition, PINN can be extended to solve integro-differential equations [71], fractional PDEs [86] and stochastic PDEs [113]. Furthermore, by using a discrete time model (Runge-Kutta methods) to link two distinct temporal snapshots, the number of collocation points for time-dependent PDEs can be reduced significantly.

3.2.4 Application to parameter identification

Notably, PINNs are also suitable for parameter identification of PDEs. Given a set of observed data points, the unknown parameters of the PDE can be optimized alongside the parameters of the solution network u_Θ . From an implementation point of view, PINNs can therefore be applied to parameter identification problems requiring minimal additional work, see [15, 44, 72, 87, 88, 111].

While the identification/learning of scalar parameters is quite straightforward, that of function-valued (e.g. space-dependent and/or time-dependent) parameters require some additional effort. For function-valued parameters such as the right side, λ in equation 8 or the coefficient λ in 52 of a certain PDE, one usually introduces an additional neural network λ_Θ for the searched functions. The idea behind these networks is comparable to u_Θ which parameterize the PDE solution as described in 2, i.e. we input the space and/or time variables and the network should output an approximation of the searched function at these values. The training process then consists of a combination of physics-informed loss and data loss. Via the data loss the network u_Θ learns an interpolation of the given (measured) data. A physics-informed loss, like the $MSE_{\mathcal{L}}$ term in 11, then enables us to learn the searched functions, by using the learned interpolation u_Θ . During minimization of the sum of both loss terms, the corresponding weights of all appearing networks then are optimized simultaneously via automatic differentiation. The resulting loss function which is optimised, e.g. in the case of the Poisson problem 8 is thus

$$L = \underbrace{\frac{1}{N_{\mathcal{P}}} \sum_{i=1}^{N_{\mathcal{P}}} |\Delta u_\Theta(x_{\mathcal{P}}^i) - \lambda_\Theta(x_{\mathcal{P}}^i)|^2}_{\text{Physics loss}} + \underbrace{\frac{1}{N_{\mathcal{D}}} \sum_{j=1}^{N_{\mathcal{D}}} |u_\Theta(x_{\mathcal{D}}^j) - u(x_{\mathcal{D}}^j)|^2}_{\text{Data loss}}, \quad (12)$$

where $N_{\mathcal{P}}$ is the number of collocation points, and $N_{\mathcal{D}}$ is the number of known data points, such that $\{x_{\mathcal{P}}^i \in \Omega : i = 1, \dots, N_{\mathcal{P}}\}$ and $\{x_{\mathcal{D}}^j \in \partial\Omega : j = 1, \dots, N_{\mathcal{D}}\}$.

In the case of noisy data, the physics can also act as a regularization for the learned interpolation, since the loss also influences u_Θ . Even when only discrete data points of the solution are available, the physics loss may be evaluated on arbitrary points, because of the interpolation properties of u_Θ . Moreover, the flexible framework of PINNs allows to include further a-priori knowledge on the solution or parameter functions, such as their regime or boundary values, by similar incorporation into the loss.

In the numerical experiments in Section 5, we will use simple fully connected neural networks (FCNNs), consisting of multiple FC layers. As an activation function we will use $\phi(x) = \tanh(x)$.

3.2.5 Theoretical Background

In contrast to the large number of applications of PINNs, they still lack a rigorous theoretical background. First consistency results under additional assumptions for linear elliptic and parabolic PDEs, can be found in [108]. Some estimates on the generalization error of PINNs approximating solutions for forward and inverse problems are proven in [77, 78]. The authors derive an error estimation in terms of training error and training points by exploitation of stability properties of the underlying equation. More general convergence results of the PINN approach still have to be found.

Some studies of the convergence rate were carried out in [102, 103]. There the Neural Tangent Kernel (NTK) theory [42] was applied to the PINN framework, which gave first insight on the convergence behaviour of the different loss terms and spectral bias of PINNs. With the NTK theory special weights for the different terms can be found, to achieve more robust and accurate results. In [100], The same approach was also applied to the DeepONet architecture, that will be introduced in Section 4.3.

3.2.6 Generalizations and extensions of PINN

Lastly, we want to give a short overview of possible extensions and generalizations for PINNs. Since the literature in this regard is vast, we can not represent every approach.

- **Quadratic Residual Networks (QRES)** [11]: Extends PINNs by including quadratic terms in each layer. The used architecture consist of FC layers with additional weight matrices, see Figure 5. In each Layer, The output of the FC layer matrix and additional matrix are pointwise multiplied and added

to the FC layer output, to create a quadratic term. This may lead to faster convergence and better parameter efficiency with respect to network width and depth.

- **Residual-based adaptive refinement** [71]: The idea of RAR is to add more residual points in the locations where the PDE residual is large during training process, conceptually similar to FEM refinement methods.
- **Gradient-enhanced PINN (gPINN)** [111]: If the PDE residual $\mathcal{L}u$ is zero, then it is clear that the gradient of the PDE residual, i.e $\nabla \mathcal{L}u$, should also be zero. Thus, the gradient-enhanced PINN (gPINN) uses a new type of loss functions by leveraging the gradient information of the PDE residual to improve the accuracy and training efficiency of PINNs.
- **XPINN and cPINN** [43, 44]: The XPINN and cPINN apply domain decomposition, then different subdomains use independent neural networks to approximate the solutions. In addition to the loss function used in PINN, interface conditions are introduced to stitch the decomposed subdomains together in order to obtain a solution of the governing PDEs over the complete domain. These extensions efficiently lends itself to parallelized computation and are cable to solve more general PDEs, e.g. PDEs with jump parameter functions.

For further details on the PINN approach, we suggest the paper [18], which contains a comprehensive and nicely written survey for the current state of the art of the PINNs. Mentioning different applications, extensions, theory, general challenges and currently open questions.

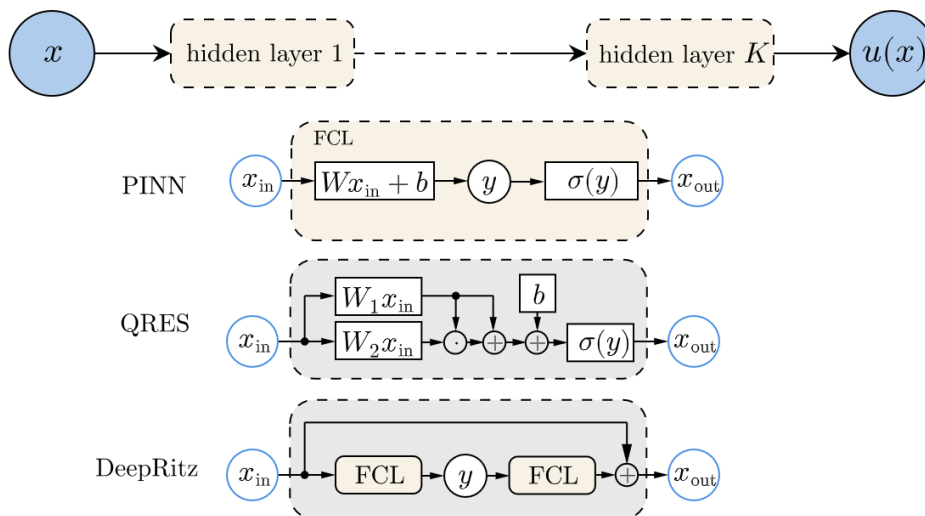


Figure 5: Overview and comparison of network architectures used in PINN, QRES and Deep Ritz. With weight matrix W , bias vector b and activation function σ .

3.3 Weak Adversarial Networks

3.3.1 Motivation

Similar to PINN and Deep Ritz, the method of weak adversarial networks [112] also parameterizes the solution as a neural network and is a physics-informed method. However, the weak adversarial network is based on the weak formulation of the PDE and the loss function is defined as an operator norm to be minimized. For simplicity, consider the following weak formulation of the Poisson problem with either Dirichlet or Neumann boundary conditions on an arbitrary domain $\Omega \in \mathbb{R}^d$:

$$\langle \mathcal{L}[u, \lambda], \varphi \rangle := a(u, \varphi; \lambda) = \int_{\Omega} (\nabla u \cdot \nabla \varphi - \lambda \varphi) dx = 0, \quad \text{for all } \varphi \text{ in } H_0^1(\Omega), \quad (13)$$

$$\mathcal{B}(u, \lambda) = 0 \quad \text{on} \quad \partial\Omega. \quad (14)$$

From the above formula, we see that for each $u \in H^1(\Omega)$, it defines a linear functional (operator) $\mathcal{L}[u, \lambda]$ such that $\mathcal{L}[u, \lambda](\varphi) = a(u, \varphi; \lambda)$. A function $u \in H^1(\Omega)$ satisfying the boundary condition is the weak solution of the equation if and only if the operator norm:

$$\|\mathcal{L}[u, \lambda]\|_{op} := \max\{\langle \mathcal{L}[u, \lambda], \varphi \rangle / \|\varphi\|_2 \mid \varphi \in H_0^1(\Omega), \varphi \neq 0\} \quad (15)$$

is equal to 0. Hence, the solution satisfies the boundary condition and solves the following minmax problem:

$$\min_u \max_{\varphi} |\langle \mathcal{L}[u, \lambda], \varphi \rangle|^2 / \|\varphi\|_2^2. \quad (16)$$

This weak formulation inspires an adversarial approach, where one network u_θ with parameter θ is used to parametrize the solution of the PDE and another network φ_η with parameter η approximates the test function.

3.3.2 Network architecture

As just stated, in weak adversarial networks, the solution is parameterized as a neural network u_θ with parameter θ , which is learned by minimizing the operator norm $\|\mathcal{L}[u_\theta]\|_{op}$. The test function, however, is parameterized by an adversarial network φ_η with parameter η and is trained by maximizing $\langle \mathcal{L}[u_\theta], \varphi_\eta \rangle / \|\varphi_\eta\|$, hence it approximates the operator norm $\|\mathcal{L}[u_\theta, \lambda]\|_{op}$. Thus, it is an adversarial training in a way that the test function criticizes on the solution network where the PDE is violated, and the solution network corrects itself at those spots until the PDE system is satisfied (almost) everywhere in the domain. Thus the network version of (16) can be formulated as:

$$\min_{\theta} \max_{\eta} |\langle \mathcal{L}[u_\theta, \lambda], \varphi_\eta \rangle|^2 / \|\varphi_\eta\|_2^2. \quad (17)$$

Both networks u_θ and φ_η can be general architectures, e.g. FNN, ResNet, CNN, RNN. However, the choice of the neural networks can affect the efficiency and accuracy. For example, using a ResNet for parameterizing the trial and test function usually has better performance than using a fully connected network.

3.3.3 The algorithm

The main challenge of the WAN method is how to design an efficient algorithm for solving the minimax problem (17), or equivalently for

$$\min_{\theta} \max_{\eta} L_{int}(\theta, \eta) \quad \text{where} \quad L_{int}(\theta, \eta) = \log |\langle \mathcal{L}[u_\theta, \lambda], \varphi_\eta \rangle|^2 - \log \|\varphi_\eta\|_2^2. \quad (18)$$

In addition, the weak solution u_θ also needs to satisfy the boundary condition, which can be realized by minimizing

$$L_{bdry}(\theta) = \int_{\partial\Omega} |u_\theta(x) - g(x)|^2 dx. \quad (19)$$

The total objective function is the weighted sum of the two objectives and we seek to compute a saddle point that solves the minimax problem:

$$\min_{\theta} \max_{\eta} L(\theta, \eta) = \min_{\theta} \max_{\eta} L_{int}(\theta, \eta) + \alpha L_{bdry}(\theta). \quad (20)$$

where $\alpha > 0$ is an user-chosen balancing parameter. Typical algorithms use alternating updates, i.e. the objective function is alternatively minimized and maximized and the parameters θ and η are alternately updated such that the primal network can approximate the solution gradually.

Given the objective function (8), the key ingredients in the network training are the computation of $L(\theta, \eta)$ and its gradients with respect to θ and η , respectively. By denoting

$$I(x, \theta, \eta) = \nabla u_\theta(x) \cdot \nabla \varphi_\eta(x) - \lambda(x) \varphi_\eta(x), \quad (21)$$

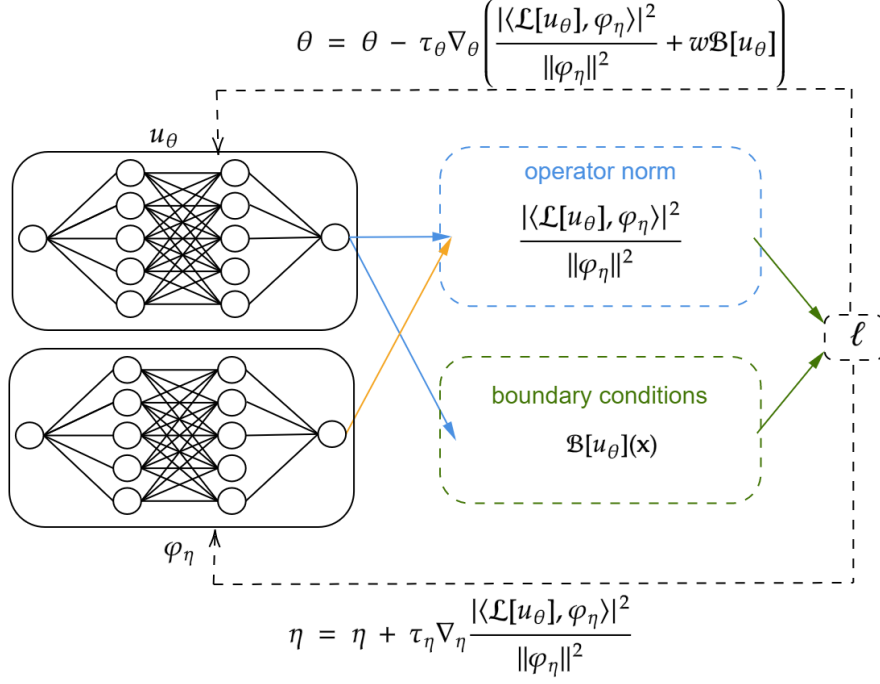


Figure 6: Architecture of the WAN

we have

$$\nabla_\theta I(x, \theta, \eta) = \nabla(\nabla_\theta u_\theta(x)) \cdot \nabla \varphi_\eta(x) - \lambda(x) \varphi_\eta(x); \nabla_\eta I(x, \theta, \eta) = \nabla u_\theta(x) \cdot \nabla(\nabla_\eta \varphi_\eta(x)) - \lambda(x) (\nabla_\eta \varphi_\eta(x)), \quad (22)$$

and

$$\nabla_\theta L_{int}(\theta) = 2 \left(\int_\Omega I(x; \theta, \eta) dx \right)^{-1} \left(\int_\Omega I(x; \theta, \eta) dx \right). \quad (23)$$

Monte-Carlo (MC) approximations can be used to approximate the integrals, i.e., we randomly sample N_r collocation points $\{x_r^{(j)}\}_{j=1}^{N_r}$ uniformly in the interior of the region and approximate the gradient $\nabla_\theta L_{int}(\theta) \approx 2 \cdot (\sum_{j=1}^{N_r} I(x_r^{(j)}; \theta, \eta))^{-1} (\sum_{j=1}^{N_r} \nabla_\theta I(x_r^{(j)}; \theta, \eta))$. The gradients $\nabla_\eta L_{int}$ and $\nabla_\theta L_{bdry}$ can be approximated by the same procedure. Using these gradients of $\nabla_\theta L$ and $\nabla_\eta L$, we can apply alternating updates to optimize the parameters θ and η . The resulting algorithm is then summarized in Algorithm 3. Details on how to adapt weak adversarial network for parabolic PDEs involving time can be found in the original paper.

3.3.4 Weak Adversarial Network for inverse problems

The weak adversarial network can be extended to solve inverse problems directly [5]. An inverse problem defined on an open and bounded domain in \mathbb{R}^d may be presented in a general form as

$$\mathcal{A}[u, \lambda] = 0, \quad \text{in } \Omega, \quad (24)$$

$$\mathcal{B}[u, \lambda] = 0, \quad \text{on } \partial\Omega, \quad (25)$$

where u is the solution and λ can be the coefficient in the inverse medium problem or the source function in the inverse source problem. $\mathcal{B}[u, \lambda] = 0$ are some observations on the boundary. Suppose that the variational form is given by

$$\langle \mathcal{L}[u, \lambda], \varphi \rangle := \int_\Omega \mathcal{L}[u, \lambda](x) \varphi(x) dx \quad \text{for all } \varphi \text{ in } H_0^1(\Omega). \quad (26)$$

Algorithm 3: Weak Adversarial Network (WAN) for Solving static PDEs.

Input: N_r/N_b : number of region/boundary collocation points;
 K_u/K_φ : number of solution/adversarial network parameter updates per iteration;
 τ_θ/τ_η : learning rates for θ and η ;
 α : balancing weight
1 Initialize the network architectures u_θ, φ_η ;
2 **while** not converged **do**
3 Sample collocation points $\{x_r^j \in \Omega : j \in [N_r]\}$ and $\{x_b^j \in \partial\Omega : j \in [N_b]\}$
4 Update weak solution parameter
5 **for** $k = 1, \dots, K_u$ **do**
6 Update $\theta \leftarrow \theta - \tau_\theta \nabla_\theta L$ where $\nabla_\theta L$ is approximated using $\{x_r^j\}$ and $\{x_b^j\}$.
7 **end**
8 **for** $k = 1, \dots, K_\varphi$ **do**
9 Update $\eta \leftarrow \eta + \tau_\eta \nabla_\eta L$ where $\nabla_\eta L$ is approximated using $\{x_r^j\}$.
10 **end**
11 **end**

Take the inverse conductivity problem as an example, we have

$$\langle \mathcal{L}[u, \lambda], \varphi \rangle = \int_{\Omega} (\lambda \nabla u \cdot \nabla \varphi - f \varphi) dx = 0. \quad (27)$$

By defining the norm of $\mathcal{A}[u, \lambda]$ as

$$\|\mathcal{L}[u, \lambda]\|_{op}^2 := \sup_{\varphi \in H_0^1, \varphi \neq 0} \frac{|\langle \mathcal{L}[u, \lambda], \varphi \rangle|^2}{\|\varphi\|^2}. \quad (28)$$

Then, the weak formulation and the boundary condition induce a minimax problem:

$$\min_{u, \lambda} \max_{\varphi} \frac{|\langle \mathcal{L}[u, \lambda], \varphi \rangle|^2}{\|\varphi\|^2} + \int_{\partial\Omega} |\mathcal{B}[u, \lambda]|^2 dx. \quad (29)$$

By parameterizing u , λ , and φ as neural networks $u_{\theta_1}, \lambda_{\theta_2}$ and φ_{θ_3} , respectively, we have the network version of the minimax problem:

$$\min_{\theta_1, \theta_2} \max_{\theta_3} \frac{|\langle \mathcal{L}[u_{\theta_1}, \lambda_{\theta_2}], \varphi_{\theta_3} \rangle|^2}{\|\varphi_{\theta_3}\|^2} + \alpha \int_{\partial\Omega} |\mathcal{B}[u_{\theta_1}, \lambda_{\theta_2}]|^2 dx \quad (30)$$

The algorithm is then similar to that of the direct problems by updating $\theta = \theta_1 + \theta_2$ and $\eta = \theta_3$ alternately.

4 DL concepts based on operator approximation

In this section we introduce the basic concepts for DL approaches which aim at approximating the parameter-to-state operator. By construction these methods are perfectly suited for parametric studies and can be adapted directly to inverse problems. The two basic concepts for adaptation to inverse problems have already been described in Section 2.3.

4.1 Model Reduction And Neural Networks For Parametric PDEs (PCANN)

4.1.1 Motivation

PCANN, as we call it in this paper, seeks to provide a meshless operator for the evaluation of the solution of a PDE by combining ideas of model order reduction with deep learning. For given training data (λ_i, u_i) on first obtains a model reduction by use of the principal component analysis (PCA) for both the input (parameter λ)

and output (solution u) functions. Only the coefficients of a finite number of PCA components are retained. The PCA thus reduces the dimensions of both the input and output spaces to finite latent dimensional latent spaces. A neural network then maps the coefficients of the respective representations in these latent spaces as shown in Figure 2. The evaluation of this operator approximation for a novel parameter λ is then most efficient: one only needs to compute the scalar products with the specified finite number of PCA components, the neural network then maps these coefficients to the latent coefficients of the output space and an expansion using these coefficients and the PCA on the output side gives a function approximation to the solution of the PDE.

The formulation of this approach is in a function space setting and hence mesh-free. For implementation purposes, however, one has to specify how to compute the scalar products with the PCA components. These functions are only given numerically, usually by their values on a specified grid. The red arrow shows the flow during testing. The overall PCANN can be used to evaluate the solution of the PDE for any given grid size as illustrated in Algorithm 4.

In a situation where the input-to-output operator is linear, like in the case of the Poisson problem considered, it might be beneficial to use a simple linear map for the mapping of the reduced/latent dimensions. Section 5, equally shows results for this case, PCALin, where a single linear layer with no activation functions is used to map the latent dimensions. PCALin is similar to the linear method proposed in [8], only, we use a neural network instead of the normal equations. The result in both cases are similar as we later on show in 5. The combination of model order reduction with deep learning has recorded success in a number of application problems ranging from cardiac electrophysiology [27, 31], where the use of proper orthogonal decomposition (POD) further improves the results [30], to fluid flow [29] and non-linear models [16, 28]. Specifically, the PCANN operator has been used in [54, 67] in a multiscale plasticity problem to map strain to stress.

4.1.2 Network Architecture

In our numerical examples, we followed the outline of the original paper [8] and used a fully connected feed forward neural network for the mapping of the latent spaces. The number of nodes per layer is as follows $d_{\mathcal{X}}, 500, 1000, 2000, 1000, 500, d_{\mathcal{Y}}$. $d_{\mathcal{X}}$ and $d_{\mathcal{Y}}$ are considered to be hyperparameters, and for convenience, are chosen to be equal. Figure 7 shows a simplified schematic of the overall architecture.

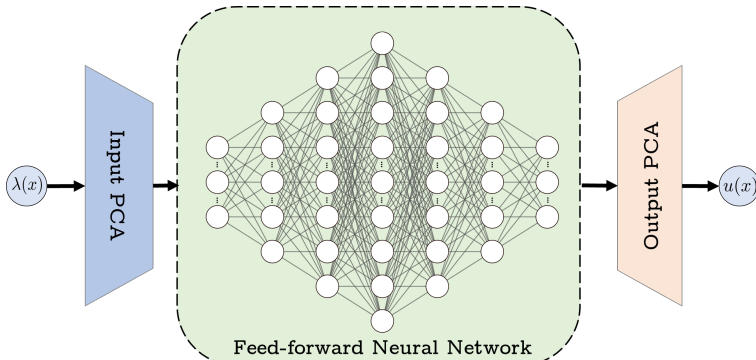


Figure 7: Architecture of the PCANN

4.1.3 The Algorithm

As a purely data-driven method, no physics or PDE is needed in the training of the model. However, the data used for the training of the network is obtained from a classical FDM for solving the underlying PDE. By training the network with these input-output (numerically-given) function pairs, we obtain a neural operator which solves the PDE for various instances irrespective of the mesh size.

Once again, we specify the algorithm for the Poisson problem in Equation 8. The training data is the pair (λ_i, u_i) , with each $\lambda_i, u_i \in \mathbb{R}^{s^2}$. Originally, λ_i, u_i are functions giving in a (square) grid of dimensions $s \times s$. By flattening these functions, we now have them in \mathbb{R}^{s^2} . Training then proceeds as in Algorithm 4, while testing/usage of the trained network proceeds as in Algorithm 5.

4.1.4 Theoretical Background

As the PCANN method combines both the PCA and Neural network (NN) to achieve the task of operator learning, the strength of its approximation therefore comes from that of both the PCA and NNs. For a good approximation, one thus needs not only a good neural network but also, appropriate PCA truncation parameters (resulting from choosing sufficient amounts of data). The existence of all these factors is shown in Theorem 3.1 of [8] which is a consequence of Theorem 3.5 of the same work.

Algorithm 4: PCANN

Input:

- (λ_i, u_i) : Training Data pair with $i = 0 \dots N_{\text{train}}$
- τ : learning rate

- 1 Initialize the network Φ_{Θ}
- 2 Compute PCA of (λ_i) , store PCA $(a_k), k = 1, \dots, d_{\mathcal{X}}$
- 3 Compute PCA of (u_i) , store PCA $(b_{\ell}), \ell = 1, \dots, d_{\mathcal{Y}}$
- 4 **for** $i \leftarrow 0, \dots, N_{\text{train}}$ **do**
- 5 | compute $c_i^k = \langle \lambda_i, a_k \rangle \in \mathbb{R}^{d_{\mathcal{X}}}$
- 6 | compute $d_i^{\ell} = \langle u_i, b_{\ell} \rangle \in \mathbb{R}^{d_{\mathcal{Y}}}$
- 7 **end**
- 8 **while** not converged **do**
- 9 | /* Train network */
- 9 | **for** $i \leftarrow 0, \dots, N_{\text{train}}$ **do**
- 10 | | Compute Loss, $L_i = \sum_{\ell=1}^{d_{\mathcal{Y}}} \left\| \frac{\Phi_{\Theta}(c_i^k) - d_i^{\ell}}{d_i^{\ell}} \right\|^2$
- 11 | **end**
- 12 | Compute the Loss, $L = \sum_{i=1}^{N_{\text{train}}} L_i$
- 13 | Optimise L using the appropriate/chosen optimisation algorithm.
- 14 | Update $\theta \leftarrow \theta - \tau \nabla_{\Theta} L$
- 15 **end**

Algorithm 5: Using/Testing the PCANN

Input:

- Input parameter functions λ_i with $i = 0 \dots N_{\text{test}}$
- Input PCA basis $(a_k)_{k=1, \dots, d_{\mathcal{X}}}$
- Output PCA basis $(b_{\ell})_{\ell=1, \dots, d_{\mathcal{Y}}}$
- Trained network Φ_{Θ} .

Result: Output solution functions \tilde{u}_i , with $i = 0 \dots N_{\text{test}}$

- 1 **for** $i \leftarrow 0, \dots, N_{\text{test}}$ **do**
- 2 | $\tilde{u}_i = \sum_{\ell} \Phi_{\Theta}(\langle \lambda_i, a_k \rangle)_{\ell} b_{\ell}$
- 3 **end**

4.1.5 PCANN adaptation for inverse problems

Following the general concepts as discussed in Section 2.3 we have two principle options. We either train a PCANN network $\Psi_{\Theta}(u)$ with training data $(u_i^{\delta}, \lambda_i)$, where we reverse the input-output order. I.e. the (u_i^{δ}) are used as input and (λ_i) as output. After training we can directly use a new measurement (u^{δ}) and compute a corresponding parameter $\hat{\lambda} = \Psi_{\Theta_{u^{\delta}}}$.

The other option is to use a trained network for the forward problem Φ_{Θ} and include this into a Tikhonov functional. The resulting algorithm is summarized as follows:

Algorithm 6: Using trained forward PCANN for Inverse Problem

Input:

- Solution function u^δ
- Input PCA basis $(a_k)_{k=1,\dots,d_x}$
- Output PCA basis $(b_\ell)_{\ell=1,\dots,d_y}$
- Trained network $\Phi_\Theta : c = (\langle \lambda, a_k \rangle) \mapsto d = (\langle u, b_\ell \rangle)$.

Result: Output parameter function $\hat{\lambda}$

- 1 Initialise c^0
 - 2 **for** $m \leftarrow 0, \dots, N$ (*large integer*) **do**
 - 3 Compute $J_\alpha(c) = \|\Phi_\Theta(c) - \langle u^\delta, b_\ell \rangle\|^2$
 - 4 Compute the loss $J_\alpha(c) := J_\alpha(c) + \alpha R(c)$.
 - 5 Optimise Loss $J_\alpha(c)$ using gradient descent
 - 6 Update $c^{m+1} \leftarrow (c^m - \sigma_m \partial J / \partial c (c^m))$
 - 7 **end**
 - 8 Compute $\hat{\lambda} = \sum_k c_k^N a_k$
-

4.2 Fourier Neural Operator

4.2.1 Motivation

Fourier neural operators (FNO) [61] are designed as deep learning architectures for learning mappings between infinite-dimensional function spaces. The Fourier neural network is formulated as an iterative architecture, where each iteration (hidden layer), inspired by the convolution theorem, is a Fourier integral operator defined in Fourier space. The main network parameters are therefore defined and learned in Fourier space rather than in physical space, i.e., the coefficients of the Fourier series of the output function are learned from the data.

While standard feed-forward neural networks (FNN) and CNN’s combine linear multiplications with non-linear activations in order to learn highly nonlinear functions, FNOs combine linear integral operators with non-linear activations in each layer to learn non-linear operators. The fast Fourier transform (FFT) makes the implementation even more efficient.

Different from DeepONet, and similar to the PCANN methods, FNO discretizes both the input function $\lambda(x)$ and the output function $u(x)$ by using point-wise evaluations in an equispaced mesh. In addition, FNO requires that λ and u be defined on the same domain and are discretized by the same discretization. The function space formulation of the approach allows to train an FNO on a dataset with low resolution and to apply it directly on a dataset with higher resolution, thus achieving the so called zero-shot super resolution.

4.2.2 Theoretical Background

The idea of FNO, stems up from an earlier paper by the same team, see [62], which also seeks to approximate a neural operator by concatenating multiple hidden layers. While standard artificial neural networks (FCN, CNN) have affine functions (weights and biases) with scalar nonlinear activation as hidden layers, neural operators rather have affine operators (usually, in addition to affine functions with weights and biases [52] [70]) with scalar nonlinear activation functions. A hidden layer numbered $j + 1$ thus performs the update of input v_j as follows

$$v_{j+1}(x) := \sigma(Wv_j(x) + b + (\mathcal{K}(a; \theta)v_j)(x)), \quad \forall x \in \Omega, \quad (31)$$

where W, b and \mathcal{K} are the respective weights, biases and neural operators. These neural operators are chosen to be integral operators of the form

$$(\mathcal{K}(\lambda; \theta)v)(x) = \int_{\Omega} \kappa_{\theta}(x, y; \lambda(x), \lambda(y))v(y)dy, \quad \forall x \in \Omega. \quad (32)$$

These operators can be realised by different concepts such as graph kernels [62], multipole expansions [63], non-local kernels [109], low-rank kernels [53], wavelet transforms [97] or multiwavelet transforms [36]. In the

special case of a convolution where $\kappa_\theta = \kappa_\theta(x - y)$, Equation 32 becomes

$$\begin{aligned}
(\mathcal{K}(\theta)v)(x) &= \int_{\Omega} \kappa_\theta(x - y)v(y)dy, \quad \forall x \in \Omega \\
&= (\kappa_\theta * v)(x), \quad \forall x \in \Omega \\
&= (\mathcal{F}^{-1}(\mathcal{F}(\kappa_\theta) * \mathcal{F}(v)))(x), \quad \forall x \in \Omega \\
&= (\mathcal{F}^{-1}(K_\theta \cdot \mathcal{F}(v)))(x), \quad \forall x \in \Omega,
\end{aligned}$$

by the use of the convolution theorem. This then leads to the parametrisation of the neural network given by κ_θ directly in the Fourier space K_θ . [52] provides a good theoretical background of FNOs and [53] offers a good overview of neural operators using different integral operators along with some theoretical justification.

4.2.3 The algorithm

The classical FNO is only possible with a uniform grid (cartesian domain), but can be extended for any mesh. We note that unlike the PCANN method, the input and output functions are inputted in their unflattened states. Once again, as an example, we consider the problem in Equation 8 and we seek to learn the operator

$$F : \Lambda(\Omega; \mathbb{R}^{d_\lambda}) \ni \lambda(x) \mapsto u(x) \in \mathcal{U}(\Omega; \mathbb{R}^{d_u}), \quad (33)$$

where d_λ and d_u depend on the discretisation used ($d_\lambda = d_u = 513^2$ if we use functions with a resolution of 513×513), Ω is a subset of \mathbb{R} while Λ and \mathcal{U} are Banach's spaces of functions taking values in \mathbb{R} .

Algorithm 7: FNO

Input:

- (λ_i, u_i) : Training data pair with $i = 0 \dots N_{\text{train}}$
 - τ : learning rate
- 1 Initialize the fully connected networks (FCN) P_θ and Q_ψ
 - 2 Initialize the linear transforms W_ϕ and R_ϕ
 - 3 Lift λ_i to a higher dimension by computing $v_0 = P_\theta(\lambda_i)$
/* Section 4.2.4 defines these FCN and linear transform networks */
 - 4 **for** $j \leftarrow 0, \dots, T - 1$ **do**
 - 5 | $v_{j+1} := \sigma(W_\phi v_j + [\mathcal{F}^{-1}(R_\phi \cdot (\mathcal{F}v_j))])$, output of Fourier layers
 - 6 **end**
 - 7 Obtain the target dimension by using Q_ψ to get $\tilde{u}_i = Q_\psi(v_T)$
 - 8 **while** not converged **do**
 - 9 | /* Train network */
 - 9 | **for** $i \leftarrow 0, \dots, N_{\text{train}}$ **do**
 - 10 | | Compute loss $L_i = \sum_{\ell=1}^{d_y} \left\| \frac{\tilde{u}_i - u_i}{u_i} \right\|^2$ using the appropriate optimisation algorithm
 - 11 | **end**
 - 12 | Compute the Loss, $L = \sum_{i=1}^{N_{\text{train}}} L_i$
 - 13 | Optimise L using the appropriate/chosen optimisation algorithm.
 - 14 | Update $\theta \leftarrow \theta - \tau \nabla_{\Theta} L$
 - 15 **end**
-

4.2.4 Network Architecture

The architecture of the FNO follows from the algorithm described in Section 4.2.3. For the special case in Equation 8, we consider a mesh of resolution $N \times M$. We denote each point in the domain Ω as x_k^l , with input $\lambda(x_k^l)$, and output $u(x_k^l)$, with $k \in \{1, \dots, N\}$ and $l \in \{1, \dots, M\}$. We equally denote $\lambda(x)$ and $u(x)$ as the input and output for the whole domain.

- The FCN P_θ takes each $\lambda(x_k^l) \in \mathbb{R}$ and maps it to a higher dimension d_{v_0} , i.e.

$$\begin{aligned} v_0(x_k^l) &= P_\theta(\lambda(x_k^l)) \in \mathbb{R}^{d_{v_0}}, \\ v_0(x) &= P_\theta(\lambda(x)) \in \mathbb{R}^{d_{v_0} \times N \times M}. \end{aligned}$$

$v_0(x)$ is thus an $N \times M$ image with d_{v_0} channels.

- To obtain $v_1(x)$ from $v_0(x)$, the following operations are applied.
 - The (2D) Fourier transform \mathcal{F} is applied to each channel of $v_0(x)$, and the first $k = k_1 \cdot k_2$ modes are kept (k_1, k_2 , being the number of modes to be kept in the first and second dimensions respectively). As a result we obtain $\mathcal{F}(v_0(x)) \in \mathbb{C}^{d_{v_0} \times k}$.
 - The linear transform \mathcal{R}_ϕ , which is realized as a weight matrix in $\mathbb{C}^{k \times d_{v_0} \times d_{v_0}}$ is applied to $\mathcal{F}(v_0(x))$. The result is $\mathcal{R}_\phi \cdot \mathcal{F}(v_0(x)) \in \mathbb{R}^{d_{v_0} \times k}$.
 - Apply the inverse FFT to $\mathcal{R}_\phi \cdot \mathcal{F}(v_0(x))$, (appended with zeros to make up for the truncated/unselected modes). The outcome is $\mathcal{F}^{-1}(\mathcal{R}_\phi \cdot \mathcal{F}(v_0(x))) \in \mathbb{R}^{N \times M \times d_{v_0}}$.
 - Finally, $v_1(x)$ is obtained from the above together with a residual connection with a weight matrix $W_\Phi \in \mathbb{R}^{d_{v_0} \times d_{v_0}}$, as follows

$$v_1(x) = \sigma(W_\Phi \cdot v_1(x) + \mathcal{F}^{-1}(\mathcal{R}_\phi \cdot \mathcal{F}(v_0(x)))) \in \mathbb{R}^{N \times M \times d_{v_0}}$$

- v_2, v_3, \dots, v_T are obtained from v_1, v_2, \dots, v_{T-1} respectively in a similar manner as above. In this way, we have T Fourier layers.
- At the end of the last Fourier layer another FCN Q_ψ is applied, which projects $v_T(x)$ to the output dimension. We therefore obtain the output function

$$u(x) = Q_\psi(v_T(x)) \in \mathbb{R}^{N \times M}$$

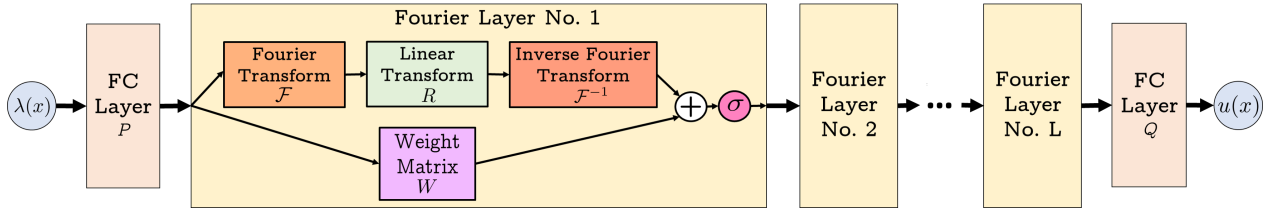


Figure 8: Architecture of the FNO

4.2.5 Generalisation and Extensions of FNOs

A detailed guide for implementation and an illustration of how to extend FNO to operators with inputs and outputs defined on different domains can be found in [70]. There, also two cases of generalisation are considered:

- C 1:** As motivation take a parabolic PDE, where the initial condition at time $t = 0$ is the input for the parameter-to-state operator. The output is the solution for all times $t \in [0, T]$. This leads to the general setting where the output space is that of functions defined on a product space, where the first component is the same as for the input space and the second component is arbitrary. i.e.

$$F : \Lambda(\Omega; \mathbb{R}^{d_\lambda}) \ni \lambda(x, 0) \mapsto u(x, t) \in \mathcal{U}(\Omega \times [0, t]; \mathbb{R}^{d_u}),$$

where Ω is a subset of \mathbb{R} while Λ and \mathcal{U} are Banach's spaces taking values in \mathbb{R}^{d_λ} and \mathbb{R}^{d_u} (with $d_\lambda = d_u$, depending on the discretisation of the functions) respectively. In order to match dimensions before applying an FNO, the output domain could be shrunk by use of a Recurrent Neural Network (RNN) or the input domain could be extended to incorporate the time, t as an extra coordinate.

C 2: The input space is a subset of the output space, like in the case of the operator F , mapping the boundary conditions of the domain to the solution of the PDE in the whole domain.

$$F : \mathcal{G}(\partial\Omega; \mathbb{R}^{d_g}) \ni g(x) \mapsto u(x) \in \mathcal{U}(\Omega; \mathbb{R}^{d_u}),$$

where $\partial\Omega \subset \Omega \subset \mathbb{R}$, while \mathcal{G} and \mathcal{U} are Banach's spaces taking values in \mathbb{R}^{d_g} and \mathbb{R}^{d_u} (defined in a similar way as above in the first case) respectively. For this situation, a zero padding could be applied or better still, an appropriate transformation could be used to map the boundary condition to a lower dimension. This then brings us back to the previous case.

It is worth noting that the use of the FFT in the algorithm of the FNO restricts its applicability to situations where the input and output are defined on a cartesian domain (square, rectangle domain in 2D and cube, cuboid in 3D). This introduces a challenge when dealing with complex geometries. A practical workaround is as followd.

W 1: Define a new domain which is the minimum bounding box of the complex domain, and perform a zero padding for the area within this bounding box, but out of the complex domain. However, in practise this makes the resulting function discontinuous in the 'rectangle' and usually yields larger errors.

W 2: Use same minimum bounding of the complex domain, as previously described, but padding is done with the nearest function values within the complex domain, instead of zeros.

Though somewhat successful, the extensions provided in [70] do not seem to favour FNO. A better approach to complex domains is by transforming/deforming this complex domain to a cartesian domain by use of neural networks (NN), positioned before and after the FNO as proposed in [60]. These neural networks could either be fixed or learned together with the FNO parameters. The resulting NN-FNO-NN network is said to be 'geometry aware' and is called Geometry-Aware FNO (Geo-FNO).

Besides these structural considerations, the following generalizations have recently gained increasing attention:

4.2.5.1 From conv-FNO to U-FNO:

Possibly the most recent variant of the FNO, the U-FNO [106] introduces the famous U-Net to the architecture in the so called U-Fourier layer. The U-FNO thus has both Fourier and U-net layers: it starts off with the former and ends with the latter. Essentially, a U-Fourier layer is similar to the Fourier layer, but has both a weight matrix and a two-step U-Net layer in the residual. In contrast to the update performed by the Fourier layer in Equation 31, the U-Fourier layer performs the update in Equation 34, with U being the two-step U-Net

$$v_{t+1}(x) := \sigma(Uv_t(x) + Wv_t(x) + b + (\mathcal{K}(a; \theta)v_t)(x)), \quad \forall x \in \Omega. \quad (34)$$

As compared with methods based on CNNs, the baseline FNO achieves a good accuracy for single-phase flow problems, but it doesn't seem to do so well with multiphase flows [105]. On the other hand, conv-FNO does better than CNN-based methods, and the U-FNO even improves on that. conv-FNO are implemented by using a standard convolution in place of the U-Net.

4.2.5.2 Multiwavelet based operator (MWT):

In a more recent work [36], a neural operator which evaluates the kernel operator in (32) using a different approach is introduced. The idea here is to leverage the successes in signal processes of both orthogonal polynomials and wavelet basis (notably, vanishing moments and orhgonality). Multiwaveletes therefore do not just project the function onto a single wavelet function as wavelets do, but rather, they project the function onto a subspace of degree-restricted polynomials.

For an understanding of the concept, the space of piecewise polynomials of degree up to $k \in \mathbb{N}$ with $n \in \mathbb{Z} \cup \{0\}$ is defined on $[0, 1]$:

$$\mathbf{V}_n^k = \bigcup_{l=0}^{2^n-1} \{f \mid \deg(f) < k \text{ for } x \in (2^{-n}l, 2^{-n}(l+1)) \wedge 0, \text{ elsewhere}\}.$$

For each $k \in \mathbb{N}$ with $n \in \mathbb{Z} \cup \{0\}$, we have that $\dim(\mathbf{V}_n^k) = 2^n k$ and

$$\mathbf{V}_{n-1}^k \subset \mathbf{V}_n^k. \quad (35)$$

We note that, as n increases, so does l , and \mathbf{V}_n^k is defined from a lower(coarser) to a higher(finier) resolutions; these resolutions being each time a power of 2. As a result, the method is restricted to discretisations which are a power of 2. Appropriate padding or interpolation could be applied to the function if its resolution is not a power of 2.

Given the basis $\phi_j, j = 0, 1, \dots, k-1$ w.r.t a measure μ_0 of \mathbf{V}_0^k , it is possible to obtain the basis of subsequent $\mathbf{V}_n^k, n > 0$ by appropriate shifts and scales of ϕ_j :

$$\phi_{jl}^n(x) = 2^{n/2} \phi_j(2^n x - l), \quad j = 0, 1, \dots, k-1, \quad l = 0, 1, \dots, 2^n - 1, \text{ w.r.t. } \mu_n \quad (36)$$

One then defines the multiwavelet subspace W_n^k , which is related to the spaces of orthogonal polynomials as below:

$$\mathbf{V}_{n+1}^k = \mathbf{V}_n^k \oplus \mathbf{W}_n^k, \quad \mathbf{V}_n^k \perp \mathbf{W}_n^k. \quad (37)$$

Similarly, the basis of $\mathbf{W}_n^k, n > 0$ can be obtained by appropriate shifts and scales if the basis $\psi_j, j = 0, 1, \dots, k-1$ w.r.t a measure μ_0 of \mathbf{W}_0^k is known. A similar expression as in Equation 36 can be obtained

Equations 35 and 37 informs us that the basis of \mathbf{V}_n^k and W_n^k can be written as linear combinations of that of \mathbf{V}_{n+1}^k . As a result, for a given function it is possible to obtain a relationship between its coefficients in these bases. Specifically, the function $f \in \mathbb{R}^d$ has coefficients in the space of orthogonal polynomials (multiscale coefficients) $\mathbf{s}_l^n = [\langle f, \phi_{il}^n \rangle_{\mu_n}]_{i=0}^{k-1} \in \mathbb{R}^{k^d \times 2^n}$ and coefficients in the multiwavelet subspace (multiwavelet coefficients) $\mathbf{d}_l^n = [\langle f, \psi_{il}^n \rangle_{\mu_n}]_{i=0}^{k-1} \in \mathbb{R}^{k^d \times 2^n}$, which are related by the *decomposition* equations:

$$\mathbf{s}_l^n = H^{(0)} \mathbf{s}_{2l}^{n+1} + H^{(1)} \mathbf{s}_{2l+1}^{n+1}, \quad (38)$$

$$\mathbf{d}_l^n = G^{(0)} \mathbf{s}_{2l}^{n+1} + G^{(1)} \mathbf{s}_{2l+1}^{n+1}, \quad (39)$$

and *reconstruction* equations

$$\mathbf{s}_{2l}^{n+1} = \Sigma^{(0)} (H^{(0)T} \mathbf{s}_l^n + G^{(0)T} \mathbf{d}_l^n), \quad (40)$$

$$\mathbf{s}_{2l+1}^{n+1} = \Sigma^{(1)} (H^{(1)T} \mathbf{s}_l^n + G^{(1)T} \mathbf{d}_l^n). \quad (41)$$

$H^{(0)}, H^{(1)}, G^{(0)}, G^{(1)} \in \mathbb{R}^{k^d \times k^d}$ are the reconstruction filters while $\Sigma^{(0)}, \Sigma^{(1)}$ are the correction terms. The theory and derivation of these terms are well covered in [36], we only highlight it here for better explanation of the steps involved in the method. In Equations 38-39, $H^{(0)}$ and $G^{(0)}$ act on the even terms of the multiscale coefficient while $H^{(1)}$ and $G^{(1)}$ act on the odd terms. The result of these operations are visibly a down-sampling from the higher to a lower resolution (half the original resolution), thus the term decomposition. On the other hand, Equations 40-41 perform the reverse of this operation, leading to the recovery of the higher resolution.

So far, we walked through multiwavelet representation of a function $f \in \mathbb{R}^d$. This notion will be applied to the input and output functions of the neural network/operator. A different notion, known as Non-Standard Form is used to obtain the multiwavelet representation of the kernel function. This method essentially reduces the operator kernel in Equation 32 $Kv = w$ to the set of equations.

$$U_{dl}^n = A_n d_l^n + B_n s_l^n,$$

$$U_{sl}^n = C_n d_l^n,$$

$$U_{sl}^L = \bar{T} s_l^L,$$

with U_{dl} and U_{sl} (respectively d_l^n and s_l^n) being the respective multiscale and multiwavelet coefficients of w (respectively v). L here is the index corresponding to the coefficients of the lowest resolution (output of the last decomposition). A_n, B_n, C_n and \bar{T} are then parametrised with a CNN (which could be done in Fourier space as in FNO or not) network followed by a ReLU activation then linear layer which we learn during training. In practice we use same neural networks for all n : thus $A_n = A_{\theta_A}, B_n := B_{\theta_B}, C_n := C_{\theta_C}$ and $\bar{T} := \bar{T}_{\theta_T}$. For a given input, the multiwavelet operator performs a series of operations as shown in Figure 9.

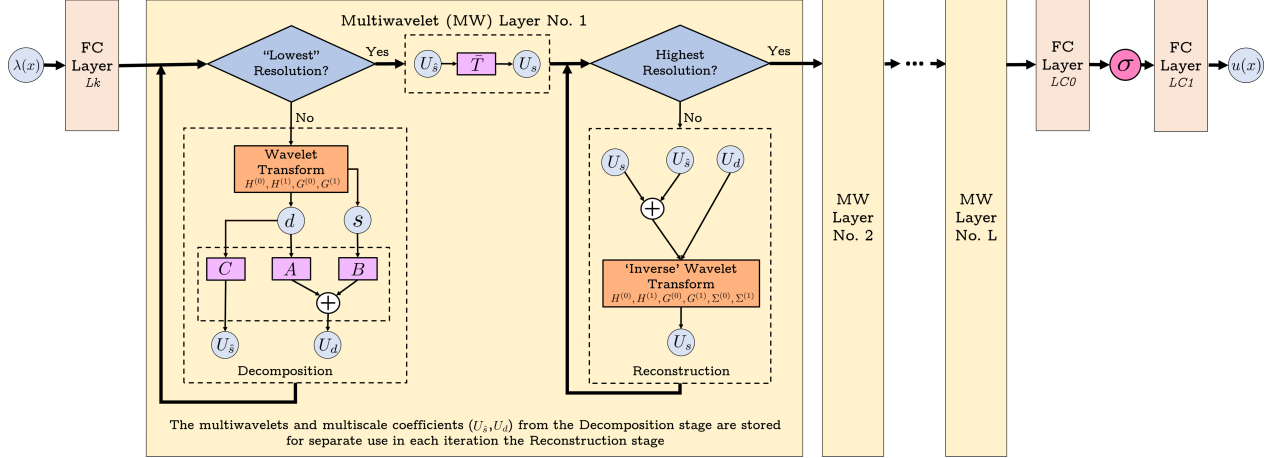


Figure 9: Architecture of the MWT Operator

4.2.5.3 Physics Informed (Fourier) Neural Operator - PINO

This method combines the operator learning of FNOs and function learning PINNs, in a quest to alleviate the challenges faced in the individual cases [64]. While PINNs face a challenge in optimisation when dealing with complex problems as in multiscale dynamics, FNO needs a wealth of data which might not be readily available. PINO combines both concepts by introducing two stages in the learning process:

- Firstly, the operator is learned using either/both a **data loss** (same loss as in FNO), or/and a **PDE loss** (physics informed loss), in a phase termed Pre-training. This case reduces to the normal FNO method, if no PDE loss is used.
- Secondly, for a specific instance of the input (parameter, for forward problem), the learned operator from the first stage is further fine-tuned, using the **PDE loss** and an **operator loss**. The latter minimises the difference between the initial network resulting from the pre-training phase and the further optimised networks. This phase is the test-time optimisation stage.

A strength of the PINO is in its ability to achieve competitive errors with fewer data as demonstrated in [64]. This is mainly due to the introduction of the PDE loss. Notably, this PDE loss is evaluated in a not-so-usual way as the input of the network is the function and not a set of collocation points. Automatic differentiation as we know it, is thus not possible. Three methods for gradient descent are outlined in [64]. One option is numerical differentiation, i.e. a finite difference method (FDM), which we use for our experiments in later sections.

4.2.6 FNO usage for inverse problems

FNO is an operator learning concept, hence both general concepts as outlined in Section 2.3 can be used for solving inverse problems. We will report on the achieved results in our section on numerical examples. FNO does remarkably well, despite its rather linear and Fourier-centric approach. However, it allows to incorporate fine details related to high frequencies in a consistent way, nevertheless understanding the success of FNO methods for solving inverse problems should be an important direction for future research.

4.3 DeepONet

4.3.1 Motivation

It is widely known that deep neural networks are universal approximators, i.e., they can approximate any finite-dimensional function to arbitrary accuracy [19,41]. This has been extended to an universal approximation theorem for operators [14], which states that a neural network with a single hidden layer can approxi-

mate accurately any nonlinear continuous operator. This theorem and its extension to multi-layer networks, see [69], provides the motivation for the concept of DeepONet.

4.3.2 Network architecture

The DeepONet [69] mirrors the structure of the universal approximation theorem of operators with a novel network architecture. Let us consider an operator \mathcal{F} that maps an input function λ to an output function u , i.e. $u = \mathcal{F}(\lambda)$. A DeepONet G_θ takes an input function λ , which is sampled at fixed predefined collocation points, and provides an approximation for $u(x)$ at arbitrary points x by the combination of a trunk and branch net in the following way:

$$u(x) \approx G_\theta(\lambda)(x) = \sum_{k=1}^p \underbrace{b_k(\lambda(s_1), \lambda(s_2), \dots, \lambda(s_m))}_{\text{branch}} \underbrace{t_k(x)}_{\text{trunk}} = \sum_{k=1}^p b_k(\lambda) t_k(x). \quad (42)$$

The trunk net $\mathbf{t} = \mathbf{T}(x; \theta_t)$ takes the continuous coordinates x as the input, and outputs a feature vector $\mathbf{t} = [t_1, \dots, t_p] \in \mathbb{R}^p$, which can be considered as p functions of x . The branch net $\mathbf{b} = \mathbf{B}(\lambda; \theta_b)$ takes $\lambda = [\lambda(s_1), \lambda(s_2), \dots, \lambda(s_m)]$, the discretization of the input function, as input and returns a feature vector $\mathbf{b} = [b_1, \dots, b_p] \in \mathbb{R}^p$ as output. The branch and trunk nets are then combined by a inner product to approximate the underlying operator.

This DeepONet is named as "unstacked DeepONet", while it is called "stacked DeepONet" if each $b_k(\lambda), k = 1, \dots, p$ is an individual neural network, i.e., $[b_1, \dots, b_m] = [\mathbf{B}(\lambda; \theta_b^1), \dots, \mathbf{B}(\lambda; \theta_b^m)]$. Several numerical results have shown that unstacked DeepONets typically have larger training error as compared with stacked DeepONets, but the test error is smaller and unstacked DeepONets lead to smaller generalization errors. Both branch net and trunk net can have general architectures, e.g., FNN, ResNet, CNN, RNN. However, as x is usually in low dimensional space, a standard FNN is commonly used as the trunk net. A bias can also be added to the last stage of the DeepONet to improve performance.

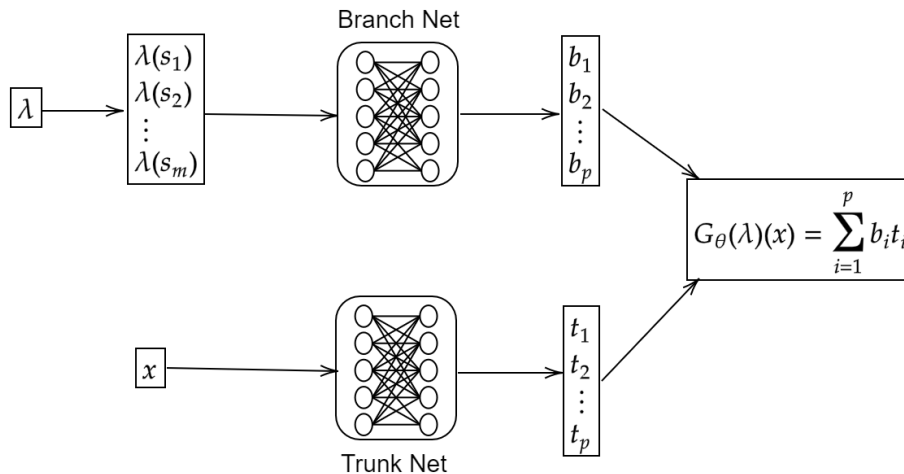


Figure 10: Architecture of the DeepONet

The novelty of the DeepONet is that its network architecture is composed of these two sub-networks, which treat the input λ and x differently, thus it is consistent with a prior knowledge. In addition, there is no need to discretize the domain to approximate the solution space, and the evaluated solution functions are defined in the whole domain. The only condition required is that the sensor locations $[s_1, s_2, \dots, s_m]$ should be consistent for the training dataset. There also are some generalizations which encode the input functions to the branch net by a feature vector, for example, we can use the coefficients of λ with respect to some chosen basis as input.

Once the DeepONet is trained, it is easy to see that the numerical solutions will lie in the linear space $\text{Span}\{t_1(x), \dots, t_p(x)\}$, i.e., $\{t_k(x)\}_{k=1}^p$ are actually the trained basis to approximate the solution space, and $\{b_k(\lambda)\}_{k=1}^p$ are the corresponding coefficients. Since usually p is not large, e.g. approximately 100 for our

Algorithm 8: Fast implementation of DeepONet

Input: data: $\{(\lambda_i, x_j, u_i(x_j)) | i = 1, 2, \dots, N; j = 1, 2, \dots, M\}$
Number of sensors: m , and the locations of the sensors: $S = (s_1, \dots, s_m)$
Let $\lambda = [\lambda_1(S), \dots, \lambda_N(S)] \in \mathbb{R}^{N \times m}$; $X = [x_1, \dots, x_M] \in \mathbb{R}^M$, $U = [u_1, u_2, \dots, u_M] \in \mathbb{R}^{N \times M}$
 p : the number of basis to be learned.
 τ_b/τ_t : learning rates of the branch net and trunk net

- 1 Initialize the branch net B_{Θ_b} and trunk net T_{Θ_t}
- 2 **while** not converged **do**
- 3 $B = B_{\Theta_b}(\lambda) \in \mathbb{R}^{N \times p}$ and $T = T_{\Theta_t}(X) \in \mathbb{R}^{M \times p}$
- 4 Output $= BT^T \in \mathbb{R}^{N \times M}$
- 5 $L(\theta) = \frac{1}{MN} \|U - \text{Output}\|$
- 6 Update $\theta \leftarrow \theta - \tau \nabla_{\Theta} L$
 /* The fast algorithm can be easily extended to the mini-batch case and the computation of the derivatives in PI-DeepONet. */
- 7 **end**

2 dimensional problems, the DeepONet can be regarded as a model reduction method in which the reduced basis is obtained by training.

4.3.3 The algorithm

Based on the architecture of the DeepONet, the parameters can be optimized by minimizing the following mean square error loss:

$$L(\theta) = \frac{1}{NP} \sum_{i=1}^N \sum_{j=1}^P |G(\lambda_i)(x_{i,j}) - G_{\theta}(\lambda_i)(x_{i,j})|^2 = \frac{1}{NP} \sum_{i=1}^N \sum_{j=1}^P |u_i(x_{i,j}) - \sum_{k=1}^p b_k(\lambda_i) t_k(x_{i,j})|^2. \quad (43)$$

There are two important hyper-parameters which should be determined before training: the positive integers m and p , i.e., the number of sensors for encoding the input functions and the number of basis used to approximate solutions. Larger m and p means smaller encoding error and reconstruction error, respectively. However, increasing them usually does not necessarily reduce the total error due to the increased complexity of the optimization problem. The locations of the sensors are not necessarily equispaced. However, they should be consistent with the training dataset.

Note that a pair of the training data in DeepONet is $\{\lambda_i, x_{i,j}, u_i(x_{i,j})\}$, thus it is slightly different from most neural operator methods, i.e. the full field observation of solutions is not necessary for the DeepONet and the DeepONet can work with only partially observed solutions. This is of particular importance for real applications where more often than not the available data is not complete. In addition, for different types of data sets, we can use different implementations for DeepONet to dramatically reduce the computational cost and memory usage by orders of magnitudes. For example, different branch input λ may share the same trunk net input x , and different input x may share a same input λ , see [70] for details. This computation technique can also be applied to the extension PI-DeepONet [101] when computing the derivatives of the output functions.

4.3.4 Generalizations of DeepONet

Several extensions of DeepONet have also been developed.

- In [70], a feature expansion for the trunk net input is proposed in order to satisfy some desirable properties of the output function, e.g., oscillating structures or decay properties. Feature expansion for the branch net can also be used to incorporate a feature which is a function of x . E.g. the POD-DeepONet as proposed in [70] precomputes a basis by performing proper orthogonal decomposition (POD) on the training data. Thus, POD-DeepONet shares the same idea with PCANN for the output

space. Employing such feature vectors might be particularly advantageous for non-smooth parameters or solutions, i.e., discontinuous or highly oscillatory functions.

- The Bayesian B-DeepONet [66] uses the Bayesian framework of replica-exchange Langevin diffusion to enable DeepONets training with noisy data. The B-DeepONet and Prob-DeepONet as proposed in [80] were shown to have good predictive power along with uncertainty quantification. In [32], a further generalisation 'Variational Bayes DeepONet' was introduced, in which the weights and biases of the neural network are treated as probability distributions instead of point estimates, and their prior distributions are updated by Bayesian inference..
- A universal approximation theorem of continuous multiple-input operators was proved and the corresponding MIONet was proposed to learn multiple-input operators in [47]. Similarly, The authors in [94] proposed a new enhanced DeepONet, in which multiple input functions are represented by multiple branch DNN sub-networks, which are then combined with an output trunk network via inner products to generate the output of the whole neural network.
- Several extensions for dealing with particular function properties were recently proposed. E.g., a multiscale DeepONet [68] was proposed to approximate a nonlinear operator between Banach spaces of highly oscillatory continuous functions. The shift-DeepONets proposed in [39] extends Deep Operator Networks for discontinuous output functions by elevating the linear basis expansion of the classical DeepONet architecture to a non-linear combination. This can make the basis functions themselves dependent on the input function by exposing explicit shift and scale parameters. In the paper [93], the authors introduce the Deep Graph Operator Network, a combination of DeepONet and Graph neural networks, by using GNN-Branch Net to exploit spatially correlated graph information. The authors in [79] developed a framework named Fed-DeepONet to allow multiple clients to train DeepONets collaboratively under the coordination of a centralized server.

4.3.5 Theoretical Background

In addition to the universal theorem, several analytic results have been published for DeepONet. In the original paper, a theoretical analysis was presented which allows to estimate the approximation properties for ODE operators with respect to an underlying probability distribution. The analysis depends on the number of sensors and the related approximation of the input functions.

In [57], the universal approximation property of DeepONets was extended to include measurable mappings in non-compact spaces. By a decomposition of the error into encoding, approximation and reconstruction errors, both lower and upper bounds on the total error were derived, relating it to the spectral decay properties of the covariance operators associated with the underlying measures. For four prototypical examples of nonlinear operators it was proved that DeepONets can break the curse of dimensionality.

In [21] the convergence rates of the DeepONet were considered for both linear and non-linear advection-diffusion equations with or without reaction. The conclusion is that the convergence rates depend on the architecture of the branch network as well as on the smoothness of inputs and outputs of the operators. The paper [33] gives a bound on the Rademacher complexity for a large class of DeepONets.

5 Numerical experiments

The core of this paper is a numerical comparison of the described methods. The aim is to develop a guideline for scientist who want to start working with DL methods for PDE-based problems and face the problem of determining suitable methods.

We will perform numerical experiments on different levels. First of all we will investigate the performance for solving the forward Poisson problem. This linear problem is most commonly used and -despite its limited value for generalisations to non-linear problems - already yields some insight into the performance of the chosen methods. We then perform tests for the inverse Poisson problem, where the source term is the sought after parameter.

After that we turn to analyzing the behaviour of the chosen methods for forward and inverse Darcy flows. A particular emphasis is on evaluating and, comparing the respective numerical schemes in terms of accuracy but also computational time and storage needed for parametric studies.

After these basic numerical tests we do report on how learned PDE solvers behave for two industrial projects.

We want to acknowledge that there already exists a growing list of publications devoted to testing DL concepts for the solution of PDEs, see e.g. [34, 70]. However, these studies focus on PDE based forward problems, in contrast, our experiments for comparing forward solvers is a preliminary step towards our main goal, namely a comparison of DL methods for PDE based parameter identification problems.

We start this section by an outline of our data generation procedure, which follows [8, 62, 63]. In summary this section is organized as follows

- Generating training and test data
- Poisson problem
 - Forward problem
 - Inverse problem trained with exact data
 - Inverse problem trained with noisy data
- Darcy flow
 - Forward problem
 - Inverse problem trained with exact data
 - Inverse problem trained with noisy data
- Industrial applications
 - A moving domain problem (Bosch)
 - Identification of material model parameters from stress tensor (Volkswagen)

5.1 Generating training and test data

The outline of our numerical experiments for the linear differential equations $\Delta u = \lambda$ on Ω , $u = g$ on $\partial\Omega$ (Poisson problem) as well as simulations for the Darcy flow follows the approach of [8]. Hence, we do a performance analysis in terms of accuracy as well as computational load and the parameter λ is randomly generated as a Gaussian random field. As a gold standard for comparison we use a standard FDM code, which is tuned to high precision and also provides the ground truth data for training the networks.

Learning operators implies learning mappings between function spaces. For a supervised learning task, we need input-output data pairs for training, which in our case are the parameter and solution functions. We start with Gaussian Random Fields, commonly used in the stochastic modeling of physical phenomena as e.g. described in [8, 62, 63, 70]; more precisely we use as base measure the Gaussian distribution

$$\mu_G = \mathcal{N}(0, (-\Delta + 9I)^{-2}),$$

with a zero Neumann boundary condition on the operator Δ , which yields random but smooth test data for the Poisson problem. Other interesting measures are μ_L and μ_P which are the push-forwards of μ_G under the exponential and piecewise constant maps respectively, so that $\mu_L = \exp_{\sharp} \mu_G$ and $\mu_P = T_{\sharp} \mu_G$, with

$$T(s) = \begin{cases} 12 & s \geq 0 \\ 3 & s < 0 \end{cases}$$

For our experiments with the Darcy flow we used piecewise constant parameters. We show some examples in Figure 11.

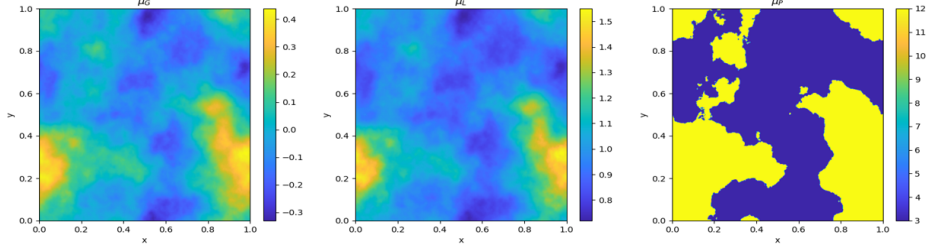


Figure 11: Example of samples from the GRF probability measures μ_G , μ_L and μ_P .

To complete the data pair, we use the generated samples as right hand sides of the Poisson problem and use a finite difference method (FDM) in order to get the solution for the considered problem: As an example, we consider the Poisson problem given by

$$\begin{aligned} -\Delta u(s) &= \lambda(s) & s \in (0,1)^2 \\ u(s) &= 0 & s \in \partial(0,1)^2, \end{aligned} \quad (44)$$

where the forcing term $\lambda(s)$ is sampled from the GRF $\lambda \sim \mu_G$. Then, the domain $(0,1)^2$ is discretised as shown in Figure 12, and a second order FDM scheme is used to evaluate the Laplacian, reducing the Poisson equation to a system of linear equations given by Equation 45, where $i = 0, \dots, N_y$ and $j = 0, \dots, N_x$ for a resolution of $(N_x + 1) \times (N_y + 1)$

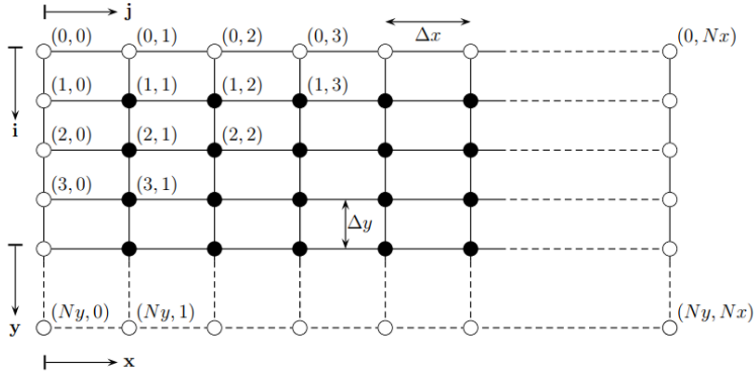


Figure 12: Computational grid showing interior grid points (black) and boundary grid points (white) .

$$\frac{\Delta y}{\Delta x} (-u_{i,j-1} + 2u_{i,j} - u_{i,j+1}) + \frac{\Delta x}{\Delta y} (-u_{i-1,j} + 2u_{i,j} - u_{i+1,j}) = \Delta x \Delta y \lambda(x_j, y_i) \quad (45)$$

Our numerical tests are done using baseline implementations of the mentioned DL algorithms and we did some extensive hyperparameter search every method, for details see the appendices. Nevertheless, hyperparameter search and fine tuning the optimization scheme in search of global minima is a never ending story. Hence, the presented results should be understood as the best we could achieve within the given time and with the available computing capacity (specified in A.2). All methods were treated equally and we believe, that this leads to a fair basis for comparison.

In addition, we are well aware of the extensive body of literature dealing with sometimes rather refined extensions and improvements of these methods, e.g. there are several extensions of the PINN approach and a survey on different Physics-informed neural operator networks variants has been published recently, [34]. However, these extensions most often come with the necessity to finetune additional hyper parameters or they do apply only to special cases. Hence, as said before we focus on a comparison of the basic implementations in this section. In order to give proper credit to the different approaches, we assigned different co-authors to different concepts and everybody was doing his best to ‘defend’ the respective concepts.

Furthermore, let us clarify the criteria for our evaluation. There are a number of obvious categories such as achievable mean accuracy, training time, time for solving the forward Poisson problem after training, but also degrees of freedom of the networks used, stability with respect to hyper parameter tuning, etc. Nevertheless, in the following we will mainly discuss two criteria, namely accuracy and the potential for parametric studies/inverse problems, i.e. the computational time needed to run the algorithm after training for novel sets of parameters.

5.2 Poisson problem

5.2.1 Forward problem

Testing different DL concepts for training a **forward solver** for the Poisson problem (44) is the most basic academic example which is used by almost all relevant publications in this context. This linear problem can be solved by all other methods considered and the errors are as reported in Table 2. These errors do not differ too much, they are below 1% relative error except for DRM, which has an error of approximately 2,5%. Still, there are some notable differences. The overall winner is PCALin both in terms of achievable accuracy as well as in terms of complexity of the network. However, none of the methods was able to achieve an accuracy comparable with fine-tuned FDM or FEM methods. The advantage of DL concepts in this case lies in the potential for large scale parametric studies, where the executing time for testing novel parameters has to be minimal.

However, not all DL concepts are suitable for parameteric studies. In general DL concepts aiming for a function approximation do require expensive retraining of the network for every additional parameter and do have limited value for large scale parameter variations. Hence, we focus on DL concepts for operator approximations, see Table 1. In our experiments DeepONet and their physics-informed versions performed best in terms of efficiency (run time for testing). The differences in testing time for these methods are below the variance introduced by the random sampling of test data.

The comparison with respect to different resolutions of u do show the expected, but interesting result, that operator approximations, which are based on a functional analytic reasoning in function spaces rather than discrete settings, indeed show an independent accuracy across scales, see Table 3. This cannot be matched by function approximations where the error increases by several orders of magnitude for coarse discretizations.

These numerical findings for the linear Poisson problem in a standard domain do have little value for generalizations to other PDE problems. Nevertheless, as a punch line for simple linear PDE problems we would stress the old saying ‘keep it simple’ and suggest to apply ‘easy to use’ concepts such as PCALin with a suitable but comparatively small network.

PINNs do also offer an easily accessible concept, which is easy to adapt to other PDE, but it requires retraining, i.e. PINN in their original version are not suitable for parametric studies, and they did exhibit a slightly larger L_2 -error in our scenario.

As an alternative, MWT requires a more advanced implementation but seems to be more efficient for parametric studies, however, training times are rather high.

5.2.2 Inverse problem

The investigation of the performance of DL concepts for PDE based inverse problems for parameter identification is the core of this survey. In this subsection we summarize the results for the inverse Poisson problem, i.e. determining λ in Equation 8 from a measured version of u . Iterative methods for solving such an inverse problems as well as parametric studies require multiple evaluations of the parameter-to-state map F . As already mentioned, DL concepts based on operator approximations are better suited in this context and we will focus on these methods. The only exception is the extension to inverse problems of PINNs and QRES as described in Section 3.2.4

Our tests for PDE based inverse problems are organized in terms of how we attack the inverse problem and which data is used for training. First of all there are two primary approaches for dealing with inverse problems, see Section 2.3, i.e. we can either train the inverse problem with a reversed input-output structure or we can integrate a learned forward solver in a Tikhonov approach. Secondly, we can train the network with either noiseless data or with noisy data with different noise levels. Both tests are meaningful for applications depending on whether some clean data obtained in research labs or measured data from field

experiments is available. As it is common for inverse problems, after training these networks will be evaluated for reconstruction problems with noisy data. The case of testing with noise-free data is included for reason of completeness.

Training is always done with 1000 training samples, where λ is computed as a smoothed random Gaussian field, see Section 5.1. The parameter-to-state map, $u = F(\lambda)$, is then computed with a high precision finite difference scheme. The resulting solution u is then perturbed with normally distributed random noise of different levels, δ .

$$u^\delta(x) = u(x) + \delta \cdot \|u\| \cdot N(0, 1)$$

For the evaluation of the methods we use additional $N = 5000$ samples of u^δ , which are computed by the same procedure, i.e. drawing additional random samples for λ_{true} , computing the corresponding solution u and adding noise.

These perturbed solutions are the input for the inverse problem during evaluation. The resulting estimation of the parameter $\hat{\lambda}$ is then compared with the original, true parameter λ_{true} . As a standard measure of success we average over the different evaluation samples and take the mean L_2 -error, $E(\|\hat{\lambda} - \lambda_{true}\|)$.

For certain applications, i.e. control problems the output error is also of importance and for some experiments we also report the difference between the solution obtained with $\hat{\lambda}$ and the true, unperturbed solution u as shown in Tables 8b and 8c.

Let us comment on the different test scenarios (inverse learning or Tikhonov, noise free or noisy data for training) in more detail.

The tests with unperturbed data, i.e. the case where the networks were trained and evaluated with perfect noise-free data are reported in Table 2 and Table 3 for different resolutions. For operator approximation methods the inverse problem in these tables is always solved by inverse learning (backward operator training). Also, PINN and QRES can be extended to parameter learning directly by a doubling of the network, see Section 3.2.4. This results in a doubling of the network parameters as shown in the second column of both tables. As a general observation we remark that the achievable accuracy for the inverse problem is considerably below the accuracy of the forward problem, which reflects the ill-posedness of the inverse problem. Also, the baseline implementations of PCANN, PINN and DeepONet do perform less reliable as compared with their extensions such as PCALin, U-FNO, PINO or MWT. After training run times of the different methods are the same as for the forward problem.

Due to the linear nature of the problem and the missing noise in the data one should not overestimate the value of these tests. In particular testing with noisy data is essential for inverse problems.

To this end, we have done experiments where the networks were trained with noiseless data but evaluation was done with noisy data, see Table 6. We clearly see, the networks trained with noise-free data do not generalize to the case of noisy data. The error exceeds 100% in most cases. The only notable exception are surprisingly DeepONet and PI-DeepONet. Even for high noise levels, these methods still produce errors in the reconstructed parameter which are approx. 4 – times larger than the noise in the data, which is the range of errors one would expect for optimal regularization schemes for ill-posed problems.

Tables 7 and 8 are the most meaningful ones for inverse problems. Here we report results on networks, which are trained and evaluated with noisy data. Table 7 reports results obtained by reversed/backward operator training, i.e. the network is trained to take u^δ as input and to return directly an estimate for the parameter λ . Table 8 reports results obtained by first training a forward network $u_\Theta(\lambda)$ and then computing an approximation to the parameter by solving a Tikhonov minimization problem

$$\min_{\lambda} \|u_\Theta(\lambda) - u^\delta\|^2 + \alpha R(\lambda).$$

In these experiments R was always taken as a discretization of the L_2 -norm and α was optimized by numerical experiments. Depending on the problem, one could add an additional regularization term as shown in Equations 54 and 55.

Both approaches, i.e. inverse learning and embedding a learned forward operator into a Tikhonov scheme do give comparable results. All errors in the reconstructions are naturally larger than the error in the input data, as is to be expected for ill-posed problems. The Tikhonov results maybe slightly better, but they require to solve a minimization problem for each new data set and are computationally more expensive. We should remark on the suboptimal results obtained by DeepONet. Here the error margins are considerably larger but almost constant over different noise levels. This might indicate, that the dominant error is not

stemming from inversion and noise, but rather from a structural disadvantage of the network architecture or suboptimal training. We have tested several larger DeepONet network architectures, which however did not cure the problem. This might be interesting to investigate further.

Tables 8b and 8c are based on experiments, where the reconstructed parameter $\hat{\lambda}$ was used to compute the corresponding solution $\hat{u} = F(\hat{\lambda})$. This is then compared with either the true solution u , see Table 8c), or the noisy data, which was used for training, see Table 8b). This is considered as a test for how well these parameter estimation problems can be used to solve control problems, which however is not the focus of this paper and this case is not investigated further.

5.2.3 Summary Poisson problem

In summary, for the forward problem the investigated DL concepts are less accurate as compared with finite difference methods on a fine grid. However, these DL concepts do produce competitive results for solving inverse problems with different noise levels. DL concepts for operator approximation perform best and offer a significant advantage in run time. Hence, either large scale parametric studies or iterative solvers for parameter identification decisively benefit from well trained DL concepts.

For the somewhat simple Poisson problem with vanishing boundary data, where both the forward as well as the inverse operator are linear, there is not much difference between the DL concepts. Overall, we propose to use PCALin, PCANN or PINN for first testing due to their ‘easy-to-use’ structure. They produce acceptable results for a wide range of hyper-parameters and are comparatively easy to train. For more accurate results, we propose to use PINO or MWT, which are somewhat more involved, for implementation details see the respective appendices.

5.3 Darcy flow

5.3.1 Forward problem

We now summarize our findings concerning numerical experiments for Darcy flow problems. We start with a discussion of the forward problem, i.e. computing the solution u in Equation 52, for a given piecewise constant diffusion coefficient λ . In all experiments, $\lambda(x) \in \{3, 12\}$, i.e. the domain of definition is segmented randomly into two regions with known values.

Surprisingly, the errors for PINN and QRES are relatively high, even if the network is trained and evaluated with noise-free data, see Table 4. All other methods solve this non-linear forward problem reliably. MWT is the overall winner for solving the forward problem with noise-free data. This also holds for most levels of resolution.

Again, the comparison with respect to different resolutions of u do show the expected result that operator approximations based on a functional analytic reasoning in function spaces indeed show an independent accuracy across scales, see Table 5.

5.3.2 Inverse problem

The investigation of the performance of DL concepts for inverse Darcy flows again either uses inverse training or embedding of a forward solver into a Tikhonov functional. The testing scenarios are similar to those of the Poisson problem, i.e. 1000 random samples were used for training and 5000 samples for evaluation.

In view of different applications we have either used no further assumption on λ , see Figure 16, or we have assumed that we know, that λ is a segmentation of the domain of definition into two components with known value, see Table 11. This e.g. models the problem of the mixing of two liquids with known density. We notice the strength of the FNO, U-FNO, MWT, and PINO to identify the discontinuity in Figure 16, when no prior information about the values is provided. As before, we have done experiments where the networks were trained with noiseless or noisy data. The results of inverse training with perfect data for training and evaluation are stated in Tables 4 and 5, they mimic the results of the forward training and do not yield additional insights. As for the Poisson problem, training with noise-free data does not generalize to noisy data, see Table 6, even only 1% error in the evaluation data yields reconstruction errors of 30% and larger. The only noticeable exception is DeepONet which shows errors of about 25% for all noise levels tested.

This might indicate that the error is dominated by a structural mismatch but otherwise good reconstruction qualities.

Tables 7 and 9 state the results most important for inverse problems. They show some remarkable difference between the considered concepts. Most methods (PINN, QRES, PCANN, PCALin, DeepONet, PI-DeepONet) do show approximately the same errors for all noise levels. This indicate that a structural approximation error domoinates the influence of the data noise. We have tested differnt hyperparameter settings for all of these methods, which however, did not change the result. As a consequence, these methods do not yield comeptitive results for small levels of data noise. Nevertheless, PCANN exhibits about 10% error in the reconstructions even for 5% data error, which is remarkably good. In our test scenarios, there are clear winners: U-FNU and MWT for small noise levels and PCANN for larger noise levels. It si surprising, that a 'linear' concept such as PCANN performs so well for a non-linear problem, and non-linear concepts such as DeepONet and its physics-informed variant PI-DeepONet, as well as PINO do not seem to be suitable for Darcy inverse problems.

Inverse training generally yields slightly better results as compared with Tikhonov embedding, as shown in Figure 9b. Errors are consistently larger, which might be partially explainable by the difficulty of choosing suitable regularization parameter α . We have also include the accuracy metric which measures the segmentation error rather than the functional L_2 error. Here results again are similar for all methods, see Table 9a.

We estimated the output error by feeding the reconstructed $\hat{\lambda}$ into the respective neural networks and comparing the resulting \hat{u} with the exact data u and its noisy version u^δ , see Figures 9c and 9.

5.3.3 Summary Darcy flow

In summary, the investigated DL concepts do produce competitive results for solving inverse problems with different noise levels. DL concepts for operator approximation perform best and offer a significant advantage in run time. Hence, either large scale parametric studies or iterative solvers for parameter identification decisively benefit from well trained DL concepts. This training has to be done with the same noise level, training with noise free data does not generalise to noisy data. As a general procedure, we would recommend to favour backward operator training over Tikhonov minimization.

for choosing appropriate methods, as indicated in our test scenario, U-FNO and MWT did best for small noise levels and, surprisingly, the linear concept PCALin was best for solving the non-linear inverse Darcy flow problem with higher noise levels.

Networks	# of Parameters	Forward Problem			Inverse Problem		
		Rel. L2 Error	Training (s/epoch)	Testing (s)	Rel. L2 Error	Training (s/epoch)	Testing (s)
DRM	6,721	0.0251	0.0514	~ 480	-	-	-
PINN	5,301 10,602	0.0075	0.1034	~ 1,315	0.1650	0.2368	~ 3,370
QRES	5,509 11,018	0.0076	0.1581	~ 2,150	0.1549	0.4186	~ 5,730
PCANN	5,155,150 5,205,200	0.0073	0.0142	0.6063	0.0981	0.0161	0.6179
PCALin	62,750	0.0013	0.0077	0.7453	0.0244	0.0090	0.7640
FNO	2,368,001	0.0066	42.6249	0.0168	0.0415	42.6245	0.0174
U-FNO	3,990,401	0.0053	97.6730	0.0346	0.0254	97.6434	0.0343
MWT	9,807,873	0.0036	114.2043	0.0488	0.0159	113.2655	0.0483
DeepONet	640,256 768,128	0.0042	0.1098	0.0002	0.1035	0.1201	0.0002
PINO	2,368,001	0.0031	42.6289	0.0166	0.0301	42.8172	!0.0143
PI-DeepONet	640,256 739,712	0.0061	0.4637	0.0002	0.1068	0.4462	0.0002

Table 2: Performance of different methods for the Poisson Problem, using a 513×513 resolution. In the second column, for the forward and inverse problems, if the same amount of parameters is used, only one number is specified. If different amounts are used, two numbers are given. Where the left one corresponds to the forward problem and the right one to the inverse case. The networks were trained with noiseless data and backward operator training was used for solving the inverse problem.

Grid size, s	<i>Forward Problem Rel. Errors</i>				<i>Inverse Problem Rel Errors</i>			
	65	129	257	513	65	129	257	513
DRM	0.0397	0.0289	0.0244	0.0251	-	-	-	-
PINN	0.0245	0.0088	0.0084	0.0075	0.1715	0.1694	0.1653	0.1650
QRES	0.0288	0.0082	0.0088	0.0076	0.1598	0.1565	0.1542	0.1549
PCANN	0.0078	0.0075	0.0073	0.0073	0.0989	0.0979	0.0981	0.0981
PCALin	0.0016	0.0013	0.0013	0.0013	0.0303	0.0271	0.0253	0.0244
FNO	0.0066	0.0061	0.0067	0.0066	0.0299	0.0341	0.0366	0.0416
U-FNO	0.0063	0.0056	0.0062	0.0054	0.0292	0.0277	0.0288	0.0254
MWT	0.0047	0.0047	0.0048	0.0036	0.0357	0.0202	0.0198	0.0159
DeepONet	0.0047	0.0041	0.0041	0.0042	0.0983	0.0992	0.1041	0.1044
PINO	0.0031	0.0030	0.0034	0.0031	0.0263	0.0273	0.0319	0.0301
PI-DeepONet	0.0081	0.0057	0.0060	0.0061	0.1074	0.1068	0.1067	0.1068

Table 3: Error variation with resolution for the Poisson problem. The networks were trained with noiseless data and backward operator training was used for solving the inverse problem.

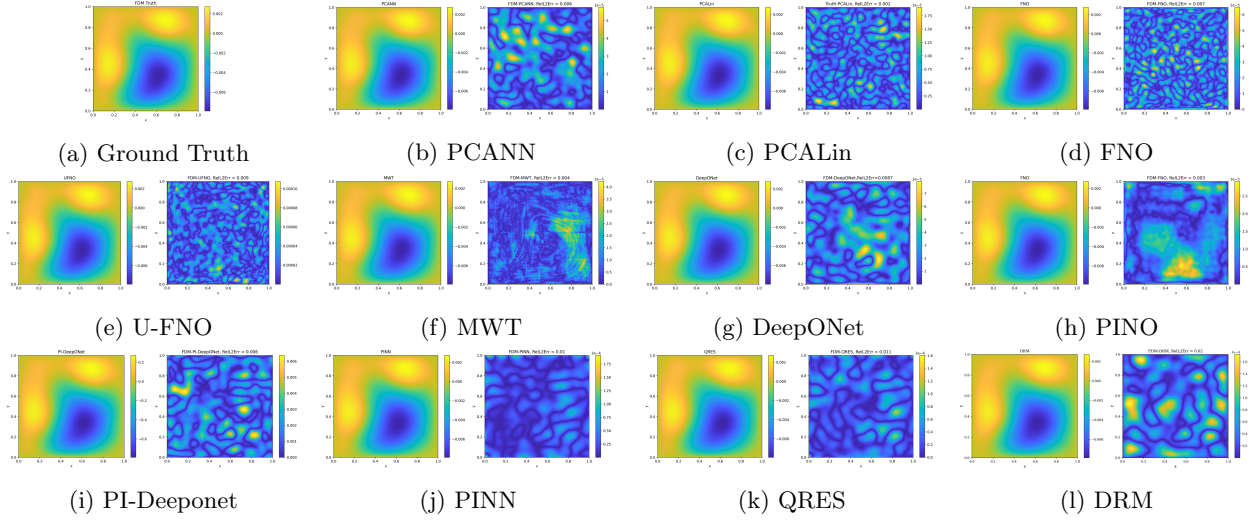


Figure 13: Test examples for Poisson forward problem using resolution of 513×513

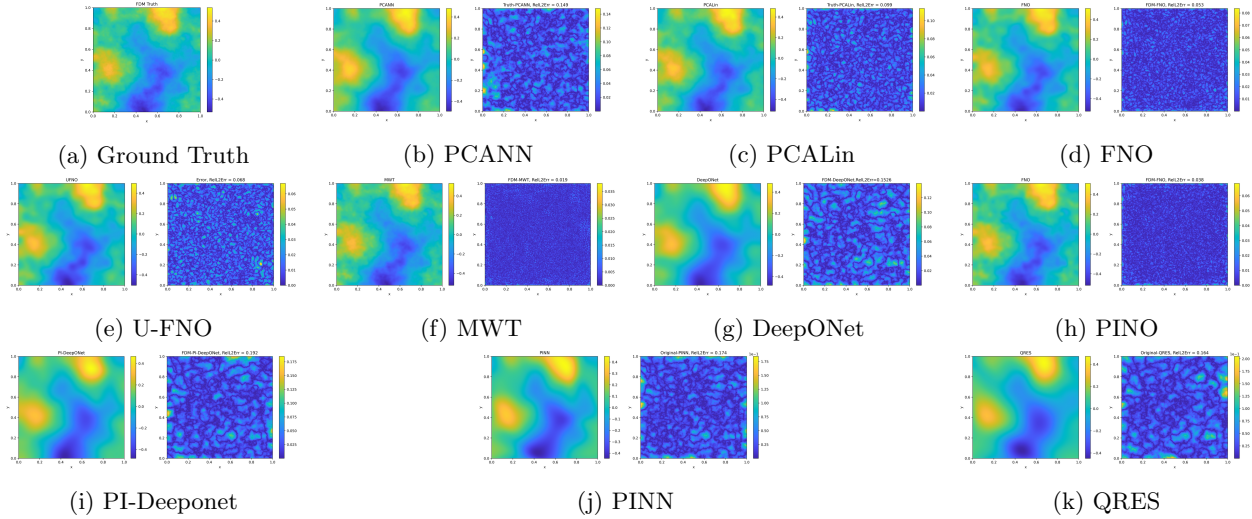


Figure 14: Test examples for inverse Poisson problem using resolution of 513×513

Networks	# of Parameters	Forward Problem			Inverse Problem		
		Rel. L2 Error	Training (s/epoch)	Testing (s)	Rel. L2 Error	Training (s/epoch)	Testing (s)
DRM	22, 201	0.0369	0.0859	~ 1, 050	-	-	-
PINN	6, 291 7, 972	0.1995	0.1164	~ 2, 010	0.1988	0.2528	~ 4, 790
QRES	6, 562 8, 895	0.2017	0.2108	~ 3, 320	0.1975	0.4221	~ 6, 420
PCANN	5, 155, 150 5, 035, 030	0.0253	0.0136	0.6108	0.0988	0.0487	0.1548
PCALin	10, 100	0.0656	0.0075	0.3290	0.2203	0.0139	0.3108
FNO	2, 368, 001	0.0109	41.6857	0.0165	0.1490	42.0596	0.0163
U-FNO	3, 990, 401	0.0095	97.9580	0.0344	0.0085	98.8170	0.0345
MWT	9, 807, 873	0.0058	112.4575	0.0637	0.0156	112.8750	0.0403
DeepONet	568, 320 1, 047, 644	0.0295	0.0606	0.0011	0.2220	0.0659	0.0011
PINO	2, 368, 001	0.0084	42.8685	0.0168	0.2345	42.7417	0.0142
PI-DeepONet	568, 320 684, 288	0.0384	0.2513	0.0011	0.2720	0.4905	0.0011

Table 4: Performance of different methods for the Darcy flow problem with piece-wise constant coefficients and using a 513×513 resolution. A similar convention is used for the second column as in Table 4. We also include here the accuracy metric for the inverse problem as the nature of the parameter makes it similar to a classification problem

Grid size, s	Forward Problem Rel. Errors				Inverse Problem Rel. Errors			
	65	129	257	513	65	129	257	513
DRM	0.0501	0.0375	0.0358	0.0369	-	-	-	-
PINN	0.2254	0.2043	0.2071	0.1995	0.2413	0.2014	0.2032	0.1988
QRES	0.2596	0.2077	0.1993	0.2017	0.2371	0.2117	0.2036	0.1975
PCANN	0.0256	0.0254	0.0253	0.0253	0.0983	0.0985	0.0987	0.0988
PCALin	0.0656	0.0656	0.0656	0.0656	0.2191	0.2198	0.2201	0.2203
FNO	0.0113	0.0106	0.0107	0.0109	0.1661	0.1536	0.1501	0.1490
U-FNO	0.0078	0.0071	0.0074	0.0095	0.0928	0.0640	0.0322	0.0085
MWT	0.0080	0.0060	0.0059	0.0058	0.1047	0.0800	0.0461	0.0156
DeepONet	0.0290	0.0292	0.0289	0.0295	0.2219	0.2261	0.2221	0.2220
PINO	0.0078	0.0066	0.0071	0.0084	0.1703	0.1997	0.2216	0.2345
PI-DeepONet	0.0390	0.0382	0.0381	0.0384	0.2706	0.2711	0.2682	0.2720

Table 5: Error variation with resolution for the Darcy Flow problem with piece-wise constant coefficients. The networks were trained with noiseless data and backward operator training was used for solving the inverse problem.

Noise level	Poisson					Darcy Flow PWC				
	0%	0.1%	1%	5%	10%	0%	0.1%	1%	5%	10%
PCANN	0.0988	0.0993	0.1171	0.3525	0.5645	0.0983	0.0983	0.0984	0.0998	0.1039
PCALin	0.0303	0.0379	0.0737	0.3134	0.6228	0.2191	0.2191	0.2192	0.2231	0.2348
FNO	0.0299	0.2966	2.6444	10.5499	19.9952	0.1341	0.1743	0.5100	3.3888	7.5197
U-FNO	0.0292	0.2102	1.1645	4.3941	8.3548	0.0896	0.1202	0.5896	1.4194	2.2052
MWT	0.0316	0.2201	1.2716	4.1969	7.6609	0.0865	0.1123	0.3668	0.6949	0.8620
DeepONet	0.0983	0.0985	0.1048	0.2059	0.3748	0.2219	0.2223	0.2224	0.2262	0.2375
PINO	0.0263	0.3457	3.3960	16.8352	33.8227	0.1703	0.1789	1.0438	6.1264	12.3570
PI-DeepONet	0.1074	0.1075	0.1120	0.1917	0.3352	0.2706	0.2706	0.2706	0.2714	0.2737

Table 6: Effects of noise on the solution for the inverse problems on a 65×65 resolution. The network is trained with noise-free data, but evaluated with noisy data. Backward operator training is used for solving the inverse problem.

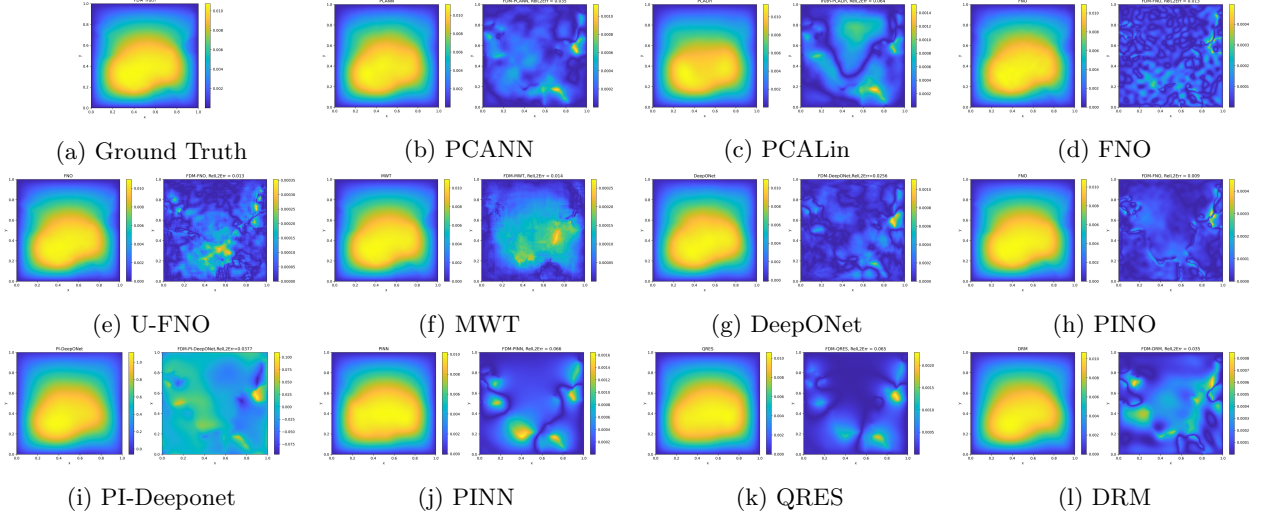


Figure 15: Test examples for forward Darcy problem using resolution of 513×513

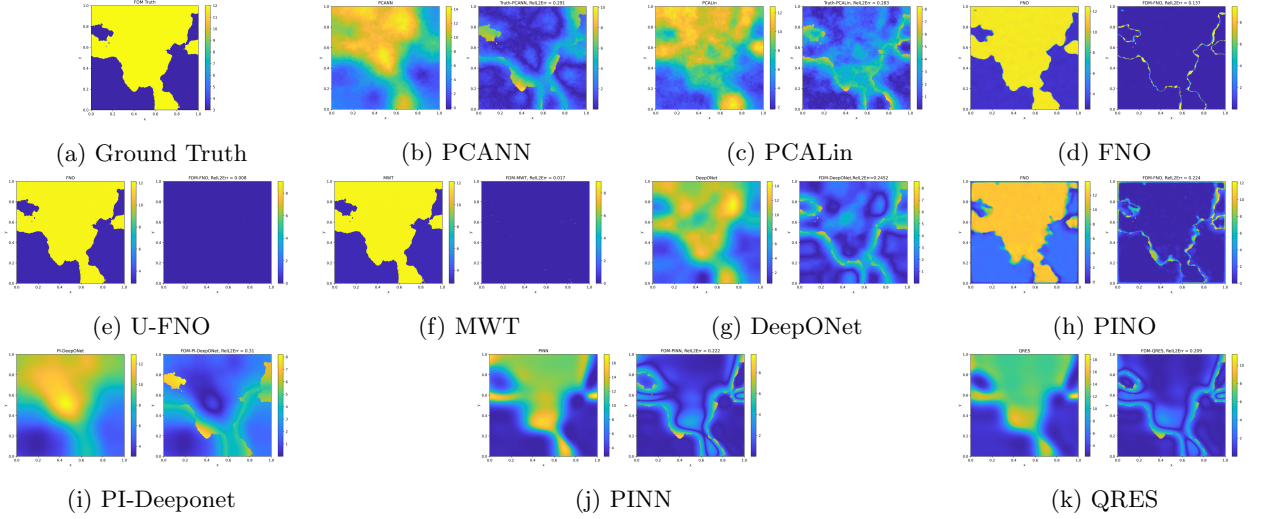


Figure 16: Test examples for inverse Darcy Flow problem using resolution of 513×513

Noise level	<i>Poisson</i>					<i>Darcy Flow PWC</i>				
	0%	0.1%	1%	5%	10%	0%	0.1%	1%	5%	10%
PINN	0.1715	0.1727	0.1734	0.2110	0.2378	0.2413	0.2407	0.2496	0.2564	0.2893
QRES	0.1598	0.1658	0.1714	0.2007	0.2256	0.2371	0.2421	0.2617	0.2789	0.2951
PCANN	0.0988	0.0991	0.1293	0.1876	0.2273	0.0983	0.0987	0.0990	0.1012	0.1093
PCALin	0.0303	0.0318	0.0840	0.1478	0.1846	0.2191	0.2191	0.2191	0.2217	0.2315
FNO	0.0299	0.0554	0.0957	0.1389	0.1678	0.1341	0.1344	0.1449	0.1770	0.2019
U-FNO	0.0292	0.0594	0.1036	0.1633	0.1839	0.0896	0.0902	0.1219	0.1649	0.1932
MWT	0.0316	0.0533	0.0966	0.1525	0.1867	0.0865	0.0893	0.1115	0.1634	0.1956
DeepONet	0.0983	0.1042	0.1084	0.1537	0.1870	0.2219	0.2283	0.2273	0.2379	0.2522
PINO	0.0263	0.0570	0.0957	0.1389	0.1678	0.1703	0.1737	0.2083	0.5147	0.9699
PI-DeepONet	0.1074	0.1086	0.1137	0.1516	0.1834	0.2706	0.2680	0.2703	0.2735	0.2742

Table 7: Effects of noise on backward operator inverse problems on a 65×65 resolution. The network is trained with noisy data and datasets with the same noise level are used for testing.

	0%	0.1%	1%	5%	10%
PCANN	0.2128	0.2128	0.2137	0.2975	0.4468
PCALin	0.0803	0.0805	0.0918	0.1534	0.2132
FNO	0.0931	0.0936	0.1082	0.1450	0.1693
U-FNO	0.0687	0.0697	0.0909	0.1397	0.1802
MWT	0.0708	0.0714	0.0878	0.1368	0.1796
DeepONet	0.1341	0.1330	0.1350	0.1660	0.2088
PINO	0.0598	0.0623	0.0890	0.1441	0.1915
PI-DeepONet	0.1573	0.1580	0.1727	0.2040	0.2298

(a) λ_{err} , the relative error of the learned parameter

	0%	0.1%	1%	5%	10%
PCANN	0.0133	0.0128	0.0130	0.0123	0.0122
PCALin	0.0010	0.0010	0.0016	0.0074	0.0158
FNO	0.0022	0.0025	0.0097	0.0464	0.0924
U-FNO	0.0009	0.0013	0.0091	0.0457	0.0914
MWT	0.0014	0.0017	0.0093	0.0459	0.0917
DeepONet	0.0053	0.0054	0.0113	0.0497	0.0988
PINO	0.0006	0.0010	0.0088	0.0454	0.0911
PI-DeepONet	0.0045	0.0047	0.0135	0.0520	0.1013

(b) \tilde{u}_{err} , the relative error between the solution of the learned parameter and the noisy solution.

	0%	0.1%	1%	5%	10%
PCANN	0.0133	0.0128	0.0131	0.0150	0.0209
PCALin	0.0010	0.0010	0.0020	0.0074	0.0133
FNO	0.0022	0.0023	0.0040	0.0089	0.0133
U-FNO	0.0009	0.0010	0.0024	0.0072	0.0124
MWT	0.0014	0.0015	0.0025	0.0072	0.0124
DeepONet	0.0053	0.0053	0.0055	0.0085	0.0137
PINO	0.0006	0.0008	0.0023	0.0072	0.0126
PI-DeepONet	0.0045	0.0046	0.0058	0.0147	0.0152

(c) u_{err} , the relative error between the solution of the learned parameter and the noiseless solution.

Table 8: Effects of noise on Tikhonov-based inverse problems for the Poisson problem and using datasets with a resolution of 65×65 . The errors shown here are averaged over 100 test samples.

	0%	0.1%	1%	5%	10%
PCANN	77.74	77.70	77.83	76.79	74.19
PCALin	90.58	90.58	90.57	90.55	90.42
FNO	96.92	96.92	96.71	95.45	94.30
U-FNO	94.23	93.83	95.20	94.14	92.48
MWT	98.26	98.33	97.84	96.42	95.04
DeepONet	93.88	93.88	93.95	93.49	92.70
PINO	97.56	97.59	97.45	96.34	95.07
PI-DeepONet	92.03	91.93	91.84	91.80	91.60

(a) $\lambda_{\text{acc}}(\%)$, the accuracy of the learned parameter

	0%	0.1%	1%	5%	10%
PCANN	0.4684	0.4692	0.4680	0.4828	0.5148
PCALin	0.3157	0.3157	0.3159	0.3163	0.3183
FNO	0.1764	0.1764	0.1823	0.2143	0.2402
U-FNO	0.2140	0.2205	0.2017	0.2371	0.2734
MWT	0.1287	0.1250	0.1435	0.1880	0.2209
DeepONet	0.2484	0.2483	0.2469	0.2547	0.2691
PINO	0.1559	0.1549	0.1607	0.1932	0.2244
PI-DeepONet	0.2792	0.2801	0.2820	0.2822	0.2861

(b) λ_{err} , the relative error of the learned parameter

	0%	0.1%	1%	5%	10%
PCANN	0.1151	0.1152	0.1144	0.1211	0.1373
PCALin	0.0929	0.0929	0.0929	0.0931	0.0934
FNO	0.0104	0.0105	0.0174	0.0711	0.1362
U-FNO	0.0477	0.0517	0.0419	0.0698	0.1145
MWT	0.0129	0.0125	0.0177	0.0544	0.1032
DeepONet	0.0480	0.0484	0.0495	0.0773	0.1190
PINO	0.0167	0.0164	0.0211	0.0567	0.1065
PI-DeepONet	0.0586	0.0593	0.0604	0.0816	0.1244

(c) \tilde{u}_{err} , the relative error between the solution of the learned parameter and the noisy solution.

	0%	0.1%	1%	5%	10%
PCANN	0.1151	0.1152	0.1144	0.1207	0.1363
PCALin	0.0929	0.0929	0.0929	0.0928	0.0923
FNO	0.0210	0.0212	0.0223	0.0329	0.0421
U-FNO	0.0477	0.0517	0.0395	0.0437	0.0496
MWT	0.0129	0.0125	0.0142	0.0209	0.0276
DeepONet	0.0480	0.0484	0.0483	0.0561	0.0597
PINO	0.0167	0.0164	0.0181	0.0250	0.0349
PI-DeepONet	0.0586	0.0593	0.0593	0.0614	0.0677

(d) u_{err} , the relative error between the solution of the learned parameter and the noiseless solution.

Table 9: Effects of noise on Tikhonov-based Inverse Problems on the Darcy Flow problem with PWC coefficients, using a dataset of resolution of 65×65 . The errors shown here are averaged over 100 test samples.

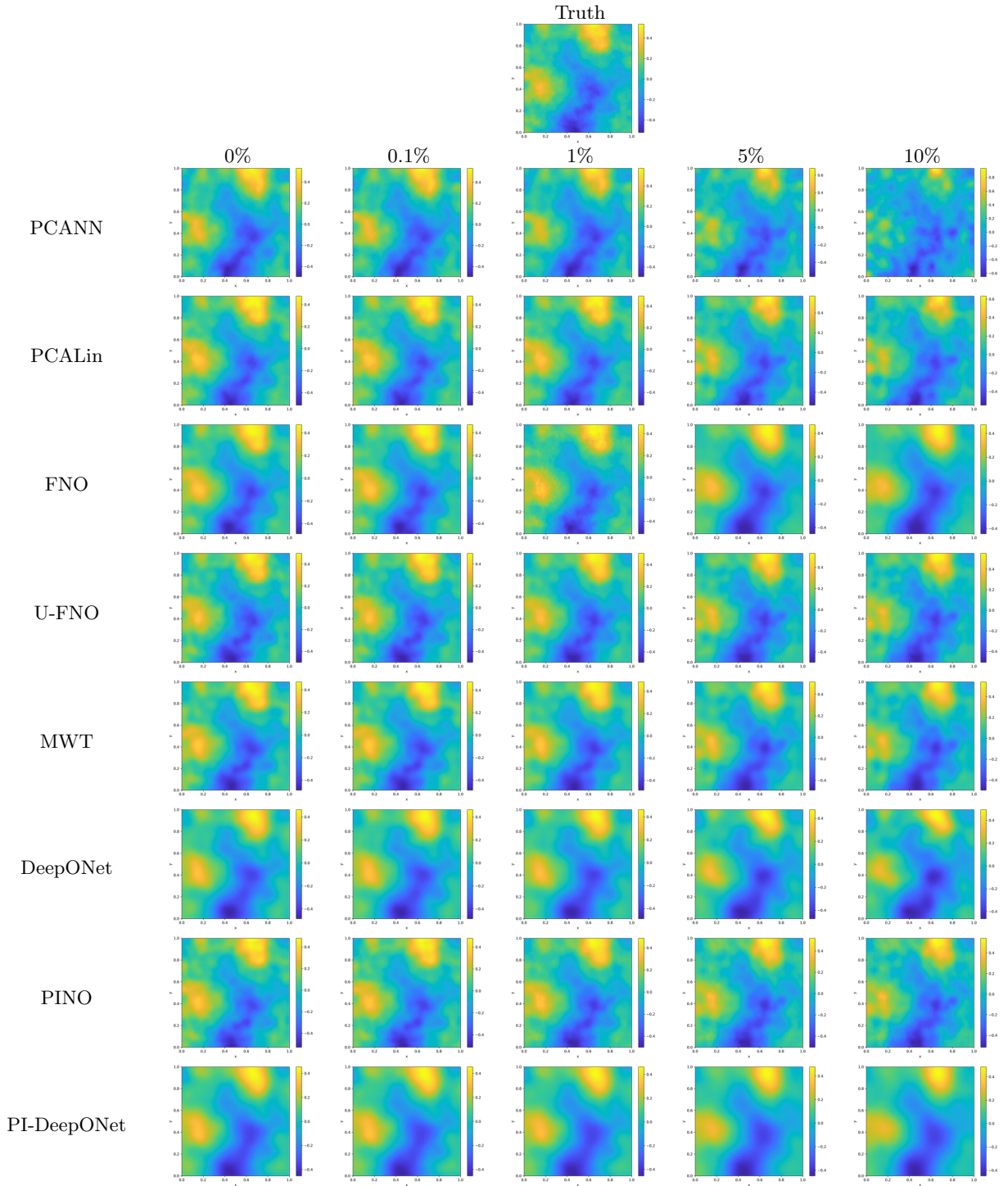


Table 10: Effects of noise on Tikhonov-based Inverse Problems on the Poisson problem, using dataset of, resolution of 65×65 .

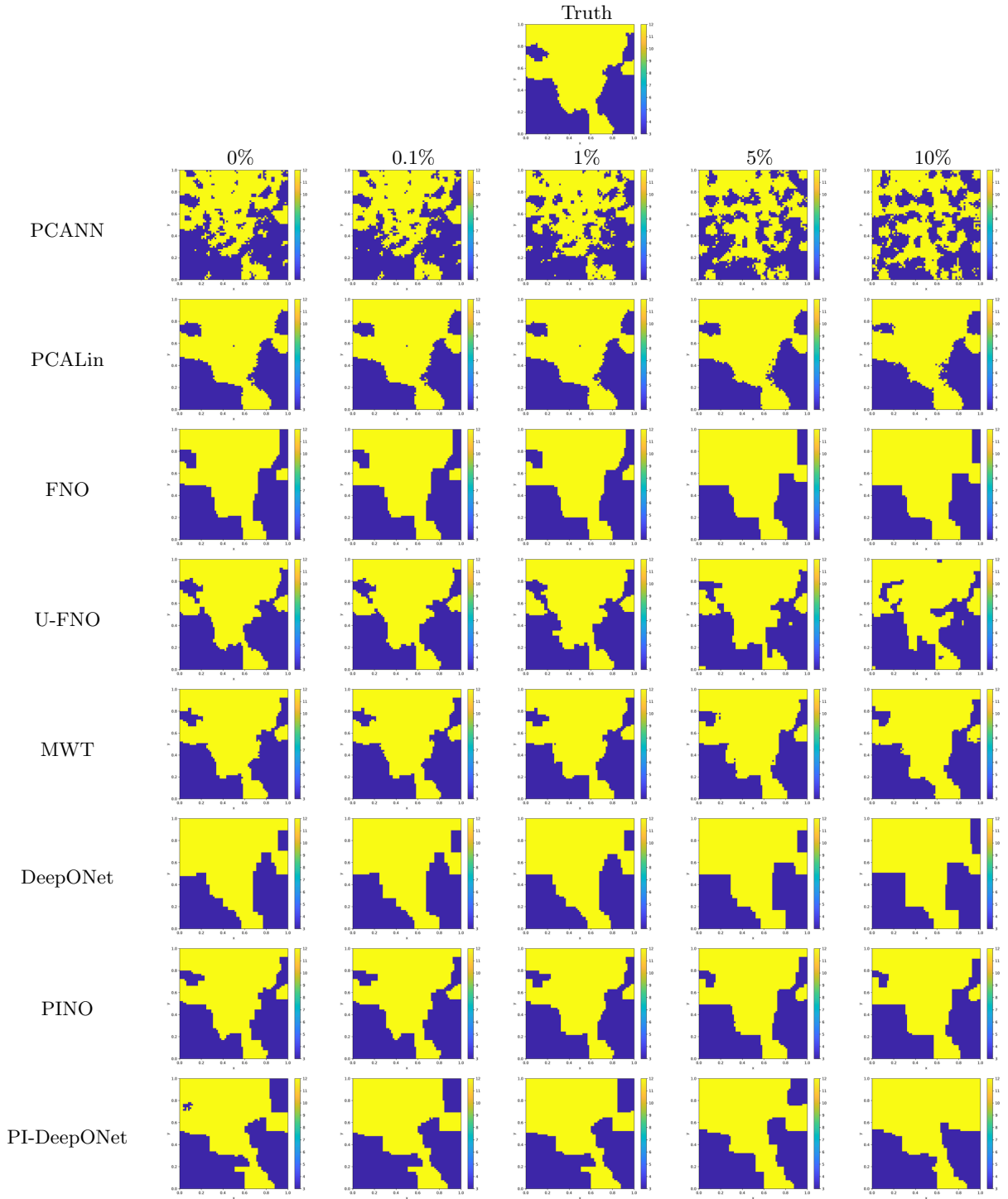


Table 11: Effects of noise on Tikhonov-based Inverse Problems on the Darcy Flow pwc problem, using dataset of, resolution of 65×65 .

5.4 Industrial Application Problems

5.4.1 A moving domain problem

Digital twins are ranked amongst the most influential technological developments of our decade, e.g. the Gartner report ranks digital twins or AI engineering amongst the Top 10 strategic development trends in all reports since 2018, [84, 85]. These digital twins combine data-driven concepts with domain specific expert knowledge, most often in the form of DL solvers for PDE models.

One particular characteristic, which sets industrial applications apart from typical academic examples, is the domain of definition. In an industrial setting, these geometries tend to be complex, e.g. given by the shape of a production device or restricted measurement geometries.

Particularly challenging are applications, where differential equations have to be solved on moving domains, e.g. the heat development inside a rotating electrical engine. The implementation of classical mesh-based methods are rather involved, e.g. computing the system matrix typically requires non-standard concepts, and they are expensive to solve. To tackle these problems, and other differential equations, with deep learning approaches, we developed, in collaboration with Bosch, the software package TORCHPHYSICS, cf. [96]. One characteristic feature of TorchPhysics is an easy-to-use generator for complex domains and geometries: Based on subtraction, addition and cross-product operations more and more complex geometries can be created from basic constituents. Another characteristic is the unbiased choice amongst several DL-coders for solving forward or inverse problems.

In this Section, we give a small insight on a problem we are currently investigating in collaboration with Bosch.

As an example for a moving domain, we consider the geometry shown in Fig. 17, which can be seen as a simplified sub-problem inside an electrical engine. The inside of the domain $\Omega(t, \omega)$ is filled with a fluid. We assume that the density of the incompressible fluid is $\rho = 1$ for simplicity. In the following, all physical values are in SI dimensions and they are not used. The blue outlined bar is rotating in time, inducing a circular motion onto the fluid. At the same time, the bar will heat up, and we also have to compute the temperature profile. Special in this problem is, that we are not only interested in one single solution, but try to approximate the system for different angular velocities ω of the rotating bar.

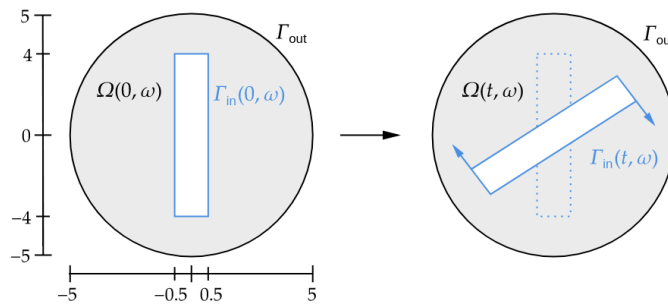


Figure 17: Time dependent rotating geometry in a circular housing

We consider the time interval $I_t := [0.0, 1.0]$ and interval for angular velocities $I_\omega := [\pi, 2\pi]$. To model the fluid inside the domain we use the incompressible Navier–Stokes equations in two dimensions, cf. [73]:

$$\begin{aligned} \partial_t u + (u \cdot \nabla) u &= \nu \Delta u - \nabla p \\ \nabla \cdot u &= 0. \end{aligned} \tag{46}$$

Here, $u(t, x)$ is the fluid velocity and ν the kinematic viscosity. For the modelling of the temperature we consider a heat equation with forced convection due to rotating geometry, cf. [26]:

$$\partial_t \theta + u \cdot \nabla \theta = a \Delta \theta \tag{47}$$

with thermal diffusion coefficient a . Convection due to a temperature depending density is not considered due the assumption of incompressibility of the fluid. Initially, at $t = 0$, we set $u = (0, 0)$, $p = 0$ and assume

a uniform temperature distribution $\theta = 270$ in the domain Ω . At the outer boundary Γ_{out} we set a no-slip condition for the fluid flow and a Dirichlet condition for the temperature θ :

$$\begin{aligned} u(x, y, t; \omega) &= (0, 0), \quad \text{for } (x, y, t, \omega) \in \Gamma_{\text{out}} \times I_t \times I_\omega \\ \theta(x, y, t; \omega) &= 270, \quad \text{for } (x, y, t, \omega) \in \Gamma_{\text{out}} \times I_t \times I_\omega \end{aligned}$$

The rotation of the rod is given by the matrix

$$A(t; \omega) := \begin{pmatrix} \cos(-\omega t(1 - e^{-\omega t})) & -\sin(-\omega t(1 - e^{-\omega t})) \\ \sin(-\omega t(1 - e^{-\omega t})) & \cos(-\omega t(1 - e^{-\omega t})) \end{pmatrix},$$

the factor $(1 - e^{-\omega t})$ is included to get a smooth start, which we scale with the rotation speed. Additionally $-\omega$ is used to get a clockwise rotation. As a heat source, a Dirichlet condition for the temperature on Γ_{in} is considered:

$$\theta(x, y, t; \omega) = 270 \text{ K} + 60(1 - e^{-\omega t}) \text{ K}, \quad \text{for } (x, y) \in \Gamma_{\text{in}}(t, \omega) \text{ and } (t, \omega) \in I_t \times I_\omega \quad (48)$$

For the fluid on Γ_{in} we again apply a no-slip condition. Because of the moving boundary, this translates to

$$u(x, y, t; \omega) = \omega d(x, y, t; \omega) \begin{pmatrix} \cos(-\omega t(1 - e^{-\omega t})) \\ \sin(-\omega t(1 - e^{-\omega t})) \end{pmatrix} (1 - e^{-\omega t} + \omega t e^{-\omega t}), \quad (49)$$

for all $(x, y) \in \Gamma_{\text{in}}(t, \omega)$ and $(t, \omega) \in I_t \times I_\omega$. Here $d(x, y, t; \omega)$ corresponds to the signed distance of the point (x, y) to the line perpendicular to the bar, which is running through the origin. This distance is given by:

$$d(x, y, t; \omega) := \begin{pmatrix} x \\ y \end{pmatrix} \cdot \begin{pmatrix} -\sin(-\omega t(1 - e^{-\omega t})) \\ \cos(-\omega t(1 - e^{-\omega t})) \end{pmatrix}$$

The distance has to be included, since points further away from the center have a higher radial velocity.

This concludes the general description of the application problem. If classical PDE solvers such as FEM or FDM solvers are used, we have to compute a new solution for each velocity value ω , that leads to costly simulations for each new parameter value. Furthermore, the most challenging part would be the implementation of discretization meshes for the moving domain. Especially, to correctly transfer the discrete solution data between different time steps to guarantee conservation of mass, momentum and energy.

By using a deep learning approach, we can try to learn the solutions for different values of ω in one single training process. Thus eliminating the need for new simulations for each ω .

This leads us to the crucial step of choosing a suitable DL method. In our case only the underlying differential equation is known, no data such as a solution for a particular parameter setting is available. Moreover only scalar parameters appear, hence we can use the classical PINN to learn the solution operator. Additionally, since PINNs are mesh-free, the implementation of the domain is easier, compared to the classical methods. One only has to correctly sample points inside the domain $\Omega(t, \omega)$ and on the boundary $\Gamma_{\text{in}}(t, \omega)$, for each combination of $(t, \omega) \in I_t \times I_\omega$, to train the needed conditions.

The library TORCHPHYSICS was developed with this time (and parameter) dependent domains in mind. Therefore, the previously explained domain can be easily defined in TORCHPHYSICS and the needed points sampled. An example for sampled points on $\Gamma_{\text{in}}(t, \omega)$, for different ω , is shown in Fig. 18. These points can then be created and used in each training step. The same is possible inside $\Omega(t, \omega)$. However, the visualization of inner points is more elaborate, so we do not show them here and refer any reader interested in more details to the TorchPhysics tutorial. To learn the problem's solution operators, we define three different neural networks $u_\Theta, p_\Theta, \theta_\Theta$, for fluid velocity, pressure, and temperature respectively. Every network has as an input the space and time variables (x, y, t) and, since we want to train the solution for different ω , also the angular velocity ω . The network u_Θ has two output neurons, for the two velocity components.

Since the neural networks have to fulfill multiple conditions, this can lead to problems while training. I.e. different loss terms may have varying preferred minimization directions. To somewhat simplify the optimization process, we apply hard constraints to naturally fulfill some of the conditions and simplify the output range of our neural networks. These constrained networks are denoted by $\tilde{u}_\Theta, \tilde{p}_\Theta, \tilde{\theta}_\Theta$. For the temperature we consider:

$$\tilde{\theta}_\Theta(x, y, t; \omega) = 60(1 - e^{-\omega t}) \left(1 - \frac{\sqrt{x^2 + y^2}}{r} \right) \theta_\Theta(x, y, t; \omega) + 270.$$

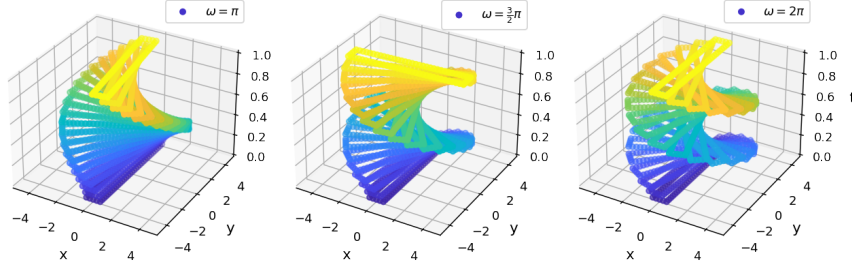


Figure 18: Example of sampled inner boundary points for the application problem. The points are only colored for visual representation.

In the following and the above equation, we omit the temperature unit. Our restricted network $\tilde{\theta}_\Theta$ fulfills the initial and outer boundary conditions. Here $r = 5$, describing the radius of the whole circle. The only constrain for the pressure is the time scale:

$$\tilde{p}_\Theta(x, y, t; \omega) = (1 - e^{-\omega t})p_\Theta(x, y, t; \omega).$$

To somewhat implement the movement of the rotating bar into our velocity network, we choose the constraints:

$$\tilde{u}_\Theta(x, y, t; \omega) = r\omega(1 - e^{-\omega t} + \omega t e^{-\omega t}) \begin{pmatrix} 1 - \frac{\sqrt{x^2 + y^2}}{r} \\ \cos(-\omega t(1 - e^{-\omega t}))u_{\Theta,1}(x, y, t; \omega) \\ \sin(-\omega t(1 - e^{-\omega t}))u_{\Theta,2}(x, y, t; \omega) \end{pmatrix}.$$

Again, \tilde{u}_Θ naturally satisfies the initial and boundary conditions on Γ_{out} . All neural networks are FCNs, with hyperbolic tangent as activation. The networks u_Θ, θ_Θ consist of seven hidden layers with 100 neurons each, and p_Θ use networks with 5 layers and 80 neurons.

The only conditions that have to be learned are the Eqs. (46)–(49)) This is done via the classical PINN approach, as described in Sec. 3.2, and applied to the constrained networks. Since the temperature does not influence the fluid profile, we first train the solution of the Navier-Stokes equations. Then, the results are used in the training of the heat equation. For the optimization process, Adam is used and randomly distributed training points are resampled in each iteration, for both the inner part and the moving boundary.

ρ	ν	a
1.0	2.0	0.5

Table 12: Material and operation parameter

The results are presented in Figs. 19 and 20. Here two aspects have to be mentioned. Firstly, getting convergence of the training loss was rather challenging, and relatively large loss values for the divergence and heat term were obtained. Secondly, no reference solution is currently available. Therefore, we can not directly measure the accuracy of the learned approximation. Solely from a physical point of view, the results appear reasonable and would allow for a first step in a rapid prototyping cycle. However, this aspect has to be further investigated, in general, the research for this problem is, from our side, in a rather early stage. This example is shown primarily to present a new application area (moving domains) for the deep learning approaches, where they may be advantageous compared to classical methods, and to demonstrate the potential of TORCHPHYSICS.

5.4.2 Identification of material model parameters from stress tensor (Volkswagen, Fraunhofer ITWM)

To shorten the design cycle of vehicles and to reduce the cost of development, automotive industries employ numerical simulation tools in the vehicle development process for testing and analysis. In this application example, we are interested in the interaction of vehicles with various roadbeds such as sand, snow, mud, etc. Vehicle stability depends largely on this interaction, and the safety of the passengers is thus a concern. To

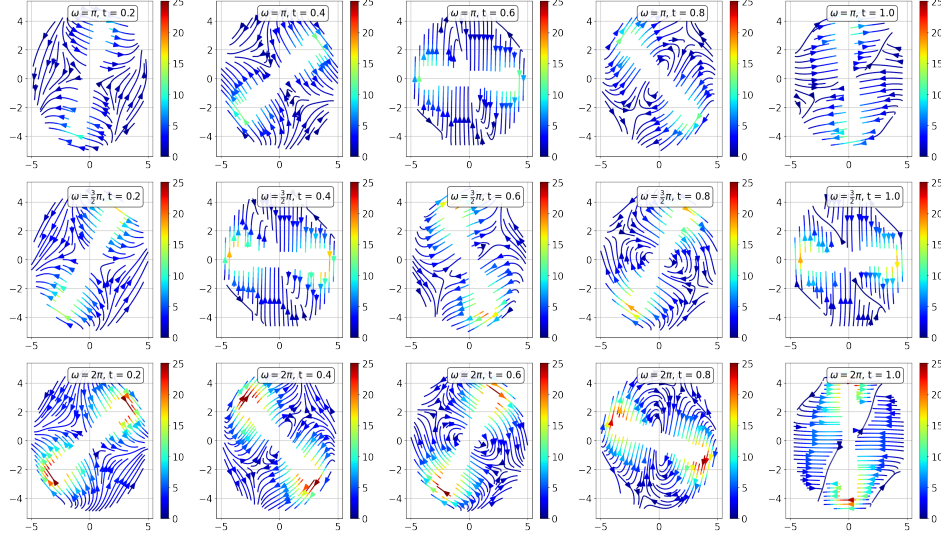


Figure 19: Learned velocity profile for different angular velocities ω , at some discrete time steps.

approach this problem, a full-body model of the vehicle dynamics is needed as well as proper modeling of the roadbed. Of interest to us, is the modeling of the roadbed consisting of granular material. This is a continuum mechanics problem that involves not only the well-known conservation equations of mass, momentum, and energy but also, supplementary phenomenological material models. While the former specify the process conditions and are generally well understood, the latter relates the applied strain to the resulting stress and comes with uncertainties as well as non-linearities. Obviously, the overall goal is for the simulations to match the real-life experiments, thus the selected material model is of great importance.

Material models have parameters that are specific to the considered material as well as its reaction to external conditions, and these models range from simple to complex. By using single-parametric models for the granular material (roadbed), for example, one notices an increasing deviation between simulations and experiments as the simulation time progresses. Also, the simulations have long running times. As a result, complex material models with many more parameters are used. Such parameters are usually determined by a great wealth of expert knowledge, and costly experiments. The barodesy model [50, 51] is one of such complex material models which conforms to the basic mechanical properties of the material. It is formulated in tensorial form by Equations (50)–(51).

$$\frac{d\mathbf{S}}{dt} = \mathbf{W}\mathbf{S} - \mathbf{S}\mathbf{W} + \mathbf{H}(\mathbf{S}, \mathbf{D}, e) \quad (50)$$

$$\frac{de}{dt} = (1 + e) \cdot \text{tr}(\mathbf{D}), \quad (51)$$

with

$$\begin{aligned} \mathbf{D} &= \frac{1}{2} \left(\nabla \mathbf{v}^T + (\nabla \mathbf{v}^T)^T \right) & \mathbf{R} &= \text{tr}(\mathbf{D}^0) \cdot \mathbf{I} + c_1 \cdot \exp(c_2 \cdot \mathbf{D}^0) \\ \mathbf{W} &= \frac{1}{2} \left(\nabla \mathbf{v}^T - (\nabla \mathbf{v}^T)^T \right) & h_b &= \sigma^{c_3} \\ \mathbf{H}(\mathbf{S}, \mathbf{D}, e) &= h_b(\sigma) \cdot (f_b \mathbf{R}^0 + g_b \mathbf{S}^0) \cdot |\mathbf{D}| & f_b &= c_4 \cdot \text{tr}(\mathbf{D}^0) + c_5 \cdot (e - e_c) + c_6 \\ \sigma &= |\mathbf{S}| = \sqrt{\text{tr}(\mathbf{S}^2)} & g_b &= -c_6 \\ \mathbf{S}^0 &= \mathbf{S}/|\mathbf{S}|, \mathbf{D}^0 = \mathbf{D}/|\mathbf{D}|, \mathbf{R}^0 = \mathbf{R}/|\mathbf{R}| & e_c &= (1 + e_{c0}) \cdot \exp\left(\frac{\sigma^{1-c_3}}{c_4 \cdot (1 - c_3)}\right) - 1 \end{aligned}$$

where

- \mathbf{S} is the Cauchy stress tensor (with principal stresses $\sigma_1, \sigma_2, \sigma_3$ in axial and lateral directions),

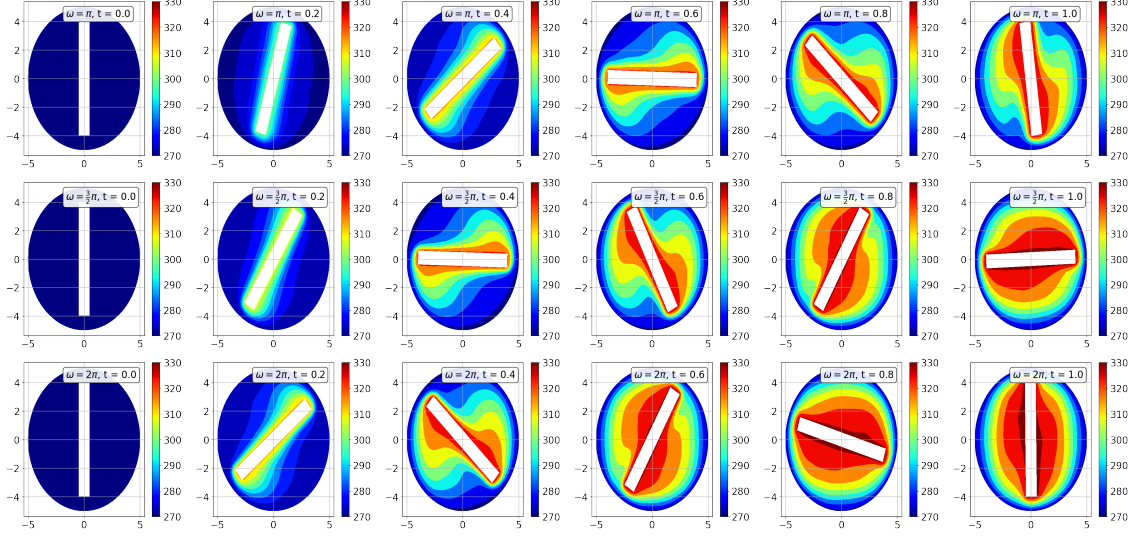


Figure 20: Learned temperature profile for different angular velocities ω , at some discrete time steps.

- \mathbf{W} is the antisymmetric part of the velocity gradient,
- \mathbf{D} is the stretching tensor (the symmetric part of the velocity gradient),
- $e = V_p/V_s$ is the void ratio, with critical void ratio e_c where V_p and V_s are the volume of pores and solids (grains).

The function \mathbf{H} introduces the material parameters $c_1, c_2, c_3, c_4, c_5, c_6$, and ec_0 , which we will identify via deep learning in a supervised task.

Using the MESHFREE software [55] we generate parameters-stress pairs to train our neural network. MESHFREE employs a Generalized Finite Difference Method (GFDM): a meshless approach to numerically solve (coupled) PDEs based on their strong formulation on a sufficiently dense cloud of points carrying the physical information (such as velocity, pressure, etc.). A weighted moving least squares method is used to approximate the required spatial partial derivatives on a finite point set [74,83]. MESHFREE has successfully been applied for the simulation of complex continuum mechanics problems in industry, like mining [75], flow inside a turbine [56], and vehicles travelling through water [45], just to name a few.

In our case, the simulation setting is that of the oedometric test: one of two benchmark problems usually considered in soil mechanics to, e.g., check and calibrate material models. It does so by simulating a one-dimensional compression; the soil (material) sample is loaded in axial direction and rigid side walls prevent any lateral expansion as demonstrated in Figure 21a. Figure 21b shows the initial point cloud configuration for this test.

PCA is used to reduce the dimensions of the principal stress component from 675 to 50. This reduced dimension is then used as input to the FCN (fully connected network) similar to that in Section 4.1. Since the parameter space is low enough, no PCA is used after the FCN. As a result, the output of the FCN yields the target parameters directly. Of the 6000 data pairs generated, 75% is used for training. During training, the relative L2 error of the individual parameters is calculated and their average is the loss function minimized for training the network. However, due to the nature of this loss function, the learning of the parameters of higher magnitude is favoured. As remedy, the parameters of lower magnitude are scaled so that they are of the same order (of thousands) as the parameters of higher magnitude. In this way, learning of all the individual parameters is achieved. We obtained an average relative L2 test error of 2.63×10^{-3} on the test data set. Figure 22 shows the comparison of the ground truth (MESHFREE simulation in blue) and the learned parameters (PCANN in orange). A detailed discussion of this application is currently in preparation [82].

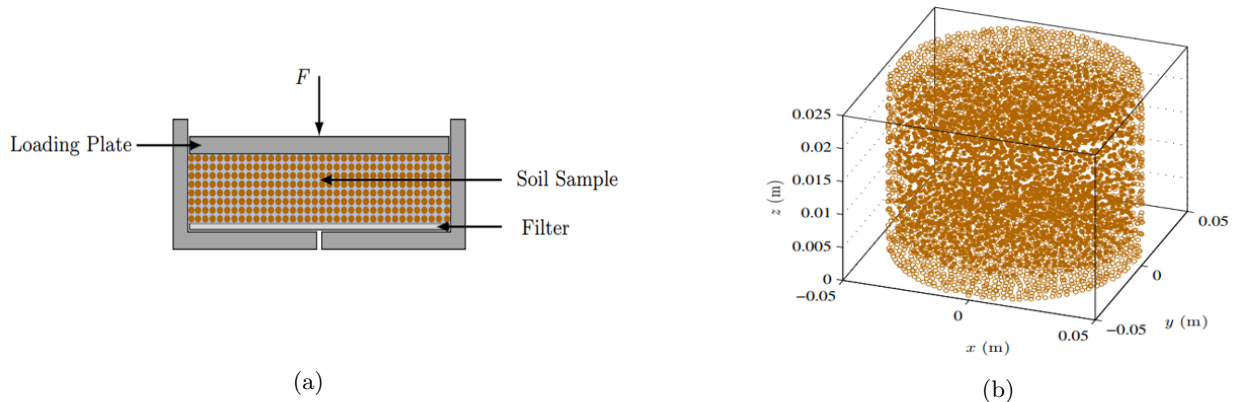


Figure 21: (a) Schematic illustration of the oedometric test. (b) Initial FPM point cloud configuration for the oedometric test (filled circles: interior points, non-filled circles: boundary points) using MESHFREE (see [83])

6 Conclusions

The presented surveys aims at developing a guideline on whether and how to use deep learning concepts for PDE based forward solvers and related inverse problems. To this end we have implemented and tested the most widely used neural network concepts as well as several of their extensions for the two most common PDE problems (Poisson, Darcy flow). In addition, we have applied neural networks concepts to two industrial projects. There is no unique criterion for determining the best method, this very much depend on the specific task at hand. Hence, we presented a survey of numerical values for each method, which should allow the user to evaluate the particular criterion relevant for its specific application and to determine a suitable method accordingly.

Nevertheless, we want to highlight some general findings. Within this restricted scope of our test environment, we have found the following conclusions. DL concepts for solely solving forward problems lack precision as compared with classical FEM methods. However, in general they achieve reasonable accuracy and offer great potential for efficient parameter studies, e.g. for applications in rapid prototyping.

Our findings differ depending on whether the underlying PDE is linear or non-linear and whether training data, i.e. sufficiently many parameter-state pairs are known, is available.

For a linear PDE and if only the PDE is known but no data is available, we propose to use PINN for solving the forward problem. If data, i.e. sufficiently many parameter-state pairs are known, then PCA or even better PCALin are an excellent starting point. As mentioned, this is only a first indication, our tests were restricted to the Poisson problem. Surprisingly, see Table 7 there is not much difference between those concepts for solving the inverse Poisson problem by backward operator training. All methods considered produce reliable results e.g. for 5% noise in the data. Hence, run times might be the criterion for decision. Obviously concepts for operator training are advantageous and DeepONet and PI-DeepONet are the overall winners in terms of efficiency.

The Poisson forward problem is a rather simple linear elliptic PDE. Hence, the numerical test should be seen as some preliminary test giving some limited insight on the behavior of DL concepts for forward linear PDEs. As we will see from the more evolved examples, the findings in this section have only a limited meaning for more general cases.

Concerning industrial applications, additional features gain influence. E.g. the simulation of heat inside a rotating engine requires to work with a time-dependent domain of definition. Most codes will require substantial additional work when dealing with such complex domains. TorchPhysics offers an accessible concept for working with such domains, which in connection with a standard PINN concept did yield good performance for a parametric study in this context.

The other industrial problem of identifying parameters in a problem of mechanical engineering reduces to a rather low-dimensional task and can be solved by PCANN. Hence, choosing a method suitable for a given industrial problem requires problem-specific considerations, which have to be evaluated task by task.

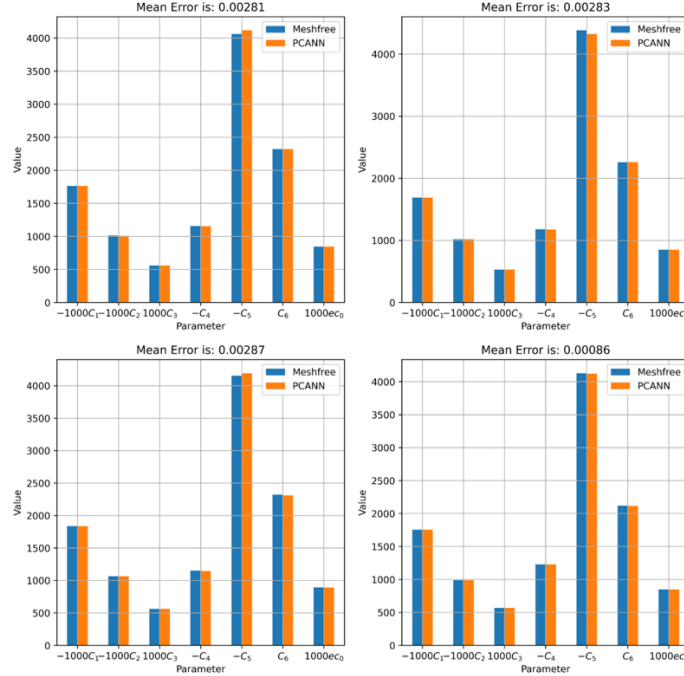


Figure 22: Comparison of ground truth(MESHFREE simulation in blue) and learned parameters (PCANN in orange) for four randomly chosen examples of the oedometric test

We should remark, that the size of the network differs considerably. We have performed rather extensive hyper-parameter searches for each method. The reported network sizes did yield the best results. E.g. the DRM does not benefit from extending the network to larger sizes for the mentioned application.

In the Table 1, we list the properties of classical methods, Deep Ritz method in [110], PINN in [88], model reduction and Neural Network in [8], DeepONets in [69] and Fourier Neural Operator [61]. We should mention that the properties only correspond to the methods in these mentioned papers, since by some modifications, they can have different properties. For example, the PINN may be used to model parameter-solution operators.

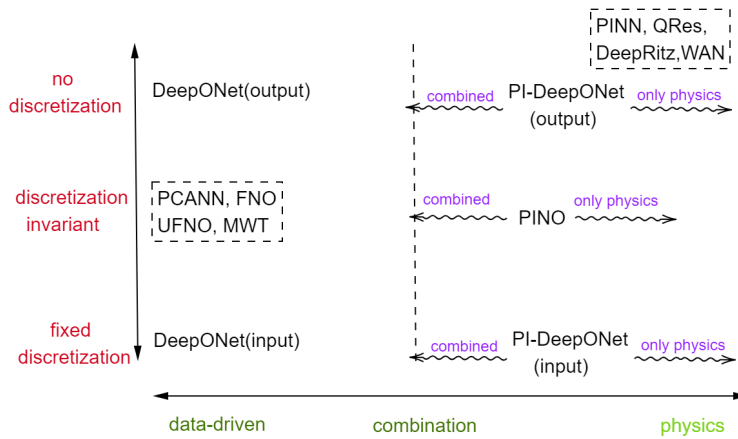


Figure 23: Deep Learning methods for PDE.

The above discussed methods have shown their high potential for solving PDEs as well as their related parametric studies and inverse problems. Whenever efficiency is an issue, these methods perform most

convincingly. However, there are still many open questions and problems that are common in deep learning community. Hyperparameter search can be very time consuming and would benefit from a sound theoretical foundation. Also the choice of activation functions and loss function can be more refined.

References

- [1] Christian Aarset, Martin Holler, and Tram Thi Ngoc Nguyen. Learning-informed parameter identification in nonlinear time-dependent pdes. *arXiv preprint arXiv:2202.10915*, 2022.
- [2] Jonas Adler and Ozan Öktem. Learned primal-dual reconstruction. *IEEE transactions on medical imaging*, 37(6):1322–1332, 2018.
- [3] Simon Arridge and Andreas Hauptmann. Networks for nonlinear diffusion problems in imaging. *Journal of Mathematical Imaging and Vision*, 62(3):471–487, 2020.
- [4] Simon Arridge, Peter Maass, Ozan Öktem, and Carola-Bibiane Schönlieb. Solving inverse problems using data-driven models. *Acta Numerica*, 28:1–174, 2019.
- [5] Gang Bao, Xiaojing Ye, Yaohua Zang, and Haomin Zhou. Numerical solution of inverse problems by weak adversarial networks. *Inverse Problems*, 36(11):115003, 2020.
- [6] Atilim Gunes Baydin, Barak A Pearlmutter, Alexey Andreyevich Radul, and Jeffrey Mark Siskind. Automatic differentiation in machine learning: a survey. *Journal of Machine Learning Research*, 18:1–43, 2018.
- [7] Christian Beck, Sebastian Becker, Patrick Cheridito, Arnulf Jentzen, and Ariel Neufeld. Deep splitting method for parabolic pdes. *SIAM Journal on Scientific Computing*, 43(5):A3135–A3154, 2021.
- [8] Kaushik Bhattacharya, Bamdad Hosseini, Nikola B Kovachki, and Andrew M Stuart. Model reduction and neural networks for parametric pdes. *arXiv preprint arXiv:2005.03180*, 2020.
- [9] Lennard Bösel, Moritz Thürlmann, and Sereina Riniker. Machine learning in qm/mm molecular dynamics simulations of condensed-phase systems. *Journal of Chemical Theory and Computation*, 17(5):2641–2658, 2021.
- [10] Susanne C. Brenner and Larkin R. Scott. *The Mathematical Theory of Finite Element Methods*, volume 15 of *Texts in Applied Mathematics*. Springer, 2008.
- [11] Jie Bu and Anuj Karpatne. Quadratic residual networks: A new class of neural networks for solving forward and inverse problems in physics involving pdes. In *Proceedings of the 2021 SIAM International Conference on Data Mining (SDM)*, pages 675–683. SIAM, 2021.
- [12] Martin Burger and Andreas Neubauer. Analysis of tikhonov regularization for function approximation by neural networks. *Neural Networks*, 16(1):79–90, 2003.
- [13] Jiun-Shyan Chen, Michael Hillman, and Sheng-Wei Chi. Meshfree methods: Progress made after 20 years. *Journal of Engineering Mechanics*, 143(4):04017001, 2017.
- [14] Tianping Chen and Hong Chen. Universal approximation to nonlinear operators by neural networks with arbitrary activation functions and its application to dynamical systems. *IEEE Transactions on Neural Networks*, 6(4):911–917, 1995.
- [15] Yuyao Chen, Lu Lu, George Em Karniadakis, and Luca Dal Negro. Physics-informed neural networks for inverse problems in nano-optics and metamaterials. *Optics express*, 28(8):11618–11633, 2020.
- [16] Ludovica Cicci, Stefania Fresca, and Andrea Manzoni. Deep-hyromnet: A deep learning-based operator approximation for hyper-reduction of nonlinear parametrized pdes. *arXiv preprint arXiv:2202.02658*, 2022.

- [17] Daniele Colombo, Ersan Turkoglu, Weichang Li, and Diego Rovetta. Coupled physics-deep learning inversion. *Computers & Geosciences*, 157:104917, 2021.
- [18] Salvatore Cuomo, Vincenzo Schiano di Cola, Fabio Giampaolo, Gianluigi Rozza, Maziar Raissi, and Francesco Piccialli. Scientific machine learning through physics-informed neural networks: Where we are and what’s next, 2022.
- [19] George Cybenko. Approximation by superpositions of a sigmoidal function. *Mathematics of control, signals and systems*, 2(4):303–314, 1989.
- [20] Maarten De Hoop, Daniel Zhengyu Huang, Elizabeth Qian, and Andrew M Stuart. The cost-accuracy trade-off in operator learning with neural networks. *arXiv preprint arXiv:2203.13181*, 2022.
- [21] Beichuan Deng, Yeonjong Shin, Lu Lu, Zhongqiang Zhang, and George Em Karniadakis. Convergence rate of deepnets for learning operators arising from advection-diffusion equations. *arXiv preprint arXiv:2102.10621*, 2021.
- [22] Sören Dittmer, Tobias Kluth, Peter Maass, and Daniel Otero Bager. Regularization by architecture: A deep prior approach for inverse problems. *Journal of Mathematical Imaging and Vision*, 62(3):456–470, oct 2019.
- [23] Patrick Dondl, Johannes Müller, and Marius Zeinhofer. Uniform convergence guarantees for the deep ritz method for nonlinear problems. *arXiv preprint arXiv:2111.05637*, 2021.
- [24] Claudia Drygala, Benjamin Winhart, Francesca di Mare, and Hanno Gottschalk. Generative modeling of turbulence. *Physics of Fluids*, 34(3):035114, 2022.
- [25] Chenguang Duan, Yuling Jiao, Yanming Lai, Xiliang Lu, and Zhijian Yang. Convergence rate analysis for deep ritz method. *arXiv preprint arXiv:2103.13330*, 2021.
- [26] N. Elsner. *Grundlagen der technischen Thermodynamik*. Akademie-Verlag, 1988.
- [27] Stefania Fresca, Luca Dede, and Andrea Manzoni. A comprehensive deep learning-based approach to reduced order modeling of nonlinear time-dependent parametrized pdes. *Journal of Scientific Computing*, 87(2):1–36, 2021.
- [28] Stefania Fresca, Giorgio Gobat, Patrick Fedeli, Attilio Frangi, and Andrea Manzoni. Deep learning-based reduced order models for the real-time simulation of the nonlinear dynamics of microstructures. *International Journal for Numerical Methods in Engineering*, 123(20):4749–4777, 2022.
- [29] Stefania Fresca and Andrea Manzoni. Real-time simulation of parameter-dependent fluid flows through deep learning-based reduced order models. *Fluids*, 6(7):259, 2021.
- [30] Stefania Fresca and Andrea Manzoni. Pod-dl-rom: enhancing deep learning-based reduced order models for nonlinear parametrized pdes by proper orthogonal decomposition. *Computer Methods in Applied Mechanics and Engineering*, 388:114181, 2022.
- [31] Stefania Fresca, Andrea Manzoni, Luca Dedè, and Alfio Quarteroni. Deep learning-based reduced order models in cardiac electrophysiology. *PloS one*, 15(10):e0239416, 2020.
- [32] Shailesh Garg and Souvik Chakraborty. Variational bayes deep operator network: A data-driven bayesian solver for parametric differential equations. *arXiv preprint arXiv:2206.05655*, 2022.
- [33] Pulkit Gopalani, Sayar Karmakar, and Anirbit Mukherjee. Capacity bounds for the deepnet method of solving differential equations. *arXiv preprint arXiv:2205.11359*, 2022.
- [34] Somdatta Goswami, Aniruddha Bora, Yue Yu, and George Em Karniadakis. Physics-informed deep neural operator networks. *arXiv preprint arXiv:2207.05748*, 2022.
- [35] Somdatta Goswami, Minglang Yin, Yue Yu, and George Karniadakis. A physics-informed variational deepnet for predicting the crack path in brittle materials. *arXiv preprint arXiv:2108.06905*, 2021.

- [36] Gaurav Gupta, Xiongye Xiao, and Paul Bogdan. Multiwavelet-based operator learning for differential equations. *Advances in Neural Information Processing Systems*, 34:24048–24062, 2021.
- [37] Joachim Gwinner and Ernst Peter Stephan. *Advanced boundary element methods*. Springer, 2018.
- [38] Eldad Haber and Lars Ruthotto. Stable architectures for deep neural networks. *Inverse problems*, 34(1):014004, 2017.
- [39] Patrik Simon Hadorn. Shift-deeponet: Extending deep operator networks for discontinuous output functions. In *Master thesis, ETH Computational Science and Engineering*. ETH Zurich, Seminar for Applied Mathematics, 2022.
- [40] Andreas Hauptmann and Ben T Cox. Deep learning in photoacoustic tomography: current approaches and future directions. *Journal of Biomedical Optics*, 25(11):112903, 2020.
- [41] Kurt Hornik, Maxwell Stinchcombe, and Halbert White. Multilayer feedforward networks are universal approximators. *Neural networks*, 2(5):359–366, 1989.
- [42] Arthur Jacot, Franck Gabriel, and Clément Hongler. Neural tangent kernel: Convergence and generalization in neural networks, 2020.
- [43] Ameya D Jagtap and George Em Karniadakis. Extended physics-informed neural networks (xpinns): A generalized space-time domain decomposition based deep learning framework for nonlinear partial differential equations. *Communications in Computational Physics*, 28(5):2002–2041, 2020.
- [44] Ameya D Jagtap, Ehsan Kharazmi, and George Em Karniadakis. Conservative physics-informed neural networks on discrete domains for conservation laws: Applications to forward and inverse problems. *Computer Methods in Applied Mechanics and Engineering*, 365:113028, 2020.
- [45] Anthony Jefferies, Jörg Kuhnert, Lars Aschenbrenner, and Uwe Giffhorn. Finite pointset method for the simulation of a vehicle travelling through a body of water. In *Meshfree methods for partial differential equations VII*, pages 205–221. Springer, 2015.
- [46] Yuling Jiao, Yanming Lai, Yisu Lo, Yang Wang, and Yunfei Yang. Error analysis of deep ritz methods for elliptic equations. *arXiv preprint arXiv:2107.14478*, 2021.
- [47] Pengzhan Jin, Shuai Meng, and Lu Lu. Mionet: Learning multiple-input operators via tensor product. *arXiv preprint arXiv:2202.06137*, 2022.
- [48] John Jumper, Richard Evans, Alexander Pritzel, Tim Green, Michael Figurnov, Olaf Ronneberger, Kathryn Tunyasuvunakool, Russ Bates, Augustin Žídek, Anna Potapenko, et al. Highly accurate protein structure prediction with alphafold. *Nature*, 596(7873):583–589, 2021.
- [49] George Em Karniadakis, Ioannis G Kevrekidis, Lu Lu, Paris Perdikaris, Sifan Wang, and Liu Yang. Physics-informed machine learning. *Nature Reviews Physics*, 3(6):422–440, 2021.
- [50] D Kolymbas. Barodesy: a new constitutive frame for soils. *Géotechnique Letters*, 2(2):17–23, 2012.
- [51] D Kolymbas. Barodesy: a new hypoplastic approach. *International Journal for Numerical and Analytical Methods in Geomechanics*, 36(9):1220–1240, 2012.
- [52] Nikola Kovachki, Samuel Lanthaler, and Siddhartha Mishra. On universal approximation and error bounds for fourier neural operators. *Journal of Machine Learning Research*, 22:Art–No, 2021.
- [53] Nikola Kovachki, Zongyi Li, Burigede Liu, Kamyar Azizzadenesheli, Kaushik Bhattacharya, Andrew Stuart, and Anima Anandkumar. Neural operator: Learning maps between function spaces. *arXiv preprint arXiv:2108.08481*, 2021.
- [54] Nikola Kovachki, Burigede Liu, Xingsheng Sun, Hao Zhou, Kaushik Bhattacharya, Michael Ortiz, and Andrew Stuart. Multiscale modeling of materials: Computing, data science, uncertainty and goal-oriented optimization. *Mechanics of Materials*, 165:104156, 2022.

- [55] Jörg Kuhnert. Meshfree simulations in car design: closing the gaps of classical simulation tools. *German Success Stories in Industrial Mathematics*, 35:130, 2021.
- [56] Jörg Kuhnert, Isabel Michel, and Reiner Mack. Fluid structure interaction (fsi) in the meshfree finite pointset method (fpm): Theory and applications. In *International workshop on meshfree methods for partial differential equations*, pages 73–92. Springer, 2017.
- [57] Samuel Lanthaler, Siddhartha Mishra, and George E Karniadakis. Error estimates for deeponets: A deep learning framework in infinite dimensions. *Transactions of Mathematics and Its Applications*, 6(1):tnac001, 2022.
- [58] R. J. LeVeque. *Finite Volume Methods for Hyperbolic Problems*. Cambridge University Press, 2002.
- [59] Housen Li, Johannes Schwab, Stephan Antholzer, and Markus Haltmeier. Nett: Solving inverse problems with deep neural networks. *Inverse Problems*, 2018.
- [60] Zongyi Li, Daniel Zhengyu Huang, Burigede Liu, and Anima Anandkumar. Fourier neural operator with learned deformations for pdes on general geometries. *arXiv preprint arXiv:2207.05209*, 2022.
- [61] Zongyi Li, Nikola Kovachki, Kamyar Azizzadenesheli, Burigede Liu, Kaushik Bhattacharya, Andrew Stuart, and Anima Anandkumar. Fourier neural operator for parametric partial differential equations. *arXiv preprint arXiv:2010.08895*, 2020.
- [62] Zongyi Li, Nikola Kovachki, Kamyar Azizzadenesheli, Burigede Liu, Kaushik Bhattacharya, Andrew Stuart, and Anima Anandkumar. Neural operator: Graph kernel network for partial differential equations. *arXiv preprint arXiv:2003.03485*, 2020.
- [63] Zongyi Li, Nikola Kovachki, Kamyar Azizzadenesheli, Burigede Liu, Andrew Stuart, Kaushik Bhattacharya, and Anima Anandkumar. Multipole graph neural operator for parametric partial differential equations. *Advances in Neural Information Processing Systems*, 33:6755–6766, 2020.
- [64] Zongyi Li, Hongkai Zheng, Nikola Kovachki, David Jin, Haoxuan Chen, Burigede Liu, Kamyar Azizzadenesheli, and Anima Anandkumar. Physics-informed neural operator for learning partial differential equations. *arXiv preprint arXiv:2111.03794*, 2021.
- [65] Yulei Liao and Pingbing Ming. Deep nitsche method: Deep ritz method with essential boundary conditions. *arXiv preprint arXiv:1912.01309*, 2019.
- [66] Guang Lin, Christian Moya, and Zecheng Zhang. Accelerated replica exchange stochastic gradient langevin diffusion enhanced bayesian deeponet for solving noisy parametric pdes. *arXiv preprint arXiv:2111.02484*, 2021.
- [67] Burigede Liu, Nikola Kovachki, Zongyi Li, Kamyar Azizzadenesheli, Anima Anandkumar, Andrew M Stuart, and Kaushik Bhattacharya. A learning-based multiscale method and its application to inelastic impact problems. *Journal of the Mechanics and Physics of Solids*, 158:104668, 2022.
- [68] Lizuo Liu and Wei Cai. Multiscale deeponet for nonlinear operators in oscillatory function spaces for building seismic wave responses. *arXiv preprint arXiv:2111.04860*, 2021.
- [69] Lu Lu, Pengzhan Jin, and George Em Karniadakis. Deeponet: Learning nonlinear operators for identifying differential equations based on the universal approximation theorem of operators. *arXiv preprint arXiv:1910.03193*, 2019.
- [70] Lu Lu, Xuhui Meng, Shengze Cai, Zhiping Mao, Somdatta Goswami, Zhongqiang Zhang, and George Em Karniadakis. A comprehensive and fair comparison of two neural operators (with practical extensions) based on fair data. *Computer Methods in Applied Mechanics and Engineering*, 393:114778, 2022.
- [71] Lu Lu, Xuhui Meng, Zhiping Mao, and George Em Karniadakis. Deepxde: A deep learning library for solving differential equations. *SIAM Review*, 63(1):208–228, 2021.

- [72] Lu Lu, Raphael Pestourie, Wenjie Yao, Zhicheng Wang, Francesc Verdugo, and Steven G Johnson. Physics-informed neural networks with hard constraints for inverse design. *SIAM Journal on Scientific Computing*, 43(6):B1105–B1132, 2021.
- [73] G. Łukaszewicz and P. Kalita. Navier–stokes equations. *Advances in Mechanics and Mathematics*, 34, 2016.
- [74] I Michel, SMI Bathaeian, J Kuhnert, D Kolymbas, C-H Chen, I Polymerou, C Vrettos, and A Becker. Meshfree generalized finite difference methods in soil mechanics—part ii: numerical results. *GEM-International Journal on Geomathematics*, 8(2):191–217, 2017.
- [75] Isabel Michel, Tobias Seifarth, Jörg Kuhnert, and Pratik Suchde. A meshfree generalized finite difference method for solution mining processes. *Computational Particle Mechanics*, 8(3):561–574, 2021.
- [76] Pedro M Milani, Julia Ling, and John K Eaton. Generalization of machine-learned turbulent heat flux models applied to film cooling flows. *Journal of Turbomachinery*, 142(1), 2020.
- [77] Siddhartha Mishra and Roberto Molinaro. Estimates on the generalization error of physics informed neural networks (pinns) for approximating a class of inverse problems for pdes, 2020.
- [78] Siddhartha Mishra and Roberto Molinaro. Estimates on the generalization error of physics informed neural networks (pinns) for approximating pdes, 2020.
- [79] Christian Moya and Guang Lin. Fed-deeponet: Stochastic gradient-based federated training of deep operator networks. *Algorithms*, 15(9):325, 2022.
- [80] Christian Moya, Shiqi Zhang, Meng Yue, and Guang Lin. Deeponet-grid-ug: A trustworthy deep operator framework for predicting the power grid’s post-fault trajectories. *arXiv preprint arXiv:2202.07176*, 2022.
- [81] Johannes Müller and Marius Zeinhofer. Deep ritz revisited. *arXiv preprint arXiv:1912.03937*, 2019.
- [82] Derick Nganyu Tanyu, Isabel Michel, Andreas Rademacher, Peter Maass, and Jörg Kuhnert. Parameter identification by deep learning of a material model for granular media. *In preparation*, 2022.
- [83] I Ostermann, J Kuhnert, D Kolymbas, C-H Chen, I Polymerou, V Šmilauer, C Vrettos, and D Chen. Meshfree generalized finite difference methods in soil mechanics—part i: theory. *GEM-International Journal on Geomathematics*, 4(2):167–184, 2013.
- [84] Kasey Panetta. Gartner top 10 strategic technology trends for 2019. <https://www.gartner.com/smarterwithgartner/gartner-top-10-strategic-technology-trends-for-2018>. Accessed: December 7, 2022.
- [85] Kasey Panetta. Gartner top 10 strategic technology trends for 2020. <https://www.gartner.com/smarterwithgartner/gartner-top-10-strategic-technology-trends-for-2019>. Accessed: December 7, 2022.
- [86] Guofei Pang, Lu Lu, and George Em Karniadakis. fpinns: Fractional physics-informed neural networks. *SIAM Journal on Scientific Computing*, 41(4):A2603–A2626, 2019.
- [87] Maziar Raissi. Deep hidden physics models: Deep learning of nonlinear partial differential equations. *The Journal of Machine Learning Research*, 19(1):932–955, 2018.
- [88] Maziar Raissi, Paris Perdikaris, and George E Karniadakis. Physics-informed neural networks: A deep learning framework for solving forward and inverse problems involving nonlinear partial differential equations. *Journal of Computational Physics*, 378:686–707, 2019.
- [89] Lars Ruthotto and Eldad Haber. Deep neural networks motivated by partial differential equations. *Journal of Mathematical Imaging and Vision*, 62(3):352–364, 2020.

- [90] Wil Schilders. Msode: Modelling, simulation and optimization in a data-rich environment. In *Mathematics: Key Enabling Technology for Scientific Machine Learning*, pages 24–30, 2021.
- [91] Justin Sirignano and Konstantinos Spiliopoulos. Dgm: A deep learning algorithm for solving partial differential equations. *Journal of computational physics*, 375:1339–1364, 2018.
- [92] John C. Strikwerda. *Finite Difference Schemes and Partial Differential Equations*. Society for Industrial and Applied Mathematics, second edition, 2004.
- [93] Yixuan Sun, Christian Moya, Guang Lin, and Meng Yue. Deepgraphonet: A deep graph operator network to learn and zero-shot transfer the dynamic response of networked systems. *arXiv preprint arXiv:2209.10622*, 2022.
- [94] Lesley Tan and Liang Chen. Enhanced deeponet for modeling partial differential operators considering multiple input functions. *arXiv preprint arXiv:2202.08942*, 2022.
- [95] Nils Thuerey, Philipp Holl, Maximilian Mueller, Patrick Schnell, Felix Trost, and Kiwon Um. Physics-based deep learning. *arXiv preprint arXiv:2109.05237*, 2021.
- [96] TORCHPHYSICS: A deep learning library to solve differential equations. <https://github.com/boschresearch/torchphysics>. Accessed: December 7, 2022.
- [97] Tapas Tripura and Souvik Chakraborty. Wavelet neural operator: a neural operator for parametric partial differential equations. *arXiv preprint arXiv:2205.02191*, 2022.
- [98] F. Tröltzsch. *Optimal Control of Partial Differential Equations*, volume 112 of *Graduate Studies in Mathematics*. American Mathematical Society, Providence, 2010.
- [99] Rui Wang, Karthik Kashinath, Mustafa Mustafa, Adrian Albert, and Rose Yu. Towards physics-informed deep learning for turbulent flow prediction. In *Proceedings of the 26th ACM SIGKDD International Conference on Knowledge Discovery & Data Mining*, pages 1457–1466, 2020.
- [100] Sifan Wang, Hanwen Wang, and Paris Perdikaris. Improved architectures and training algorithms for deep operator networks, 2021.
- [101] Sifan Wang, Hanwen Wang, and Paris Perdikaris. Learning the solution operator of parametric partial differential equations with physics-informed deepnets. *arXiv preprint arXiv:2103.10974*, 2021.
- [102] Sifan Wang, Hanwen Wang, and Paris Perdikaris. On the eigenvector bias of fourier feature networks: From regression to solving multi-scale PDEs with physics-informed neural networks. *Computer Methods in Applied Mechanics and Engineering*, 384:113938, oct 2021.
- [103] Sifan Wang, Xinling Yu, and Paris Perdikaris. When and why pinns fail to train: A neural tangent kernel perspective, 2020.
- [104] E Weinan, Jiequn Han, and Arnulf Jentzen. Algorithms for solving high dimensional pdes: From nonlinear monte carlo to machine learning. *Nonlinearity*, 35(1):278, 2021.
- [105] Gege Wen, Catherine Hay, and Sally M Benson. Ccsnet: a deep learning modeling suite for co2 storage. *Advances in Water Resources*, 155:104009, 2021.
- [106] Gege Wen, Zongyi Li, Kamyar Azizzadenesheli, Anima Anandkumar, and Sally M Benson. U-fno—an enhanced fourier neural operator-based deep-learning model for multiphase flow. *Advances in Water Resources*, 163:104180, 2022.
- [107] Hui Xie, Chuanlei Zhai, Li Liu, and Heng Yong. A weighted first-order formulation for solving anisotropic diffusion equations with deep neural networks, 2022.
- [108] Shin Yeonjong, Jerome Darbon, and George Em Karniadakis. On the convergence of physics informed neural networks for linear second-order elliptic and parabolic type PDEs. *Communications in Computational Physics*, 28(5):2042–2074, jun 2020.

- [109] Huaqian You, Yue Yu, Marta D’Elia, Tian Gao, and Stewart Silling. Nonlocal kernel network (nkn): a stable and resolution-independent deep neural network. *arXiv preprint arXiv:2201.02217*, 2022.
- [110] Bing Yu et al. The deep ritz method: a deep learning-based numerical algorithm for solving variational problems. *arXiv preprint arXiv:1710.00211*, 2017.
- [111] Jeremy Yu, Lu Lu, Xuhui Meng, and George Em Karniadakis. Gradient-enhanced physics-informed neural networks for forward and inverse pde problems. *Computer Methods in Applied Mechanics and Engineering*, 393:114823, 2022.
- [112] Yaohua Zang, Gang Bao, Xiaojing Ye, and Haomin Zhou. Weak adversarial networks for high-dimensional partial differential equations. *Journal of Computational Physics*, 411:109409, 2020.
- [113] Dongkun Zhang, Lu Lu, Ling Guo, and George Em Karniadakis. Quantifying total uncertainty in physics-informed neural networks for solving forward and inverse stochastic problems. *Journal of Computational Physics*, 397:108850, 2019.
- [114] Yinhao Zhu and Nicholas Zabaras. Bayesian deep convolutional encoder–decoder networks for surrogate modeling and uncertainty quantification. *Journal of Computational Physics*, 366:415–447, 2018.

A Appendix

A.1 Application Problems

A.1.1 Darcy Flow

For this problem, we consider the steady-state of the 2-d Darcy Flow equation on the unit box which is the second order, linear, elliptic PDE

$$\begin{aligned} -\nabla \cdot (\lambda(s)\nabla u(s)) &= f(s) & s \in (0, 1)^2 \\ u(s) &= 0 & s \in \partial(0, 1)^2 \end{aligned} \tag{52}$$

with a Dirichlet boundary where $a \in L^\infty((0, 1)^2; \mathbb{R}_+)$ is the diffusion coefficient, $f = 1 \in L^2((0, 1)^2; \mathbb{R}_+)$ is the forcing function and $u \in H_0^1((0, 1)^2; \mathbb{R})$ is the unique solution of the PDE. Some few applications of this PDE are seen in the domains of modeling the pressure of subsurface flow, the deformation of linearly elastic materials, and the electric potential in conductive materials.

A.1.2 Poisson Equation

We are interested in the PDE

$$\begin{aligned} -\Delta u(s) &= \lambda(s) & s \in (0, 1)^2 \\ u(s) &= 0 & s \in \partial(0, 1)^2 \end{aligned} \tag{53}$$

which is a special case of Equation 52 where the diffusion coefficient is constant and equals to 1 everywhere in the domain $\Omega = (0, 1)^2$.

A.2 Setting of Numerical Implementations

The details of the experiments provided in Section 5. The computing environment is described below:

- CPU: 8x nVidia GeForce GTX 2080 Ti
- CPU: Intel Xeon Gold 6234 (8 cores, 32 threads)
- RAM: 1500 GB of system RAM
- OS: Ubuntu 16.04.7 LTS

While the parameters for the Poisson problem are sampled from the distribution μ_G , those for the Darcy Flow are sampled on μ_P (piece wise constant). These distributions are described in Section 5.

For the operator learning scenarios (PCANN, FNO, UFNO, DeepONet), for both forward and inverse problems of the Poisson and Darcy Flow problems, we train the neural operator on 1000 training data-set pairs we evaluate on 5000 test pairs. This also holds for the pre-training phase of the PINO.

The experiments for DRM, PINN, QRES, DeepONet and PI-DeepONet were all done in the deep learning library TORCHPHYSICS [96], the code is available online.

A.2.1 DRM, PINNs and QRES

Hyperparameter		PINNs & QRES				DRM	
		<i>Forward</i>		<i>Inverse</i>		<i>Forward</i>	
		ADAM	LBFGS	ADAM	LBFGS	ADAM	LBFGS
Poisson	Learning rate	0.001	0.2	0.001	0.5	0.001	0.2
	Iterations	5,000	8,000	5,000	10,000	5,000	5,000
	Scale factor s	100		100		100	
	$(\omega_{\mathcal{L}}, \omega_{\mathcal{B}}, \omega_{\mathcal{D}})$	(1, 10,000, 0)		(1, 0, 10,000)		(1, 10,000, 0)	
Darcy Flow	Learning rate	0.001	0.25	0.005	0.5	0.002	0.25
	Iterations	5,000	12,000	5,000	15,000	5,000	8,000
	Scale factor s	0.01		100		0.01	
	$(\omega_{\mathcal{L}}, \omega_{\mathcal{B}}, \omega_{\mathcal{D}})$	(1, 100, 0)		(1, 0, 100)		(1, 100, 0)	

Table 13: Used parameters for the DRM, PINNs and QRES in the simulations.

Since the general training procedures of DRM, PINNs and QRES are closely related, we explain the implementation for all 3 approaches at the same time.

The accuracy of the results mainly depends on the size of the network, the number of training points and the range of the solution. To get a fair comparison between PINN and QRES, we choose the networks in such a way that they have roughly the same number of trainable parameters. We considered both accuracy and training time while choosing the network architecture. All other Hyperparameters for PINNs and QRES are the same. In the inverse problem we use two networks (u_{Θ}, f_{Θ}) . Where u_{Θ} interpolates the given data and f_{Θ} approximates the searched data function.

In the Poisson problem for PINNs we use a FCN with 3 hidden layers and 50 neurons. For QRES the architecture 5 with 3 layers and 36 neurons is utilized. In the inverse problem, (u_{Θ}, f_{Θ}) have both the same structure as in the forward problem. The used neural network in the Deep Ritz method consists of 2 residual blocks, and the initial and last FC layer. Where each layer has 40 neurons.

For the Darcy equation, deeper neural networks were in general more advantageous. Therefore, the Deep Ritz network consisted of 3 residual blocks with 60 neurons. For the forward problems with PINNs we applied an architecture with 4 layers, where the number of neurons of layer k was the k -th entry in $(50, 50, 50, 20)$. Analogue, for QRES a network with the structure $(36, 36, 36, 15)$ was used. For the inverse problem, the PINN u_{Θ} was given by $(50, 50, 20)$ and for QRES by $(36, 36, 15)$. For the network of the data function f_{Θ} , we choose for PINNs $(30, 40, 40, 20, 20)$ and for QRES $(25, 35, 25, 15, 15)$.

The strong formulation of the Darcy equation (52) with a piece wise constant coefficient λ is ill posed at the points where the jump occurs. This leads to an additional challenge for the training of the forward problem with PINNs and QRES. When the derivatives of λ become large, so does the loss function, and the optimization is mainly focused on reducing the influence of the derivatives. Which leads overall to a worse approximation of the real solution. To avoid this problem, in [107] a special weight function is introduced. The function is constructed in such a way, that the weight is zero at the interfaces where the discontinuities are and $\mathcal{O}(1)$ away from the interfaces. If we apply this idea to our problem, we have to remove all points where the discrete jumps occur and the equation reduces everywhere else to $\lambda \Delta u = f$, since our parameter is piece wise constant. For the DRM we can use the original PDE (52). This is also possible in the inverse case, since there the unknown parameter λ is approximated by a smooth neural network.

Additionally, neural networks can best work with values in the range of $[-1, 1]$, because of this we scale our data by a factor s . The used values are listed in table 13. For the forward problem the given data function is scaled, for the inverse problem the known solution u is multiplied by s .

Training is done with a combination of Adam and LBFGS. We start with a fixed number of iterations of Adam and then switch over to LBFGS, like usually done in the literature. Since two different optimization algorithms are used, the needed time per iteration (epoch) in table 2 is an average over both algorithms. For LBFGS we use the PyTorch implementation and set the *max_iteration* variable to 2. In the inverse case, both data fitting and the minimization of the PDE loss are trained at the same time. For LBFGS all available points have to be used in each training step, this leads to a rather slow training process for higher resolutions. Using lower resolutions leads to roughly the same accuracy, but speeds up the training considerably.

To control the influence of each condition we add additional weights ($\omega_{\mathcal{L}}, \omega_{\mathcal{B}}, \omega_{\mathcal{D}}$). The used values are presented in table 13. Since the magnitude of the loss of the PDE condition is much larger than the loss of the other conditions, we use a large weight for the boundary and data conditions. If the weight is zero, in table 13, this means the condition did not appear in the training. E.g. no additional boundary condition in the inverse case and data of the solution in the forward problem. Lastly we want to mention, that if the boundary condition is build into the network architecture better results can be achieved.

A.2.2 PCANN, PCALin

The obtained error for the PCANN, depends largely on the reduced/latent dimension used for the PCA. For each reduced dimension $d_{\mathcal{X}} = d_{\mathcal{Y}} \in [30, 50, 70, 100, 150, 200, 250]$, the hyperparameters were grid searched. The choice of this range was based on [8], which showed how larger dimensions do not necessarily guarantee better approximations for the PCANN. However, larger dimensions could lead to better results for the PCALin. The results shown in Tables 2 and 5 are for the best performing cases. We present the hyperparameter setting for each separate case in the Table 14. ADAM was used in PCALin while SGD is was used in PCANN.

Hyperparameter	Poisson				Darcy Flow			
	PCANN		PCALin		PCANN		PCALin	
	<i>Forward</i>	<i>Inverse</i>	<i>Forward</i>	<i>Inverse</i>	<i>Forward</i>	<i>Inverse</i>	<i>Forward</i>	<i>Inverse</i>
Latent dimension	150	200	250	250	150	30	100	100
Weight decay	0.1	0.1	0.015	0.1	0.5	0.1	0.1	0.15
Batch size	500	500	1000	1000	500	100	1000	200
Learning rate	5×10^{-7}	1×10^{-5}	0.01, 0.001, 0.0025		1×10^{-6}	1×10^{-4}	1×10^{-3}	1×10^{-3}
Step size	2000	2500	2500, 5000		7500	2500	-	2500
Gamma	0.5	0.1	0.01, 0.1		0.5	0.01	-	0.01
Epochs	20000	10000	6000		20000	5000	2000	1000
Dropout	0	0.001	0		0	0.01	0	0
Weight Initialisation	kaiming normal		xavier		kaiming normal		xavier	

Table 14: Best performing hyperparameters for the PCANN method and its linear version-PCALin

A.2.3 FNO, UFNO, MWT, PINO

We use same hyper parameters for the 2D FNO/MWT problem as in the paper, and the code made available. Notably, training is done for 500 *epochs*, with a *batch-size* of 10. The ADAM algorithm is used for optimisation, with a *learning rate* of 0.001 which reduced by a factor of 0.5 (a.k.a. *gamma*) after every 100 (a.k.a. *step size*) epochs. An L-2 regularisation is added to the loss function with a *weight decay* of 1×10^{-4} . Specific to the FNO, UFNO. and PINO methods are the fourier modes and width, We truncate 12 *fourier modes* and uses a *width* size of 32.

On the other hand, in the MWT, Convolutional Neural Networks (CNNs) are used to parametrised the networks A, B, C and T is a single $k \times k$ linear layer with $k = 4$. The Legendre orthogonal polynomial basis is used as it produces better results as reported in [36].

For the PINO, we optimise the loss function L , given by:

$$L = L_{\text{data}} + 0.2 \cdot L_{\text{pde}}$$

A.2.4 DeepONet

For poisson problem, we use linear model for the branch net, while the trunk net is a neural network with width 128 and 6 hidden layers, and Tanh as the activation function . For Darcy-flow with piece-wise constant coefficients, we use the convolutional neural network for branch net, while the trunk net is a neural network with width 128 and 4 hidden layers, and ReLU as the activation function. However, for the inverse training of Darcy-flow problem, we use sin as the activation for the trunk net, which can achive better result than using general activation functions. We use the fast implementation to train the neural network as described in algorithm. The training is done for 50000 epochs, with a batch-size of 125. The Adam algorithm is used for optimization with a learning rate 0.002 which reduced by a factor 0.9 after every 1250 epochs.

We need to note that the resolution size will affect the size of the branch net of DeepONet. For example, for 513×513 resolution case, the number of parameters in the branch net would be $513 \times 513 \times 128 \approx 3.0 \times 10^7$ and the server we use will face the memory limitation problem. Thus, for high resolution case, an adaptive average pooling is first used in the branch net to reduce the size of the data, which can reduce the number of parameters and training time.

A.2.5 PI-DeepONet

In our experiments on PI-DeepONet, we add an additional physics loss to the optimization of a data-driven DeepONet described above. Therefore, we use architectures that are similar to the experiments done on DeepONet. In the case of inverse operator training for the Darcy-flow problem, we increase the size of the convolutional branch net and its adaptive average pooling.

In all cases, we rescale the input and output data such that the values are roughly in the range of $[-1, 1]$ to improve the training performance. All terms in the physics loss are scaled accordingly.

The construction of a physics-based loss in the inverse operator training requires the derivatives of the discrete PDE solution. To obtain these, we come up with a concept that is inspired by the solution of inverse problems in PINN: We introduce a second trunk net that is optimized to interpolate the solution via mean squared error and shares the same branch network. The derivatives of the solution can then be computed via gradient descent and be included in the physics-based loss to reconstruct the parameter. As a result, in addition to the data- and physics-based loss, we have to minimize an interpolation loss $MSE_{\mathcal{I}}$. Both trunk nets are optimized simultaneously.

One has to choose the weights $\omega_{\mathcal{L}}, \omega_{\mathcal{B}}, \omega_{\mathcal{D}}$ (and $\omega_{\mathcal{I}}$) of the physics-informed, boundary condition, data-based (and interpolation) parts of the loss function. In most cases, we choose all weights to have the value 1. Only in the Darcy-flow inverse operator learning, we scale the interpolation loss by $\omega_{\mathcal{I}} = 5$ to improve the influence of the learned derivatives.

Hyperparameter	Poisson		Darcy Flow	
	α_1	α_2	α_1	α_2
PCANN	0.0005	0.05	0.0001	0.005
PCALin	0.00001	0.025	0.001	0.001
FNO	0	0.25	0	0.025
UFNO	0	0.05	0	0.005
MWT	0	0.05	0	0.005
PINO	0	0.05	0	0.005
DeepONet	0	0.05	0	0.025
PI-DeepONet	0	0.05	0	0.025

Table 15: Hyperparameter configurations for Tikhnov-based methods for Inverse Problems.

In all settings, we train for 1,650,000 iterations that consist of 128 branch inputs and 100 randomly sampled trunk input points. We reduce the learning rate in an iterative scheme every 50,000 steps. For the Poisson forward problem, we use an initial learning rate of $5e - 4$ and reduce it iteratively by a factor of 0.8. For the inverse operator training, we end up using an initial learning rate of $1.5e - 4$ (Poisson) respectively $2.5e - 4$ (Darcy) and a factor of 0.85.

During training, we use the full dataset, to ensure comparability to the other used methods. The advantages of a physics-informed approach might however come better into play in a setting in which only partial

data is available, therefore, this might not be the optimal use case for PI-DeepONets.

A.2.6 Tikhonov-based methods for Inverse Problems

For learning the parameter, we used a learning rate of 0.1 and trained for 10000 epochs, decreasing the learning rate by a factor of 0.5 every 2000 epochs. The below loss functions are used.

$$Loss(\lambda)_{\text{poisson}} = \|G_{\theta}\lambda - u_{\delta}\|_2 + \alpha_1\|\lambda\|_2 + \alpha_2\|D(\lambda)\|_2 \quad (54)$$

$$Loss(\lambda)_{\text{darcy}} = \|G_{\theta}\lambda - u_{\delta}\|_2 + \alpha_1\|\lambda\|_2 + \alpha_2\text{Var}(\lambda), \quad (55)$$

where G_{θ} is the forward operator, $D(\lambda)$ is the first difference quotient of λ , and Var is the Total Variation loss. Using same hyperparameter configuration, testing was done on 100 test examples and the results were reported in Tables 8 and 9. For a visual appreciation of the results, we also show in Tables 10 and 11 the learned parameter for both Poisson and Darcy Flow with piece-wise constant parameter problems.